Statistical Failure Properties of Fiber-Reinforced Composites

Von der Fakultät Physik der Universität Stuttgart
zur Erlangung der Würde eines Doktors der
Naturwissenschaften (Dr. rer. nat.) genehmigte Abhandlung

vorgelegt von

Raúl Cruz Hidalgo

aus Holguín, Kuba

Hauptberichter: Prof. Dr. H. J. Herrmann
Mitberichter: Prof. Dr. Dr. h.c. H. -W. Reinhardt

Tag der mündlichen Prüfung: 28. Juli 2003

Institut für Computeranwendungen 1 der Universität Stuttgart

2003

To Carmen Rosa,
To Carmen Aimara,
To my parents,
To my grandparents.

Contents

Chapter 1

Deutsche Zusammenfassung

Ein Verbundwerkstoff ist ein kompliziertes festes Material, das aus zwei oder mehr Bestandteilen besteht. Auf einer makroskopischen Skala hat es strukturelle und funktionelle Eigenschaften, die in jedem einzelnen Bestandteil nicht vorhanden sind. In der Regel werden sie hergestellt, um die besten Eigenschaften ihrer Bestandteile aufzuweisen.

Die Natur hat Verbundwerkstoffe wie Meerespflanzen, Holz und Knochen geliefert. Außerdem gibt es viele zahlreiche künstliche Strukturen wie bewehrter Beton und Faserverbundwerkstoffe. Überraschenderweise sind sie nicht neu im alltäglichen Leben. Sogar die alten Ägypter benutzten Sperrholz und die Römer Beton. Heutzutage wiegen neue Faserverbundwerkstoffe ungefähr ein Fünftel von Stahl, aber sie können in Steifigheit und Stärke vergleichbar sein. Das ist abhängig von Fasergehalt und Lagebestimmung. Diese Faserverbundwerkstoffe verrosten oder korrodieren nicht wie Stahl oder Aluminium. Eine der wichtigsten Errungenchalten ist, dass die Automobilindustrie Trägergewicht nahe zu um 60% verringern und Trägerbrennstoffersparnis erheblich erhöhen konnten.

Ein Faserverbundwerkstoff wird aus Fasern gebildet, die in einem schützenden Material eingebettet werden, das Matrix genannt wird. Eine Kopplung mit dem Medium wird an die Fasern angebracht, um die Adhäsion der Faser zum Matrixmaterial zu verbessern. Die Funktionen der Matrix, ob organisch, keramisch oder metallisch, ist es, die Fasern zu stützen und zu schützen. Außerdem dient die Matrix als Medium für die Übertragung der Spannungsüberhöhung zwischen Fasern.

Der Lastsausfall der Faserverbundwerkstoffe wird im Allgemeinen durch den Ausfall der Faserbündel bestimmt. Wenn eine einachsige Last in die Richtung parallel zu den Fasern angewendet wird, kann die tatsächliche Spannung σ_T als

$$\sigma_T = \sigma_f V_f + (1 - V_f)\sigma_m \tag{1.1}$$

ausgedrückt werden, wobei V_f den Faservolumenbruch bezeichnet, σ_f ist die durch die Fasern getragene Spannung und σ_m die normalerweise kleinere durch die Matrix getragene Spannung.

Die Matrix in Metallmatrix-Verbundwerkstoffen trägt Last mit. Aber in Keramikmatrix-Verbundwerkstoffen (C/C-SiC), trägt nach dem Bruch der Matrix diese fast Nulllast. Damit kann die Matrixbelastung σ_m normalerweise vernachlässigt werden. Jedoch fährt Spannungsüberhöhung zwischen den Fasern durch die Matrixtätigkeit trotz der stufenweisen Beschädigung fort. Folglich hat sie eine sehr wichtige Rolle in der Lastneuverteilung.

Um den Ausfall der Faserverbundwerkstoffe zu verstehen muß, man sich auf das Reissen der Fasern konzentrieren. Folglich sind die zwei Faktoren, die den Faserausfall in den Faserverbundwerkstoffe steuern,

- die statistische Faserfestigkeit
- der Lastumlagerungstyp (type of load sharing).

Die Spannung entlang der Faser hängt von der angewandten externen Spannung ab, aber auch davon, wie die Spannung einer defekten Faser auf die umgebenden intakten Fasern und in die Umgebung der Matrix übertragen wird. Diese Spannungsübertragung wird durch die elastischen Eigenschaften der Bestandteile und durch die Faser/Matrix Schnittstelle geregelt. Es ist schwierig, sie bei mehr als einer defekten Faser zu erhalten. Für eine realistische Modellierung des Beschädigungsprozesses des Faserverbundwerkstoffs unter einer einachsigen Last müsste die Druckverteilung im vollständigen Volumen der Probe errechnet werden. Selbst wenn man die Zahl der unabhängigen Variablen begrenzt, die benötigt werden, um die interne Mikrostruktur des Probestücks zu beschreiben, ist eine genaue Vorhersage der Endfestigkeit eine rechnerisch anspruchsvolle Aufgabe.

Folglich basiert die Modellierung der Faserzusammensetzungen im allgemeinen auf bestimmten Vereinfachungen der Geometrie der Faseranordnung und der Spannungsneuverteilung nach Faserausfällen in der Probe. Außerdem muß die Zahl der Fasern, die das System bilden, sehr groß sein, um zuverlässige Ergebnisse zu erreichen. Dies macht die numerische Berechnung in vielen Fällen zu zeitaufwendig, um die Studie in einem angemessenen Zeitraum durchzuführen. Deswegen wurde viel Aufwand in analytischen Näherungen und einfacheren numerischen Modellen betrieben.

Eines dieser Modelle, das Faserbündelmodell, hat viel Aufmerksamkeit erhalten, da einige wichtige Größen im dessen Rahmen analytisch hergeleitet werden können. Außerdem können leistungsfähige Simulationstechniken entwickelt werden, die die Studie von großen Proben erlaubt. Trotz ihrer Einfachheit beziehen sie die wichtigsten Aspekte von Sachschäden und Zusammenbrüchen mit ein. Sie haben ein größeres Verständnis von Bruchprozessen geliefert und als Ausgangspunkt komplizierterer Modelle von Faserwerkstoffen und anderen mikro-mechanischen Modellen gedient.

Faserbündelmodelle mit kontinuierlicher Schädigung

Das Faserbündelmodell mit kontinuierlicher Schädigung ist eine Erweiterung der klassischen Faserbündelmodelle mit verallgemeinertem Schädigungsgesetz für Faserversagen. Das Modell besteht wieder aus N parallel angeordneten Fasern mit identischen Elastizitätsmoduli E_f aber zufälligen Faserfestigkeiten d_i, $i = 1, \ldots, N$. Für die Fasern nehmen wir linear elastisches Verhalten bis zu ihrem spröden Versagen an, das unter uni-axialer Belastung des Systems bei Überschreitung der Faserfestigkeit d_i eintritt. Die Besonderheit unseres Modells besteht nun darin, dass bei Faserversagen die Steifigkeit der Faser durch einen Faktor a mit $0 \leq a < 1$ auf aE_f gemindert wird. Damit wird mehrfaches Faserversagen möglich. Die maximal zulässige Zahl der Steifigkeitsabminderungen k_{max} geht als zusätzlicher Parameter in das Modell ein. Eine weitere, in Abb.1.1 dargestellte Variation kann in der Festigkeit d_i einer Faser bestehen, die entweder auf dem anfänglich zufälling gewählten Wert fixiert wird (eingefrorene Unordnung) oder aber nach jedem Versagen aus der selben Wahrscheinlichkeitsverteilung neu zugewiesen wird (ereignisabhängige Unordnung). Auf diese Weise können z.B. durch Bruchvorgänge initiierte mikroskopische Umordnungen im Material berücksichtigt werden.

Die Darstellung der Schädigung mittels eines kontinuierlichen Schädigungsparameters im Rahmen von Diskrete-Elemente-Modellen entspricht einer Systembeschreibung auf einer größeren Längenskala als der charakteristischen Rissgröße. Dies kann in mehrfacher Weise interpretiert werden: so können Fasern die kleinsten Elemente des Modells bilden, deren kontinuierliches Versagen z.B. mehrfaches Faserversagen repräsentiert, oder aber auf einer gröberen Skala werden mehrere Fasern mit Matrix als kleinste Elemente des Faserbündelmodells diskretisiert. Bei dieser Interpretation werden die mikroskopischen Schädigungsmechanismen bei graduellem Versagen von Matrix und Fasern eines Elements in Form von mehrfachem Elementversagen berücksichtigt. Wegen dieser alternativen Modellvorstellungen definieren wir die Elemente des Faserbündelmodells im Folgenden als Fasern. Für die Lastumlagerung nehmen wir $d \to \infty$, also globale Lastumlagerung und die Bedingung identischer Dehnungen an, was impliziert, dass steifere Fasern mehr Last tragen als weichere. Bei der Dehnung ε herrscht in der Faser i, bei der bereits $k(i)$ mal Versagen aufgetreten ist, die Spannung

$$f_i(\varepsilon) = E_f a^{k(i)} \varepsilon, \tag{1.2}$$

mit der aktuellen Fasersteifigkeit $E_f a^{k(i)}$. Trotz des unendlichen Wechselwirkungsradius

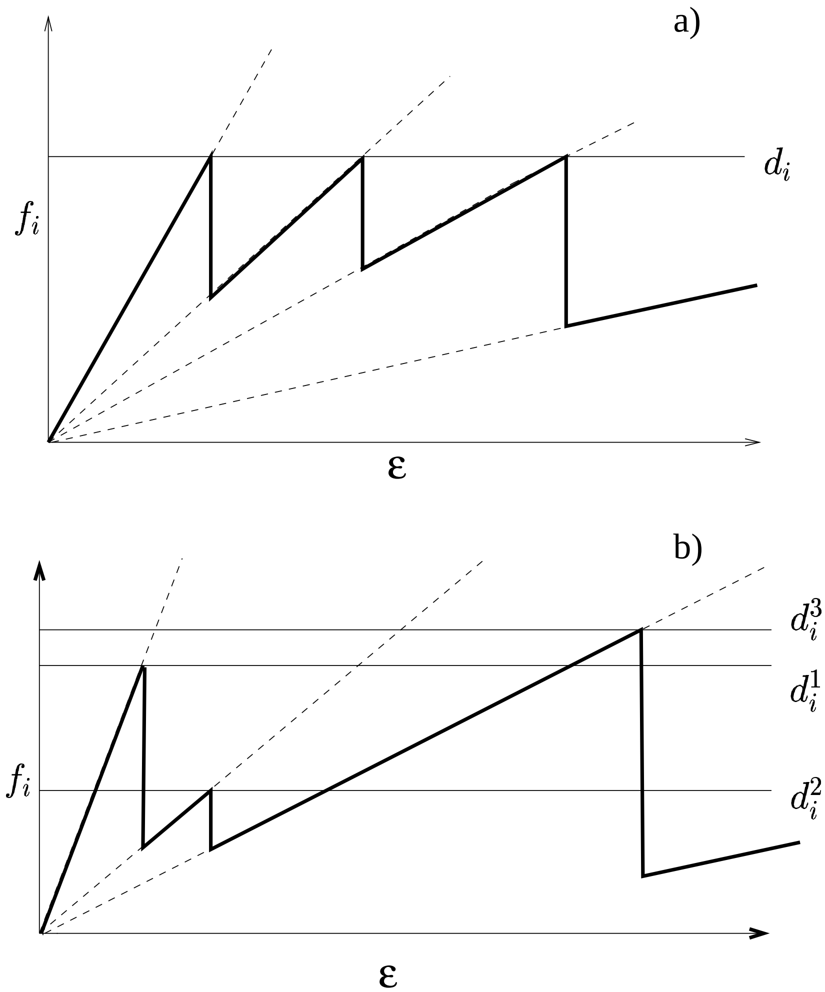

Figure 1.1: Schädigungsgesetz einer Einzelfaser i mit mehrfachem Faserversagen für (a) eingefrorene und (b) ereignisabhängige Unordnung. Die horizontalen Linien repräsentieren die Faserfestigkeit d_i.

unterscheidet sich Gl.1.2 folglich von der oben beschriebenen globalen Lastumlagerung, bei der alle intakten Fasern die selbe Last tragen.

In der folgenden Ableitung der konstitutiven Gesetze des Faserbündelmodells mit kontinuierlicher Schädigung ist E_f die Einheitssteifigkeit. Betrachtet man zunächst die konstitutive Gleichung für den Fall einfachen Faserversagens. So gilt

$$\frac{F}{N} = \varepsilon(1 - P(\varepsilon)) + a\varepsilon P(\varepsilon), \tag{1.3}$$

mit $P(\varepsilon)$ bzw. $1 - P(\varepsilon)$ als Anteil gebrochener bzw. intakter Fasern. Hieraus geht unmittelbar die Beziehung für trockene Faserbündel $(a = 0)$ [1–4], sowie für $a = 0.5$ auch das mikromechanische Modell faserverstärker Keramik-Matrix-Verbundwerkstoffe (CMC) bei Belastung in Faserrichtung hervor [5–7]. Die mikromechanische Erklärung für die Fähigkeit gebrochener Fasern in CMCs Last zu tragen, ist Faser-Matrix-Ablösung in der Nähe des Faserbruches und Spannungsaufbau in der Faser über Reibung.

Bei mehrfachem Faserversagen ist eine Unterscheidung zwischen eingefrorener und ereignisabhängiger Unordnung notwendig:

(i) Eingefrorene Unordnung: Ist zweifaches Faserversagen erlaubt, erweitert sich Gl.1.3 zu

$$\frac{F}{N} = \varepsilon(1 - P(\varepsilon)) + a\varepsilon\left[P(\varepsilon) - P(a\varepsilon)\right] + a^2\varepsilon P(a\varepsilon), \tag{1.4}$$

mit dem Anteil bereits einmal versagter Fasern $[P(\varepsilon) - P(a\varepsilon)]$ und dem Anteil bereits zweimal versagter Fasern $P(a\sigma)$. Der allgemeine Fall bei k-fachem Faserversagen führt zu:

$$\frac{F}{N} = \quad \varepsilon(1 - P(\varepsilon)) + \sum_{i=1}^{k_{max}-1} a^i\varepsilon\left[P(a^{i-1}\varepsilon) - P(a^i\varepsilon)\right] + a^{k_{max}}\varepsilon P(a^{k_{max}-1}\varepsilon) \tag{1.5}$$

(ii) Ereignisabhängige Unordnung: Für ereignisabhängige Unordnung und zweifaches Faserversagen ergibt sich

$$\frac{F}{N} = \varepsilon(1 - P(\varepsilon)) + afP(\varepsilon)(1 - P(a\varepsilon)) + a^2\varepsilon P(\varepsilon)P(a\varepsilon), \tag{1.6}$$

mit dem Anteil einmal versagter Fasern $P(\varepsilon)(1 - P(a\varepsilon))$ und dem Anteil bereits zweimal versagter Fasern $P(\varepsilon)P(a\varepsilon)$. Der allgemeine Fall, bei dem k_{max}-faches Faserversagen zugelassen ist, wird zu

$$\frac{F}{N} = \sum_{i=0}^{k_{max}-1} a^i\varepsilon\left[1 - P(a^i\varepsilon)\right]\prod_{j=0}^{i-1} P(a^j\varepsilon) + a^{k_{max}}\varepsilon \prod_{i=0}^{k_{max}-1} P(a^i\varepsilon), \tag{1.7}$$

wobei k_{max} auch unendlich werden kann.

Faserbündelmodelle zur alternativen Beschreibung des konstitutiven Verhaltens granularer Medien

In komprimiertem granularen Material werden Kräfte im System durch perkolierende Kraftlinien übertragen, die z.B. in Abb. 1.2 visualisiert sind. Die Ähnlichkeiten dieser

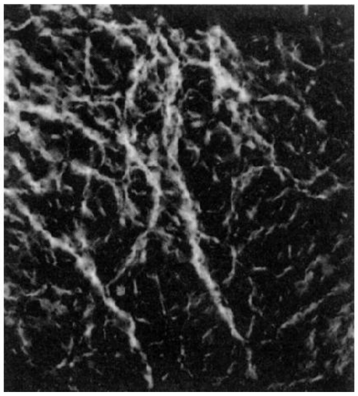

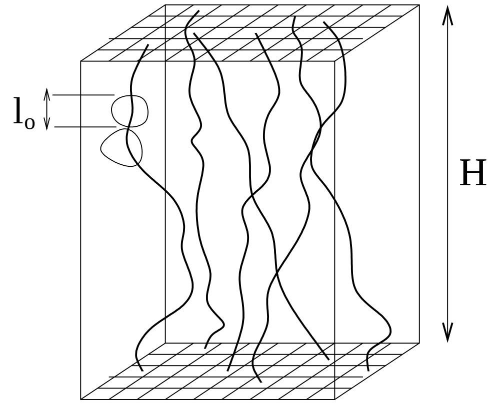

Figure 1.2: Experimentelle Visualisierung von Kraftlinien (links) und Grundmodellvorstellung (rechts).

Kraftlinien zu Fasern in Faserverbundmaterialien bilden die Grundlage unserer Modellierung. Invertiert man gedanklich die Schädigungssimulation in Faserbündelmodellen, so entsteht eine Analogie zur Ausbildung und Verstärkung von Kraftpfaden, wie sie bei der Kompression granularer Packungen beobachtet werden. Das FBM mit kontinuierlicher Schädigung bildet den Ausgangspunkt, da es graduelle Steifigkeitsänderungen der Elemente (bisher graduelles Faserversagen) berücksichtigt. Unser Modell zur Ausbildung und Verstärkung von Kraftpfaden invertiert diese Situation. Die individuellen Linien des Netzwerkes bilden in unserer Vorstellung Fasern, die anstelle von Brüchen unter Zugspannung nun unter Druck durch Umordnung von Kontakten verfestigen. Da viele Umordnungen möglich sind, bilden die FBM mit kontinuierlicher Schädigung den besten Ausgangspunkt als Modell. In dem Modell werden Kraftlinien als parallele Linien auf einem Quadratgitter angeordnet. Jeder Linie wird eine zufällige Grenzspannung d zugewiesen, bei der sich ein Kontakt entlang der Faser umstrukturiert, was typischerweise zu geraderen und steiferen Kraftlinien führt, die im Modell durch eine Steifigkeitserhöhung mit dem Faktor a berücksichtigt werden. Zudem wird beim Erreichen der k-ten Grenzspannung eine neue Grenzspannung zugewiesen, die nicht zwangsläufig höher ist als die Vorherige, aber aus einer gegebenen Wahrscheinlichkeitsdichtefunktion $P_k(d/d_c)$ stammt. d_c ist der typische Wert der Grenzspannung und erhöht sich abhängig von k wenn $d_c = d_o^k$ ist. Auf diese Weise wird bei jeder Umorientierung der Kraftlinie die Steifigkeit mit a und der effektive aber zufällige Grenzwert mit d_0 multipliziert. Die maximal mögliche Anzahl an Umstrukturierungen k_{max} ist proportional zur Anzahl der Kontakte, und damit zu H/l_0 (vgl. Abb. 1.2).

Ergänzend wurden einachsige Kompressionstests mit Glaskugeln durchgeführt. Das gemessene nichtlineare Last-Verschiebungsverhalten wird in Abb. 1.3 mit unseren Modellergebnissen verglichen.

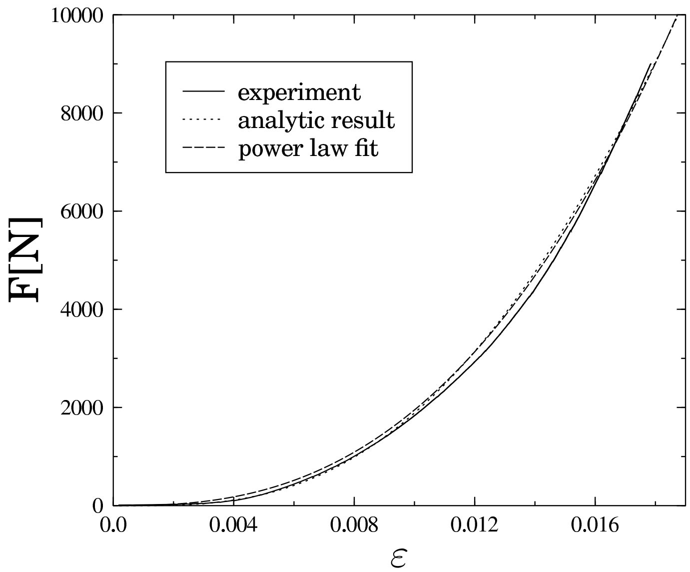

Figure 1.3: Vergleich von gemessenem und gerechnetem konstitutiven Verhalten

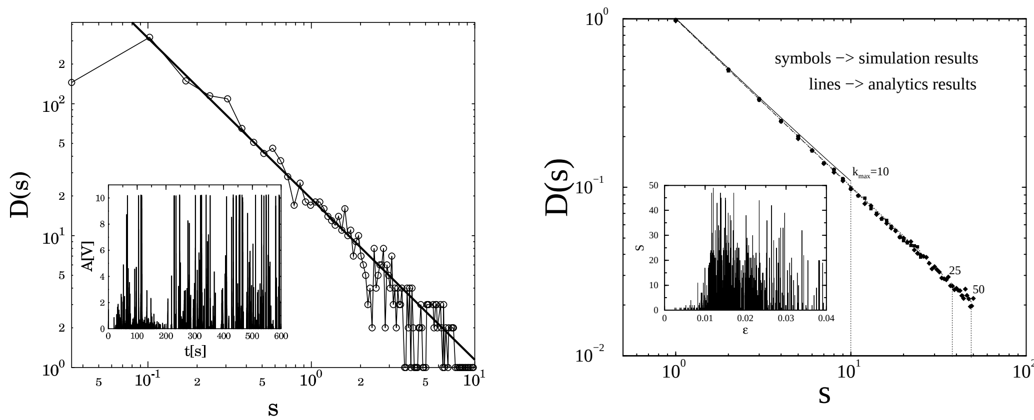

Figure 1.4: Lawinengröße s während der Belastung und ihre Größenverteilung $D(s)$.

Die Verteilung der Restrukturierungsereignisse wurde analytisch und numerisch in Abb. 1.4 verglichen. Dabei zeigt sich exzellente Übereinstimmung der Umlagerungsereignisse bei theoretischen und experimentellen Ergebnissen . Das gefundene Potenzgesetz, sowie die Werte des Exponenten und der analytischen und numerischen Lösung sind eine Konsequenz der Lokalität der Umstrukturierung aufgrund der Abwesenheit von Lastumlagerungen. Die gute Übereinstimmung weist darauf hin, dass sich dahinter der Mikromechanismus verbirgt, der für die Exponentialstatistik der akustischen Signale verantwortlich ist.

Faserbündelmodelle mit variablem Wechselwirkungsradius

Das Bruchverhalten heterogener Systeme ist charakterisiert durch stark lokalisierte Spannungskonzentrationen an der Rissspitze, die zur Bildung neuer Risse in dieser Region führen und somit zum Wachstum des Risses beitragen, der letztlich zum Systemversagen führen kann. In elastischen Materialien folgt die Spannungsumlagerung einem Potenzgesetz

$$\sigma_{add} \sim r^{-\gamma}, \tag{1.8}$$

das die Spannungsüberhöhung σ_{add} in einem Punkt im Abstand r von der Rissspitze beschreibt. Diese allgemeingültige Beziehung bezieht über den Wechselwirkungsparameter γ die Extremfälle globaler $(\gamma \to 0)$ sowie lokaler Lastumlagerung $(\gamma \to \infty)$ mit ein, die im FBM als Grenzwerte weit verbreitet sind.

Dieser allgemeine Zusammenhang aus der Bruchmechanik wurde als Lastumlagerungsgesetz in das klassische FBM eingesetzt. Ausgangspunkt bildet ein Bündel von N parallel angeordneten Fasern mit jeweils statistisch verteilter Faserfestigkeit gemäß der Wahrscheinlichkeitsverteilung $P(\sigma/\sigma_0)$, die mit dem Index i bei $1 \leq i \leq N$ versehen sind. Dabei findet die Weibullverteilung

$$P(\sigma) = 1 - e^{-\left(\frac{\sigma}{\sigma_o}\right)^{\rho}} \tag{1.9}$$

zur Repräsentation der Faserfestigkeit mit dem Formparameter ρ und dem Skalenparameter σ_0 Verwendung. Die Belastung des Systems erfolgt quasistatisch bis zum Versagen der ersten Faser i bei der Last $\sigma_i = \sigma_i^{krit}$. Die Umverteilung dieser Last auf intakte Fasern kann nun zum Versagen weiterer Fasern führen, deren Last wiederum auf die noch intakten Fasern umgelagert wird, und so fort. Dieser Prozess kann zu vollständigem Systemversagen oder aber zu einem Gleichgewichtszustand führen, bei dem die Last auf allen intakten Fasern geringer als deren individuelle Festigkeit ist. In diesem Fall wird die externe Last weiter erhöht, bis die geringste Festigkeit der zu diesem Zeitpunkt noch intakten Fasern erreicht ist. Dieser Prozess wird nun bis zum makroskopischen Systemversagen bei der makroskopischen Spannung σ_c wiederholt. Zwischen zwei aufeinanderfolgenden Lasterhöhungen bezeichnen wir die Anzahl gebrochener Fasern als Lawinengröße s und die Zahl der Lastumlagerungen als Lebenszeit T.

Wir nehmen weiter an, dass die Wahrscheinlichkeit aller intakten Fasern, von einem Schädigungsereignis unberührt zu bleiben, kleiner als eins ist, und die durch das Ereignis umgelagerte zusätzliche Last auf die Faser i von deren Abstand r_{ij} zu der zuletzt versagten Faser j bei (x_j, y_j) abhängt. Zwischen den einzelnen Fasern herrscht elastische Wechselwirkung in der Weise, dass die auf eine Faser aufgebrachte Last dem Potenzgesetz aus Gl.1.8 folgt. Die Spannungsumlagerungsfunktion $F(r_{ij}, \gamma)$ für unser diskretes

Modell ergibt sich damit zu

$$F(r_{ij}, d) = \frac{r_{ij}^{-\gamma}}{Z}, \text{ mit } Z = \sum_{i \in I} r_{ij}^{-\gamma}, \tag{1.10}$$

mit dem Normalisierungsterm Z, der aus der Summe über alle intakten Elemente I hervorgeht. Zusätzlich gelten periodische Randbedingungen, was zu einem maximal möglichen Abstand r_{max} von $(L-1)\sqrt{2}/2$ führt. Variationen des Wechselwirkungsparameters γ von stark lokalisierten bis gänzlich globalen $(\gamma \to 0)$ Wechselwirkungen beziehen grundsätzlich das gesamte System mit ein, weswegen wir fortan vom *effektiven* Wechselwirkungsradius als dem Radius eines Ereignisses reden, in dem die Wechselwirkung zu signifikanten Spannungserhöhungen führt.

Variable Wechselwirkung bei Holz unter Belastung in Faserrichtung

Reale Materialien wie Holz werden, abgesehen von wenigen Ausnahmen wie z.B. Faserbündeln ohne Matrix und Faserreibung, nicht durch die Extremfälle der globalen bzw. lokalen Lastumlagerung von versagten Materialzonen zu intakten charakterisiert. Vielmehr weist eine uni-direktionale Materialprobe bestehend aus N Fasern bei Belastung in Faserrichtung eine mit der charakteristischen Festigkeit der Fasern σ_0 normierte makroskopische Festigkeit $\sigma_c(N)/\sigma_0$ zwischen den Grenzen der globalen und lokalen Lastumlagerung auf. Mit dem in Kap. 1 beschriebenen FBM mit variablem, Lastwechselwirkungsparameter γ steht uns ein flexibles Modell zur Verfügung, dessen Parameter σ_0 und γ wir zur Beschreibung des natürlichen Faserverbundwerkstoffes Fichtenholz exemplarisch bestimmt haben.

In den Abb. (1.5,1.6) ist die Abhängigkeit der mittleren globalen Festigkeit des Faserbündels von der Systemgröße N für unterschiedliche Werte des Wechselwirkungsparameters γ dargestellt. Die numerischen Ergebnisse unserer Faserbündelmodelle bestätigen die analytischen Überlegungen von [1–4]. Auffällig ist, dass bei kleinen Werten von γ $(\gamma < 2.2)$ die Systemgröße unbedeutender wird, was im Einklang mit der Annahme globaler Lastumlagerung steht. Zunächst erfolgt eine Abschätzung der oberen und unteren Grenzen von σ_0 über die Extremfälle globaler und lokaler Lastumlagerung. Numerische Ergebnisse mit einer Weibullverteilung mit Formfaktor $\rho_s = 2$ sind in den Abb. (1.5,1.6) dargestellt. Der Fall globaler Lastumlagerung $(\gamma = 0)$ führt wegen der Unabhängigkeit von der Systemgröße in Abb. (1.6) auf die zur Abszisse parallele Linie $\sigma_c/\sigma_o = (\rho_s e)^{-1/\rho_s} = 0.429$. Diese Linie markiert die obere Grenze der Probenfestigkeit der Proben mit ca. $N = 5000$ Fasern. Mit der experimentell bestimmten Festigkeit erhält man dann die untere Grenze von $\sigma_0 = 322.8 MPa$. In identischer Weise wird mit dem zweiten Extremfall der lokalen Lastumlagerung $(\gamma = 9)$

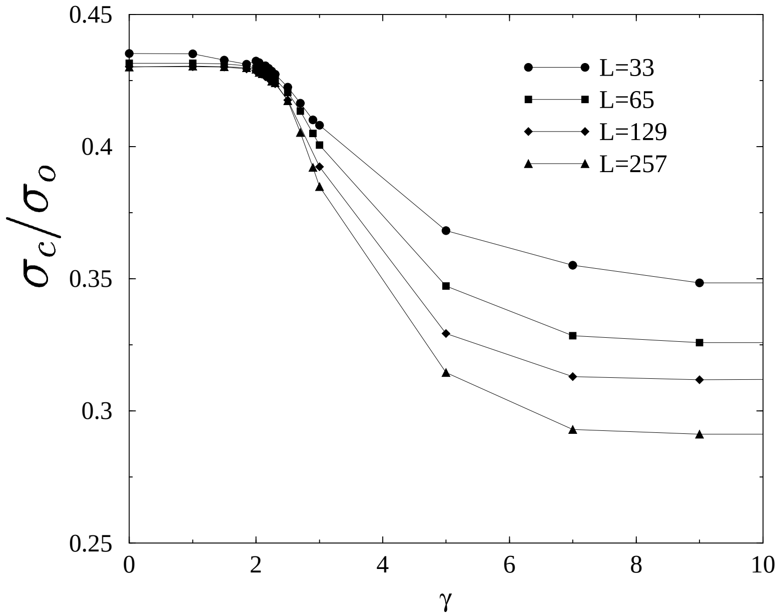

Figure 1.5: Numerische Abschätzung der Festigkeit des Faserbündelmaterials für unterschiedliche Systemgrößen L als Funktion des Wechselwirkungsparameters γ.

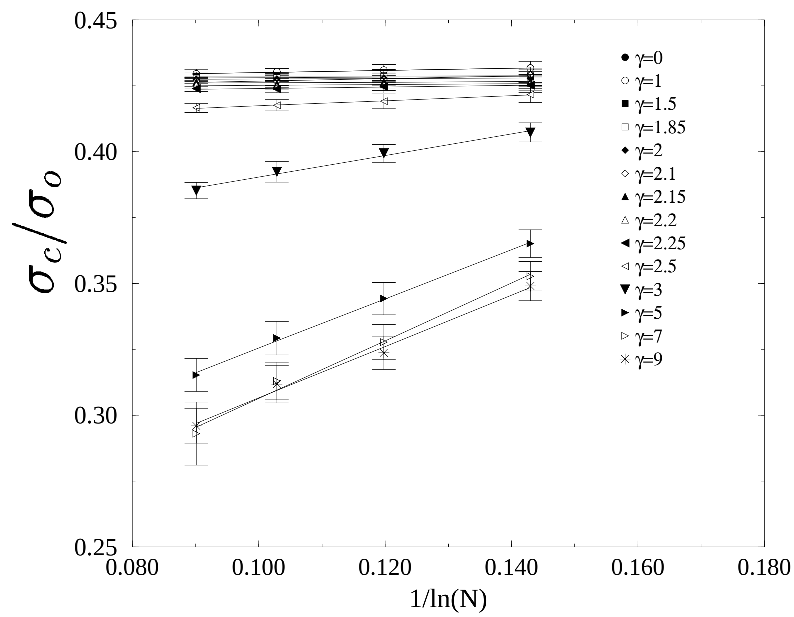

Figure 1.6: Festigkeit des Faserbündelmaterials für unterschiedliche Systemgrößen $N = L \times L$

verfahren. Die Linie $\sigma_c/\sigma_0 = 0.97(\log N)^{-1} + 0.21$ beschreibt die untere Grenze für Proben mit ca. $N = 50000$ Fasern, und damit den oberen Grenzwert $\sigma_0 = 426.5MPa$.

Auf diese Weise ist es möglich, aus experimentellen Ergebnissen über deren Festigkeit bei unterschiedlicher Systemgröße σ_0 der Einzelfasern, sowie über deren Lage in Abb. (1.6) den Wechselwirkungsparameter γ über die Steigung zu bestimmen. In Tab. 1.1 sind alle Ergebnisse zusammengefasst.

Die dargestellten Ergebnisse wurden für zwei Extremewerte des Weibull-Formparameters ρ_s errechnet, die von Thuvander u.a [8] verwendet wurden. Der invers für Fichtenholz bestimmte Wechselwirkungsparameter (vgl. Tab.1.1 und Abb.(1.6)) liegt bereits in einem Bereich, der durch rein lokale Lastumlagerung ausreichend gut beschrieben wird.

Weibull Formparameter	Weibull Skalenparameter $[MPa]$	Steigung	Wechselwirkungsparameter
$\rho_s = 1$	$384.7 < \sigma_o < 520.1$	$0.8 < \alpha < 1.1$	$6 < \gamma < 10$
$\rho_s = 2$	$322.8 < \sigma_o < 426.5$	$0.9 < \alpha < 1.3$	$5 < \gamma < 10$

Table 1.1: Aus Experimenten an unterschiedlich großen Fichtenholzproben bestimmte Modellparameter.

Faserbündelmodelle mit viskoelastischen Fasern und der langsamen Relaxation gebrochener Fasern

Unter hohen, konstanten Belastungen kann in Faserverbundwerkstoffen zeitabhängiges Kriechbruchversagen auftreten. Für die Anwendungen solcher Materialien ist die Kenntnis der Lebenszeit von hoher Bedeutung. Natürliche Faserverbundwerkstoffe wie Holz, aber auch eine Reihe anderer faserverstärkter Werkstoffe, wie z.B. Metall-Matrix-Composite (MMC) weisen Kriechbruchverhalten auf.

Zur theoretischen Beschreibung des Kriechbruchverhaltens viskoelastischer Faserverbundwerkstoffe gehen wir wieder von klassischen Faserbündelmodellen [9, 10] aus, die sehr viel zum Verständnis des Bruchverhaltens ungeordneter Materialien beigetragen haben. Unser Modell jedoch besteht aus einem Bündel von N parallel angeordneten einfachen Fasern mit viskoelastischem konstitutiven Verhalten. Diese bestehen jeweils aus einem Kelvin-Voigt Element, also aus einer einfachen Feder mit parallel angeordnetem Dämpfer, was zu der bekannten Beziehung

$$\sigma_\mathrm{o} = \beta\dot{\varepsilon} + E\varepsilon, \tag{1.11}$$

mit Dämpfungskoeffizient β und Elastizitätsmodul E der Einzelfaser führt. Eine Lösung der Differentialgleichung (Gl.1.11) liefert die zeitabhängige Deformation $\varepsilon(t)$ der Faser

$$\varepsilon(t) = \frac{\sigma_o}{E}\left[1 - e^{-Et/\beta}\right] + \varepsilon_o e^{-Et/\beta}, \tag{1.12}$$

bei gegebener, externer Spannung σ_0 und der Anfangsdehnung ε_0 zum Zeitpunkt $t = 0$. Für $t \to \infty$ konvergiert $\varepsilon(t)$ gegen σ_0/E, dem Hookschen Gesetz.

Bei Abwesenheit von Faserversagen wäre Gl.(1.12) zur Beschreibung der zeitlichen Entwicklung ausreichend. Motiviert von akustischen Emissionsmessungen an kriechenden Faserverbundwerkstoffen [11] führen wir ein Bruchkriterium für Einzelfasern ein, das erfüllt ist, sobald die Faserdehnung ihren Bruchdehnung ε_d erreicht. Diese ist eine zufällige Variable der individuellen Faser mit der Wahrscheinlichkeitsdichtefunktion $P(\varepsilon_d) = \int_0^{\varepsilon_d} p(x)dx$. Aufgrund der Gültigkeit des Hookschen Gesetzes für asymptotische Dehnungswerte bedeutet die Verwendung eines Dehnungskriteriums anstelle eines Spannungskriteriums für das Faserversagen, dass bei konstanter Last die selben Schädigungen auftreten, wie mit Spannungskriterien, nur dass Faserbrüche nicht unmittelbar auftreten, sondern über die Zeit verteilt sind.

Bei Faserversagen muss wiederum die ursprünglich von der Faser getragene Last auf intakte Fasern umgelagert werden. Als einfachster Fall wird zunächst die globale Umlagerung der Last [1–4] zu gleichen Teilen auf alle bei der Dehnung ε intakten Fasern $N_s(\varepsilon)$ untersucht, was auf die Faserlast

$$\sigma(\varepsilon) = \sigma_0 N/N_s(\varepsilon) = \sigma_0/(1 - P(\varepsilon)) \tag{1.13}$$

führt. Die zeitliche Entwicklung des Systems unter konstanter externer Belastung σ_0 lautet somit

$$\frac{\sigma_0}{1 - P(\varepsilon)} = \beta\dot{\varepsilon} + E\varepsilon, \tag{1.14}$$

und verknüpft viskoelastisches Materialverhalten mit stochastischem Faserversagen im Kontext globaler Lastumlagerung. Die Lösung von Gl.(1.14) führt auf zwei Bereiche in Abhängigkeit der externen Last σ_0: unterhalb eines kritischen Wertes σ_c führt Gl.(1.14) bei $\dot{\varepsilon} = 0$ auf die stationäre Lösung ε_s mit

$$\sigma_0 = E\varepsilon_s[1 - P(\varepsilon_s)]. \tag{1.15}$$

Solange diese Beziehung gilt, konvergiert für eine gegebene makroskopische Last σ_0 die Lösung für $\varepsilon(t)$ bei $(t \to \infty)$, und es kommt nicht zu makroskopischem Versagen. Übersteigt σ_0 jedoch σ_c, existiert keine stationäre Lösung, und $\dot{\varepsilon} > 0$. Das System versagt in diesem Fall global zum Zeitpunkt $t_f(\sigma_0)$.

Wir konnten mit unseren Modellen zeigen, dass für Kriechbruchversagen eine kritische Last σ_c existiert, die den Versagensverlauf vorherbestimmt. Unterhalb dieser Last $\sigma_o \leq$

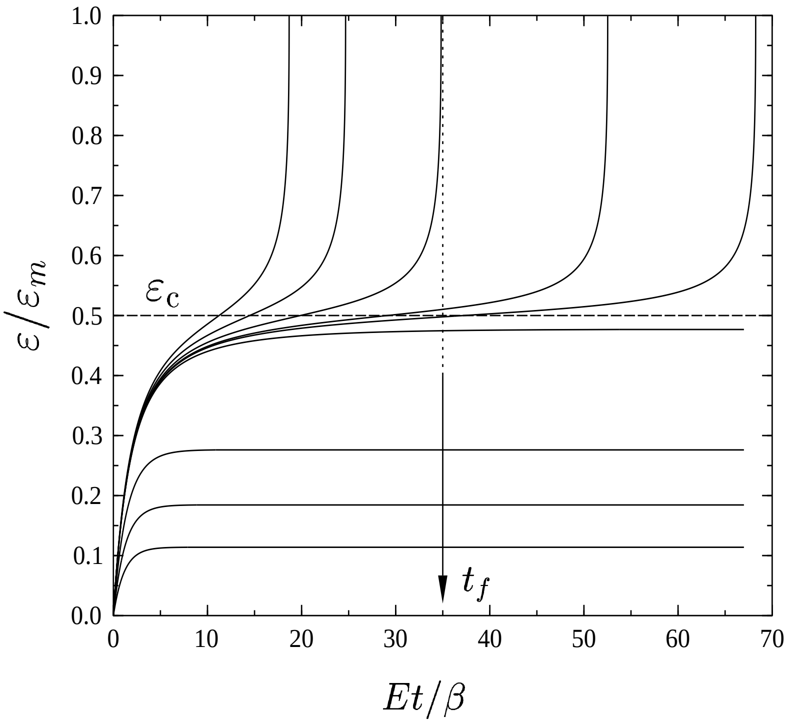

Figure 1.7: Analytische Lösungen $\varepsilon(t)$ für unterschiedliche Werte von σ_o oberhalb und unterhalb σ_c. Die kritische Dehnung ε_c ist beispielhaft für einen Wert mit seiner entsprechenden Versagenszeit t_f eingezeichnet.

σ_c wird die Lebenszeit t_f unendlich, während bei Lasten $\sigma_o > \sigma_c$ globales Versagen bei der endlichen Zeit t_f eintritt. Folglich konvergiert das Faserbündel bei abnehmender Schädigungsaktivität und bei Lasten $\sigma_o \leq \sigma_c$ gegen die stationäre Verformung ε_s (vgl. Abb. (1.7)). Die charakteristische Zeitskala dieses Prozesses τ hängt gemäß

$$\tau \sim (\sigma_c - \sigma_o)^{-1/2}, \qquad \text{für} \qquad \sigma_o < \sigma_c \tag{1.16}$$

vom Abstand zur kritischen Last ab. Interessant an diesem Ergebnis ist, dass, wenn man sich dem kritischen Punkt von unten (vgl. Abb.(1.7)) nähert, die Relaxationszeit gemäß dem universellen Potenzgesetz Gl. (1.16) mit Exponenten $-1/2$ divergiert, unabhängig von der Form der Unordnungsverteilung $P(\varepsilon)$.

Aus theoretischer und experimenteller Sicht ist es wichtig, die Abhängigkeit der Versagenszeit t_f von der aufgebrachten Last σ_o vorhersagen zu können. Analytisch konnten wir für globale Lastumlagerung beweisen dass die Beziehung

$$t_f \sim (\sigma_o - \sigma_c)^{-1/2}, \qquad \text{mit} \qquad \sigma_o > \sigma_c \tag{1.17}$$

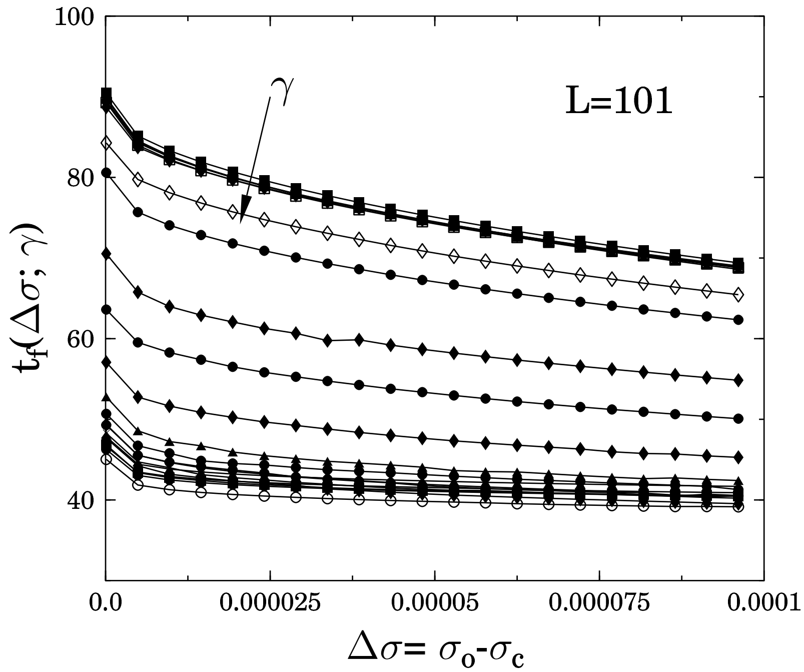

Figure 1.8: Versagenszeit t_f als Funktion von $\sigma_o - \sigma_c$ für den Wechselwirkungsparameter $0 \leq \gamma \leq 7$.

gilt. Die Versagenszeit t_f divergiert folglich ebenfalls nach einem Potenzgesetz mit identischem Exponenten und ist ebenfalls unabhängig von $P(\varepsilon)$.

Um die Auswirkungen der Lastumlagerungsstategien auf das Kriechbruchverhalten zu verstehen, haben wir untersucht, wie sich das Systemverhalten in der Umgebung des kritischen Punktes verändert, wenn die Lastumlagerung gänzlich lokal wird. Zu diesem Zweck wurden Simulationen unter Variation des effektiven Wechselwirkungsradius über den Lastumlagerungsparameter γ der Lastumlagerungsfunktion durchgeführt (vgl. Kap. 1, 1).

Das Diagramm in Abb. 1.8 zeigt die Lebenszeit t_f eines Faserbündels, dessen Fasern auf einem Quadratgitter der Kantenlänge $L = 101$ als Funktion des Abstandes vom kritischen Punkt $\Delta\sigma = \sigma_o - \sigma_c$ für unterschiedliche Wechselwirkungsparameter γ angeordnet sind. Die $t_f(\Delta\sigma;\gamma)$ Kurven formen dabei zwei Gruppen unterschiedlicher Form: eine obere Gruppe für $0 \leq \gamma \leq 1.95$, die globale Lastumlagerung beschreibt, sowie eine untere Gruppe für $\gamma > 2.9$ für lokale Lastumlagerung. Hier konvergiert $t_f(\Delta\sigma;\gamma)$ bei Erreichen der kritischen Last σ_0 rasch gegen einen konstanten Wert mit schwachem Skaleneffekt, was an einen Phasenübergang erster Ordnung erinnert. Unsere Ergebnisse deuten auf die Existenz zweier Universalitätsklassen für Kriechbruchversagen hin: vollständig globales bzw. vollständig lokales Verhalten, abhängig von dem Wech-

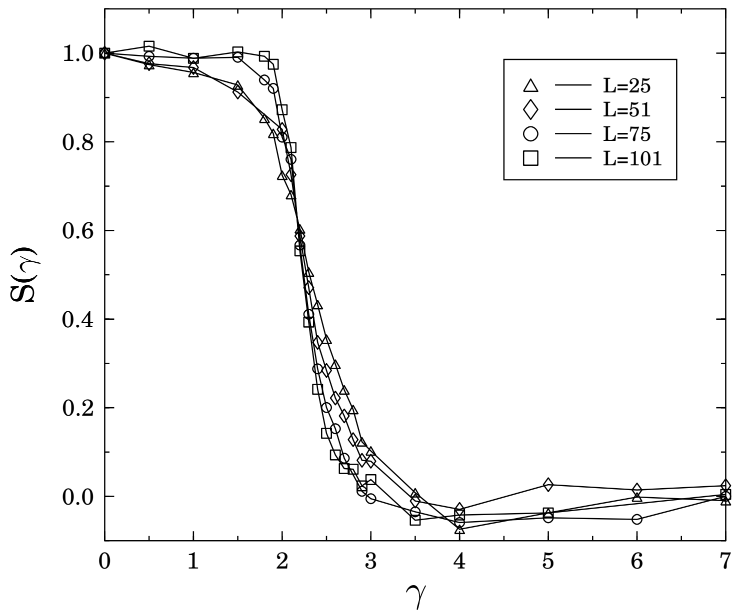

Figure 1.9: Systemgrößenabhängigkeit als Funktion von $\sigma_o - \sigma_c$ für den Wechselwirkungsparameter $0 \leq \gamma \leq 7$.

selwirkungsparameter γ mit einem scharfem Übergang. Wir führen die normierte Größe $S(\gamma) = [t_f(\gamma) - t_f(\gamma = 10)] \, / \, [t_f(\gamma = 0) - t_f(\gamma = 10)]$ ein, bei der $t_f(\gamma)$ den Wert von t_f bei kleinstem $\Delta\sigma$ zur Berechnung von $t_f(\Delta\sigma; \gamma)$ bei gegebenem γ bedeutet. Durch diese Darstellung nimmt $S(\gamma)$ bei rein lokaler Lastumlagerung den Wert 0 und 1. Auch in dieser Darstellung zeigt sich der scharfe Übergang zwischen globaler und lokaler Lastumlagerung bei einem Wert $\gamma_c \approx 2$. Mit wachsender Systemgröße wird dieser Übergang noch schärfer. Die Existenz zweier Universalitätsklassen bedeutet unter anderem, dass Ergebnisse der globalen Lastumlagerung auch jenseits $\gamma = 0$ Gültigkeit haben.

Analytische und numerische Berechnungen haben gezeigt, daß auch während der langasamen Relaxation gebrochener Fasern ein Übergang aus einem teilweise versagten Zustand unendlicher Lebenzeit in einen Zustand, in dem sich ein globales Versagen mit einer endlichen Zeit ergibt stattfindet. So divergiert die makroskopische Versagenszeit in der Nähe des kritischen Belastungswertes σ_c, gemäss der Potenzfunktion.

$$t_f \sim (\sigma_c - \sigma_\mathrm{o})^{-(m-\frac{1}{2})}, \qquad \text{für} \qquad \sigma_\mathrm{o} < \sigma_\mathrm{c} \tag{1.18}$$

Der kritische Exponent ist unabhängig von der kumulativen Festigkeitsverteilung, welche von der Natur des Relaxationprozesses abhängt ($(\beta\dot{\varepsilon})^m$ Nichtlinearität). Die Existenz von zwei Universalitätsklassen beim Kriechbruch von Faserverbundwerkstoffen wurde durch diese Ergebnisse bestätigt. Reale Materialien mit spezifischen Werten von γ fallen folglich in eine der Universalitätsklassen, weshalb wir in Experimenten entweder einen kontinuierlichen Phasenübergang mit Skaleneffekten oder sehr abruptes Versagen beobachten.

Chapter 2

Introduction

A composite material or composite is a complex solid material composed of two or more constituents. On macroscopic scale, they have structural or functional properties not present in any individual component and generally they are designed to exhibit the best properties or qualities of its constituents.

Nature has provided composite materials in biomatter such as seaweed, wood, and human bone and there are several artificial structures as reinforced concrete, fiber-reinforced composites and so on. Surprisingly, they are not new in common life, even the ancient Egyptians made plywood and the Romans had concrete.

Nowadays, the new carbon-fiber composites weigh about five times less than steel, but can be comparable or better in terms of stiffness and strength, depending on fiber orientation. These composites do not rust or corrode like steel or aluminum. Perhaps most important, the automobile industry could reduce vehicle weight by as much as 60%, significantly saving vehicle fuel.

A fiber-reinforced composite is a system made of fibers embedded in a protective material called a matrix, with a coupling agent applied to the fiber to improve the adhesion of the fiber to the matrix material. The functions of a matrix, whether organic, ceramic, or metallic, are to support and protect the fibers, and to provide a means of distributing the load among and transmitting it between the fibers without itself fracturing.

The tensile failure of fiber composites is generally dominated by failure of the fiber bundles. If an uniaxial load is applied in the direction parallel to the fibers the actual composite stress σ_T can be obtained as $\sigma_T = \sigma_f V_f + (1 - V_f)\sigma_m$, where V_f denotes the fiber volume fraction, σ_f is the mean stress carried by the fibers and σ_m is the usually small stress carried by the matrix. The matrix can carry some load in a metal or polymer matrix composite but, after matrix cracking, carries almost zero load in ceramic matrix composites. So that, the matrix stress σ_m can normally be neglected in damage modeling since already at relatively low load levels, the matrix gets multiply cracked or yields plastically limiting its load bearing capacity. However, stress transfers between the fibers by the matrix action continues despite gradual damage, therefore, it has a very important role in the load redistribution. In reconstituted artificial construction materials the range of load redistribution also called load sharing can be controlled by varying the properties of the matrix material and the fiber-matrix interface.

To understand the failure of composites one has to concentrate on the breaking of the fibers. Hence, in fiber composites the two factors controlling fiber failure are

- the statistical fiber strength
- the stress re-distribution (load sharing) after the fiber fails.

The stress along the fiber depends on the applied external stress, but also on precisely how stress is transferred from a broken fiber to the surrounding intact fibers and in the matrix environment. This stress transfer is governed by the elastic properties of the constituents and by the fiber/matrix interface, and is difficult to obtain in the presence of more than one broken fiber.

For a realistic modeling of the damage process of fiber composites under an uniaxial load, the stress distribution would have to be calculated in the whole volume of the sample. Even limiting the number of independent variables needed to describe the internal microstructure of the specimen, an accurate prediction of the ultimate strength is a computationally demanding task. Hence, in general, the modeling of fiber composites is based on certain idealizations about the geometry of the fiber arrangement and the stress redistribution following fiber failures in the specimen. Moreover , in order to obtain reliable conclusions the number of fibers forming the system has to be very large which makes the numerical problem, in many cases, too time consuming as to perform the study in a reasonable amount of time.

Thus, a lot of effort has been spent on analytical approaches and more simple numerical models which may also provide a solid ground. One of those models, the fiber bundle model, received a lot of attention because severals important quantities can be derivated analytically in their frameworks, furthermore, efficient simulation techniques can be developed which allow for the study of large samples. Despite their simplicity, they capture most of the main aspects of material damage and breakdown. They have provided a deeper understanding of fracture processes and have served as a starting point for more complex models of fiber reinforced composites and other micro-mechanical models

2.1 Overview

Firstly, in Chapter 3 we describe the general physics involved in the fiber reinforced composites modeling, when the specimens are loaded parallel to the fiber direction. The principal concepts, such as fiber bundle, load sharing, disorder distribution, creep rupture are briefly treated. In Chapter 4 we study the constitutive behavior, the damage process, and the properties of bursts in the continuous damage fiber bundle model introduced recently. This model provides various types of constitutive behaviors including also macroscopic plasticity. Furthermore, for stress controlled experiments we develop a simulation technique and explore numerically the distribution of bursts of fiber breaks assuming infinite range of interaction. Based on the analogy of force chains in granular packings and fibers in fiber reinforced composites, we propose a novel theoretical approach in Chapter 5 to describe the gradual emergence and hardening of force chains occurring under uniaxial compression. In parallel, the restructuring events that take place during the compression of a granular media were accessed experimentally. A fiber bundle model where the interaction among fibers is modeled by an adjustable stress-transfer function which can interpolate between the two limiting cases of load redistribution, the global and the local load sharing schemes are introduced in Chapter 6. By varying the range of interaction several features of the model are numerically studied. In Chapter 7 the size effect of tension strength of softwood loaded parallel to fiber direction has been numerically and experimentally studied. It was revealed that the average strength is a decreasing function of the cross-sectional specimen size. For qualitative characterization of the load sharing it has been assumed that the load-transfer function has a power law form (described in Chapter 7). A novel method to deal with the real time dependence in the breakdown process of the fiber materials is presented in Chapter 8 and 9. In Chapter 8 we develop a fiber bundle model whose fibers have viscoelastic behavior and the macroscopic damage mechanism leading to creep rupture is the strain dependent breaking of the fibers during the time evolution of the deformation of the system. On the other hand, in Chapter 9 the slow relaxation of a fiber composite was studied. In this case, the components of the solid are linearly elastic until they break, however, after breaking they undergo a slow relaxation process.

Chapter 3

Basics

3.1 Fracture of heterogeneous materials

Fracture processes have attracted the attention of the scientific community since many years. Processes involving heterogeneous systems, for which a definite and complete physical description has not been found despite the many partial successes of the last decades, are of special theoretical and practical interest [12, 13]. In particular, the latest developments of statistical mechanics have led to a deeper understanding of breakdown phenomena in heterogeneous systems, but some fundamental questions remain unsolved. The difficulties arise because in modeling fracture of heterogeneous materials, one has to deal with systems formed by many interacting constituents, each one having different statistical properties related to some breaking characteristics of the material, distributed randomly in space and/or time [12, 13].

Under applied external stress the solid materials elongate and get strained. The constitutive behavior *i.e.*, the stress σ and strain ε relation generally is linear for small stresses. After reaching the elastic limit, the weakest parts of the sample, *i.e.* defect, dislocation, pores, and so on, tend to get destabilized and microscopic internal failure is noted. Those weakest parts are often called nucleation centers, due to the cracks evolve around them, so that they play a mayor role in the breakdown properties. In that way, the internal structure of the sample becomes damaged and the nonlinearity appears in the constitutive behavior. Finally at a critical stress value σ_c, depending on the material, the amount of disorder and the specimen size, the solid breaks in two or more pieces, so that the macroscopic fracture occurs [12, 13].

The major challenge in dealing with fracture problems is to combine the statistical evolution of damage across the entire macroscopic system and the associated stress redistribution to accurately predict the point of final rupture of the material. In doing this linkage, one has to take care not to make too strong simplifications particularly in the redistribution rule, where a great deal of the physics of the problem is hidden. The complete analytical solution is in almost all cases impossible and one has to solve the problem by means of numerical simulations or to study simplified models which are analytically tractable (at least in some limits) in order to gain physical insight that guide our understanding.

Models, which computer simulations are based on, can be classified as lattice models and fiber bundle models. In lattice models the elastic medium is represented by a spring network, and disorder is captured either by random dilution or by assigning random failure thresholds to the bonds [12]. The failure rule usually applied in lattice models is discontinuous and irreversible: when the local load exceeds the failure threshold of a bond, the bond is removed from the calculations (*i.e.* its elastic modulus is set to zero). This kind of models are relevant for brittle fracture of disordered solid, laminar composites, polymers and so on, and they are a powerful tools to study the geometrical and topological properties of those systems. The fiber bundle models are the main topic of the present thesis and their properties are thoroughly described in the next sections.

3.2 Extreme statistics

The fracture or breakdown of a solid sample is always determined essentially by the extreme statistics of the most dangerous weakest defect cluster or crack within the sample volume. The general features of this extreme statistics are discussed below.

A solid of linear size L, containing n cracks within its volume is assumed. Each of these cracks has a probability $f_i(\sigma)$, $(i = 1, 2...n)$ to fail independently under an applied stress σ, as long as the perturbed or stress-released regions of each of these cracks are separate and do not overlap. Denoting the cumulative failure probability of the entire sample, under stress σ by $P(\sigma)$, the probability that the specimen does not fail under the stress σ, *i. e.* $1 - P(\sigma)$ can be written as [13]

$$1 - P(\sigma) = \prod_{i=1}^{n}(1 - f_i(\sigma)), \tag{3.1}$$

which can be approximated by

$$\prod_{i=1}^{n}(1 - f_i(\sigma)) \approx e^{-\sum_{i=1}^{n} f_i(\sigma)} \tag{3.2}$$

and finally gives

$$P(\sigma) = 1 - e^{-L^d g(\sigma)}, \tag{3.3}$$

where $g(\sigma)$ denotes the density of cracks within the sample volume L^d (coming from the sum $\sum_i$ over the entire volume), which starts propagating at and above the stress level σ. The above equation arises from the fact that the sample survives if each of the cracks within the sample survives. This is the essential origin of the extreme statistical nature of the failure probability (cumulative distribution) $P(\sigma)$ [13].

In material science, the Weibull distribution has been proved to be a good empirical statistical distribution to represent solid strength [8, 14–16],

$$P(\sigma) = 1 - e^{-\left(\frac{\sigma}{\sigma_o^b}\right)^\rho}, \tag{3.4}$$

where ρ is the so-called Weibull disorder parameter, which controls the degree of threshold disorder in the system (the bigger the Weibull index, the narrower the range of threshold values), and σ_o^b is a reference load which acts as stress unity. This cumulative distribution comes from the generally accepted assumption that the density of cracks is related to the external stress σ by a power law

$$g(\sigma) = \left(\frac{\sigma}{\sigma_o^b}\right)^\rho. \tag{3.5}$$

The Weibull distribution is one of the classical extreme value distributions. Only Weibull and Gumbel distributions

$$P(\sigma) = 1 - e^{-\frac{l}{lo}e^{\left(\frac{\sigma}{\sigma_o^b}\right)^\rho}} \tag{3.6}$$

are reasonable to describe the tensile strength of disordered materials. [8, 14–16]

3.3 Fiber bundle models

Fiber Bundle Models (FBM) form a fundamental class of approaches to the fracture problem. They are in close connection with Daniels' and Coleman's seminal works on the strength of bundles of textile fibers [9, 10] and have harbored an intense research activity in recent years[1–4, 17–50]. FBM's are important, despite their very simple nature, because they exhibit most of the essential aspects of material breakdown. In addition, they provide a deep understanding of fracture processes which has served as a starting point for more complex models [7, 28, 35, 51–55]. Generally, FBM's simulate the failure of materials by quasistatic loading, *i.e.*, by very slow steady increase in the load up to the macroscopic failure. One of the basis outputs is precisely the value of the ultimate strength. They are constructed so that a set of fibers is arranged in parallel each one having a statistically distributed strength. The most common cumulative distribution functions, used to express the breaking properties of individual elements are the Weibull Eq. 3.4 and the Gumbel distribution Eq. 3.6.

The FBM's are generally used to model specimens loaded parallel to the fiber direction, the fibers break if the load acting on them exceeds their threshold value. Once the fibers begin to fail one can choose among several load transfer rules, usually also called type of load sharing. There are two standard types of load sharing comprising the FBM and they correspond to the extreme limits of stress redistribution. In global load sharing (GLS) approach, the load of a failed fiber is equally redistributed among the active fibers remaining in the system. On the other hand, in local load sharing (LLS) the load of a failed fiber is redistributed among the intact fibers that are nearest neighbors to the failed ones. This assumes short-range interaction among the fibers and it can not, in general, be solved analytically. Moreover, some variable range of interaction models have been developed during the last ten years [7, 28, 53–55].

In fiber-reinforced composites, due to the fiber-matrix interaction a well defined symmetric stress profile $\Delta\sigma(x)$ is established in the neighborhood of the breaking points. The variable x is the distance from the break point, in the direction parallel to the fiber. This aspect has also been addressed using FBM's [35, 51, 52]. Hence, the stress $\Delta\sigma(x)$ on a given broken element of the bundle depends on the chosen cross section. The $\Delta\sigma(x)$ decreases asymptotically to zero and at a critical distance l_o from the breaking point, the stress on the broken fiber can be neglected. In the framework of the FBM's, the mean value of the stress carried by the broken elements has also been analytically deduced [35].

On the other hand, there are fiber-reinforced composites in which the microscopic damage mechanism is gradual [56, 57]. For this kind of materials a fiber bundle model with a continuous damage evolution has been recently introduced [58].

3.3.1 FBM, global load sharing approach

As it was already mentioned, the simplest case of load transfer from broken to unbroken fibers is to assume global load sharing (GLS) which means that after each fiber failure, the load of the broken fiber is equally redistributed among all the intact remaining fibers. This model, known as global fiber bundle model, is a mean field approximation where long range interactions among the elements of the system are assumed and can be solved analytically [1–4, 19, 20]. The failure process is completely random and the clusters of broken fibers formed during the evolution of the fracture process in global load sharing do not have any spatial structure since this case corresponds to the mean field approach.

GLS models have been used to predict the failure under tension in elastic yarns and cables with no twist, since in these arrangements the load supported by a failing fiber or cable is shared equally by all the remaining elements in the bundle. The existence of a loose arrangement and a tension load (for some boundary conditions) facilitates this global redistribution of load.

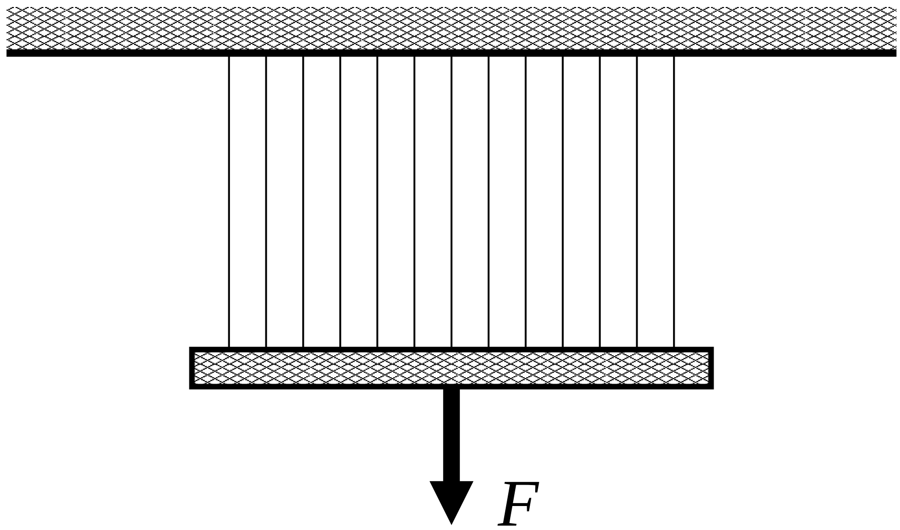

Figure 3.1: A bundle of N fibers stretched between two rigid supports with a load F

Some thermodynamics ideas

Very recently Pride et al [4] have developed a novel and interesting thermodynamics theory which easily explains the main physical aspect of the global load sharing approach.

The model is shown in Fig. 3.1. A collection of N_o fibers are stretched between two rigid supports.One support is held fixed, while the other is free to move. A load F is applied to the bundle through the free support so that the fibers are in a state of tension. Usually, the load F is normalized by N to define the overall tension stress $\sigma = \frac{F}{N_o}$. Each non-broken fiber in a bundle has the same length L. When $\sigma = 0$, this length is l_o, then the measure of strain is $\varepsilon = \frac{l-l_o}{l_o}$. Experiments may be performed on the bundle either by controlling the stress σ or the strain ε.

Each of the fibers has the same Young's modulus which is taken to be unity ($E = 1$) so that the axial strain ε of each fiber is identical to the tension in the fiber. The N_o fibers have strengths ε_1, ε_2,...ε_{N_o} which are independent random variables sampled from a distribution $p(\varepsilon)$, whose cumulative distribution is defined as $P(\varepsilon) = \int_0^\varepsilon p(x)dx$. As the strain ε of the bundle is increased, the individual fibers will break once their tension (strain) gets to their fixed strength threshold. All of this defines the fiber bundle model with global load sharing. Of interest are the mechanical properties of such bundles as averaged over all possible realizations of fiber strengths. The first needed magnitude is the probability p_j of observing one of the realizations to be in a particular state j of damage when the ensemble as a whole is at an applied strain ε. In the fiber bundle model, a damage state j is defined by which of the N fibers are broken. One could define j using a local order parameter that is 1 if a fiber is intact and 0 if the fiber is broken.

This theory postulates that the fraction p_j of all realizations observed to be in state j is obtained by maximizing Shannon's measure of disorder

$$S = -\sum_j p_j \ln p_j \tag{3.7}$$

subject to constraints. Such constraints must involve the independent variables of S. To identify the independent variables, we consider how the average energy in the ensemble of bundles changes as the strain is increased.

When ε increases to $\varepsilon + d\varepsilon$, there is both a work carried out in reversible stretching the fibers and an additional work carried out due to irreversible fiber breaks. Due to breaking, some of the members of the ensemble (individual realizations of the disorder) will be led out of their current damage state and into state j, while others that were in state j will transfer to still different states. If there is a difference in the number of members entering and leaving state j, there will be a change dp_j in the occupation probability of state j and such changes are what cause Shannon's disorder measure S to change.

The average energy density (average energy normalized by N) in the ensemble is given by $U = \sum_j p_j E_j$. Here, E_j is the energy density required to create state j at imposed strain ε and averaged over all members that have been led to state j. Depending on the breaking strengths of a given realization, the work performed in arriving at state j can be different. It is through E_j that all dependence on the quenched-disorder distribution enters the problem. The change of intern energy that occurs when ε increases to $\varepsilon + d\varepsilon$ is

$$dU = \sum_j E_j dp_j + \sum_j p_j dE_j. \tag{3.8}$$

The first term is the free energy expended in changing the disorder over the collection of realizations. It is thus proportional to the disorder change and can be written

$$TdS = \sum_j E_j dp_j. \tag{3.9}$$

The second term is written

$$f\, d\varepsilon = \sum_j p_j dE_j. \tag{3.10}$$

and represents both the reversible stretching energy in those members that did not experience breaks during the deformation increment, as well as the irreversible energy changes due to all the breaks that did not result in a net change in the occupation numbers of each state.

From these expressions it may be concluded that if U is to be treated as a fundamental function, then $U = U(S, \varepsilon)$, or equivalently if S is to be treated as the fundamental function then $S = S(U, \varepsilon)$. In other words, the independent variables that must be involved in the constraints on the maximization of S are U and ε. The proportionality constants T and f are defined

$$T = \left(\frac{\partial U}{\partial S}\right)_\varepsilon \text{ and } f = \left(\frac{\partial U}{\partial \varepsilon}\right)_S. \tag{3.11}$$

The state function f is something different than the overall tension σ since we also have that $\sigma\, d\varepsilon = dU$. Thus, in general, $(\sigma_o - f)d\varepsilon = TdS$ so that $f \neq \sigma_o$ due to fibers breaking in a positive increment $d\varepsilon$. If strain were to be decreased, fibers do not break and so $dS = 0$ and the state function f would be defined using only the purely elastic part of the energy changes dE_j. Changes in f in this case are equivalent to changes in σ.

The constraint involving ε is that each non-broken fiber throughout the entire ensemble has the same length which implies $\varepsilon_j = \varepsilon$. The constraint involving U is that

$$U = \sum_j p_j E_j. \tag{3.12}$$

Carrying out the maximization of S subject to these constraints using Lagrangian multipliers gives the probability distribution as

$$p_j(\beta, \varepsilon) = \frac{e^{-\beta E_j(\varepsilon)}}{Z(\beta, \varepsilon)} \tag{3.13}$$

where $\beta = 1/T$ and where the partition function Z is defined

$$Z(\beta, \varepsilon) = \sum_j e^{-\beta E_j(\varepsilon)}. \tag{3.14}$$

The average work density (Hamiltonian) required to create the state j (with n_j broken fibers) averaged over all realizations of the quenched disorder is then in general

$$E_j = \left(1 - \frac{n_j}{N}\right)\frac{\varepsilon^2}{2} + \frac{1}{P(\varepsilon)}\int_0^\varepsilon \frac{x^2}{2}p(x)dx \tag{3.15}$$

where the first term denotes the potential energy accumulated in the system, the second the average energy that is lost when each fiber breaks. and $P(\varepsilon) = \int_0^\varepsilon p(x)dx$

For example, under the special assumption that the breaking strengths are randomly sampled from a uniform distribution in the interval $0 \leq \varepsilon_m \leq 1$, we have that $p(\varepsilon) = 1$, $P(\varepsilon) = \varepsilon$,

$$E_j = \varepsilon^2/2 - (n_j/N)\varepsilon^2/3. \tag{3.16}$$

Nevertheless, the following analysis is valid for any properly normalized quenched-disorder distribution $p(\varepsilon)$.

There are two key average properties upon which all the thermodynamic functions depend; namely, the average fraction of broken fibers in each bundle $\langle n_j/N\rangle$ and the average of this fraction squared $\langle (n_j/N)^2\rangle$. Using the exact probability of Eq. (3.13) one obtains

$$\left\langle \frac{n_j}{N} \right\rangle = \sum_j p_j \frac{n_j}{N} = P(\varepsilon), \tag{3.17}$$

which is a known result consistent with the meaning of $P(\varepsilon)$. For $\langle (n_j/N)^2\rangle$ results

$$\left\langle \left(\frac{n_j}{N}\right)^2 \right\rangle = P(\varepsilon)^2 + \frac{P(\varepsilon)(1-P(\varepsilon))}{N}. \tag{3.18}$$

Using these two results, the other averages defining the thermodynamic variables are easily read off.

The average stress $\sigma(\varepsilon)$ is thus obtained to be

$$\sigma(\varepsilon) = \sum_j p_j \sigma_j \tag{3.19}$$

which gives

$$\sigma(\varepsilon) = (1 - P(\varepsilon))\varepsilon, \tag{3.20}$$

where $P(\varepsilon)$ and $1 - P(\varepsilon)$ are the fraction of failed N_f and intact fibers N_s, respectively. This constitutive behavior is shown in figure 3.2 for different thresholds cumulative distributions.

The global strength σ_c of the sample can be obtained from the maximization of Eq. (3.20)

$$\frac{d\sigma(\varepsilon)}{d\varepsilon} = 1 - P(\varepsilon) - \varepsilon \frac{dP(\varepsilon)}{d\varepsilon} \tag{3.21}$$

Then using the extreme necessary condition

$$\frac{d\sigma(\varepsilon)}{d\varepsilon} = 0 \tag{3.22}$$

we obtain

$$1 - P(\varepsilon_c) - \varepsilon \frac{dP(\varepsilon_c)}{d\varepsilon} = 0 \tag{3.23}$$

For an uniform cumulative distribution $P(\varepsilon) = \frac{\varepsilon}{\varepsilon_o}$ the relation (3.23) is valid for

$$\varepsilon_c = \frac{\varepsilon_o}{2}, \tag{3.24}$$

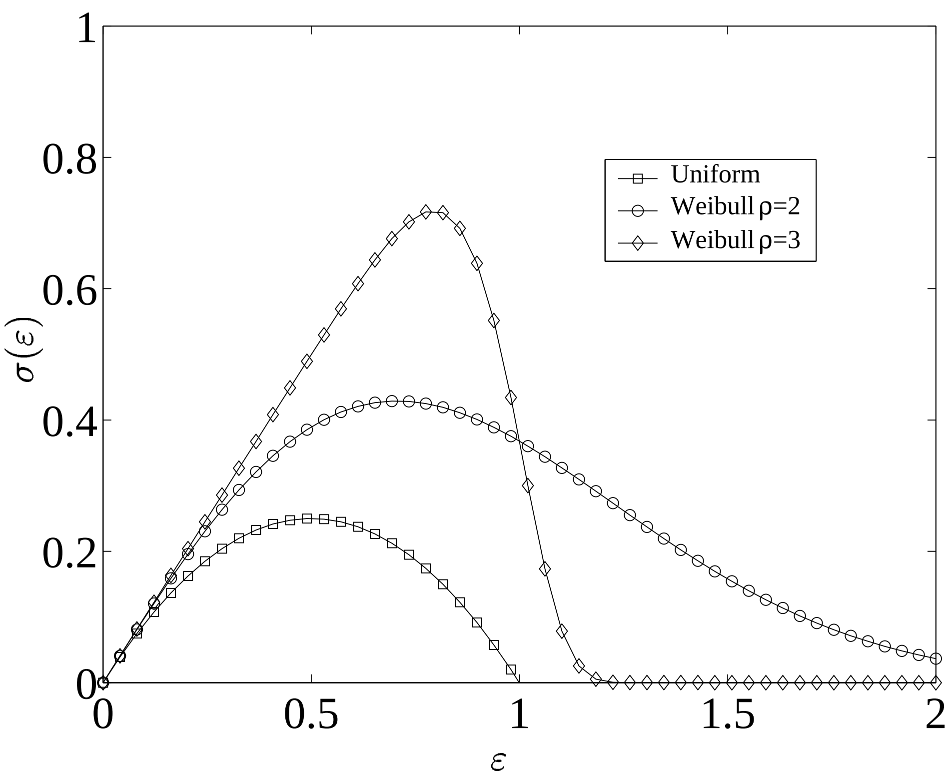

Figure 3.2: Numerical (lines) and analytical (symbols) constitutive behaviors of the dry bundle model in global load sharing approximation, using different thresholds cumulative distributions

and the strength value is

$$\sigma_c = \frac{\varepsilon_o}{4}. \tag{3.25}$$

Each of the fibers has the same Young's modulus which is taken to be unity. Hence, the axial strain ε of each fiber is identical to the tension in the fiber. On the other hand for using a Weibull type cumulative distribution

$$P(\varepsilon) = 1 - e^{-\left(\frac{\varepsilon}{\varepsilon_o}\right)^\rho} \tag{3.26}$$

relation (3.23) is valid for

$$\varepsilon_c = \varepsilon_o \rho^{\frac{1}{\rho}} \tag{3.27}$$

and the strength becomes

$$\sigma_c = \varepsilon_o (\rho e)^{-\frac{1}{\rho}}. \tag{3.28}$$

Note that those results are independent of the system size, which is characteristic of this mean field approach.

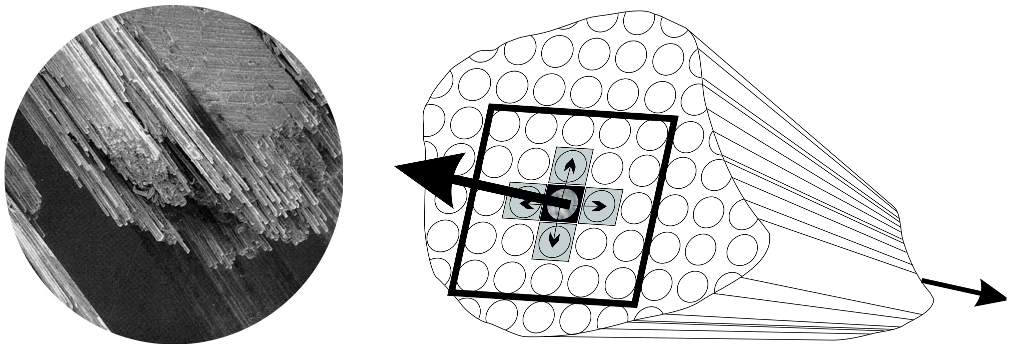

Figure 3.3: Pure local load sharing approach, after one fiber breaks the load is redistributed among the first near neighbors. Fiber composites microscopic real scenario and sketch of a fiber bundle model.

3.3.2 FBM, local load sharing approach

In the local load sharing (LLS) approach for the fiber bundle model the load borne by failing elements is transferred to their nearest neighbors which represents short range interactions among the fibers (see Fig. 3.3). In this case the damage in the system is completely localized. Initially, the evolution of independent clusters of broken fibers is observed and then global failure is initiated when one cluster reaches a critical size s_c after which the cluster becomes unstable, which induces the macroscopic fracture of the system.

The size effects on the strength of fiber bundle models in LLS have been extensively studied. Actually, when local load sharing rules are assumed, the mean strength σ_c decreases with increasing composite size [19, 26, 28, 31, 59]. The relatively weak fibers in the composite initiate the failure process and govern the strength of the composite. Larger composites contain a larger number of these weaker fibers. In the local load sharing framework, these weaker fibers may also serve as potential nucleation sites from which eventually the critical cluster could grow.

In Ref. [19, 26] the asymptotic dependence between the strength and the system size of a linear fiber bundle was found to be $\sigma_c \sim \frac{\alpha}{\ln N}$. Moreover, for some modalities of stress transfer, which can be considered as intermediate between global and local load sharing, σ_c decreases for large system sizes following the relation $\sigma_c \sim \frac{1}{\ln(\ln N)}$ as in the case of hierarchical load transfer models [31, 59].

The Local Load Sharing approach has its application in the failure of composite materials, and more specifically in the fiber-reinforced composites with elastic fibers embedded in a brittle matrix. There, as fiber breaks appear, the matrix serves the important function of transferring the shear traction to the neighborhood of the fiber. This arrangement results in a very short range of interaction, both laterally across fibers and longitudinally along the fibers axis, with most of the load going to the nearest neighbors.

3.3.3 Burst statistics and acoustic emission

One of the most interesting aspects of the damage mechanism of disordered solids is that the breakdown is preceded by an intensive precursor activity in the form of avalanches of microscopic breaking events [19, 20, 34, 45]. Under a given external load F in a bundle of fibers a certain fraction of fibers fails immediately. Due to the load transfer from broken to intact fibers this primary fiber breaking may initiate secondary breaking that may also trigger a whole avalanche of breaking. If F is large enough the avalanche does not stop and the material fails catastrophically. For the dry FBM it has been shown by analytic means that in the case of global load transfer the size distribution of avalanches follows asymptotically a universal power law

$$D(s) \sim s^{-\tau} \tag{3.29}$$

with an exponent $\tau = \frac{5}{2}$, *i.e.* it does not depend on the disorder distribution. [3, 19, 20, 60]. However, in the case of local load transfer no universal behavior exists, and the characteristic size of the avalanche is bounded [3, 19–21]. In spite that a power law for the burst-avalanche distribution is also approximately correct, the exponent τ is not universal, since it depends on the strength distribution as well as the size of the system [3, 19–21] .

It is well known that the breakdown of a disordered solid is preceded by intense precursors in the form of avalanches. That is why acoustic emission has been used for developing of a wide class of non-destructive testing (NDT) techniques for practical applications. It has been observed that the response acoustic emission (AE) to an increasing external stress takes place in bursts distributed over a wide range of scales. Examples are found in the fracturing of wood [61], cellular glass [62], and concrete [63]. Those experiments are usually performed increasing the external pressure slowly until the material (wood, concrete or fiberglass) macroscopically breaks. The acoustic energy is releasing and its amplitude shows a net increase as the material approaches the breakdown point. The integrated distribution of burst energies has often been found to follow a power law with an exponent between one and two [61, 62].

Application of AE for estimation of failure of disordered materials represents a complex problem and rises many questions that require solutions. Creation of the basic conception of composite failure is one of these problems. Without this conception it is impossible to explain physical processes which generates AE and, thus, to use AE for testing. Due to great varieties of types of composite materials it is a tough task to find a general model for the description of their failure. In this framework the FBM's are excellent candidate models. Despite of considerable difference between those models and the actual material they explain the main effects to understand the relation between the evolution of the damage and the acoustic emission process.

3.3.4 Continuous damage model

Recently, a novel continuous damage law has been introduced in lattice models [17] of fracture. In this model when the failure threshold of a lattice bond is exceeded the elastic modulus of the bond is reduced by a factor a ($0 < a < 1$), furthermore, multiple failures of bonds are allowed. Simulations revealed that under strain controlled loading the system develops into a self organized state, which is macroscopically plastic, and is characterized by a power law distribution of avalanches of breaks [17].

An extension of fiber bundle models by implementing a continuous damage law for the fibers, in the spirit of Ref. [17] was presented in Ref. [58]. It has been demonstrated in Ref. [58] that the continuous damage fiber bundle model (CDFBM) provides a broad spectrum of description of materials varying its parameters and for certain parameter settings the model recovers variants of fiber bundle models known in the literature. CDFBM is relevant for materials where the microscopic damage mechanism is a gradual multiple failure of components, *i.e.* matrix and fibers [56, 57]. One of the most appealing results on CDFBM was that the multiple failure of brittle elements can give rise to a macroscopic plastic behavior of the specimen, which is then followed by a hardening or softening regime, furthermore, under certain conditions damage localization occurs. However, the microscopic damage process of CDFBM had not been explored. Very recently, the CDFBM was further developed by Moral *et al.* [44] taking into account time dependence in the failure process.

The CDFBM is thoroughly described in chapter 4. One of the goals of this thesis is to reveal the microscopic failure process in order to understand the emergence of the plastic macroscopic state. Analytic results are obtained to characterize the damage process under strain controlled loading, furthermore, for stress controlled experiments we develop a simulation technique and explore numerically the distribution of bursts of fiber breaks. The effect of localization on the process of damage is clarified and a phase diagram of the model characterizing the possible constitutive behaviors and burst distributions is constructed in terms of the two parameters of the model.

3.4 Fiber reinforced composite models

More realistic modeling of the damage process of fiber composites under an uniaxial load have also been performed [7, 28, 53, 55, 64–67]. Nevertheless, even limiting the number of independent variables needed to describe the internal microstructure of the specimen, an accurate prediction of the ultimate strength is a computationally demanding task.

So early, based on the continuum theory, Hedgepeth [65] obtained the stress concentrations in two dimensional unidirectional composites consisting of elastic fibers in a matrix which can only carry shear stresses, with fiber breaks aligned transverse to the fiber direction. Later the same group extended the results to three dimensions [66] .

A powerful numerical technique to investigate the failure of fiber composites has been developed during the last ten years [7, 28, 53–55]. This technique uses 2D and 3D lattice Green functions to calculate load transfer from broken to unbroken fibers, and commonly includes important effects of fiber/matrix sliding. This Green function technique initially introduced by Zhou and Curtin in 1995, determines the tensile stress field in a model composite for an arbitrary configuration of broken fibers, and for a given pre-selected load sharing rule. A Green's function is a response function $G_{i,j}$ which relates the displacement at a point i due to a unit point force F_j applied at point j through

$$u_i = G_{i,j} F_j. \tag{3.30}$$

Moreover, the stress profiles in the direction parallel to the fibers is commonly described as a *shear-lag* action [7, 28, 53–55, 64, 67].

Shear-lag analysis is one of the most frequently used models for estimating stress distributions, stress concentrations, and failure in fiber-reinforced composites [64, 67]. The shear-lag *philosophy* treats the fibers as one-dimensional spring elements, thus neglecting the possible variations in axial stress in the fiber cross-sections, and approximates the matrix shear behavior as governed by the axial displacements of the fiber elements bounding the matrix region. The shear-lag method assumes that the matrix carries no tensile loads and that the matrix shear τ_n in the position z is governed by the smaller one of the shear stresses associated with the neighboring fiber displacements,

$$\tau_n(z) = G_m \frac{(u_n(z) - u_i(z))}{d} \tag{3.31}$$

where u_n is the displacement of the nth near-neighboring fiber to fiber i , G_m is the matrix shear modulus, and d is the distance between the fibers.

3D finite element models have recently been proposed and developed by many researchers [7, 53, 68–70]. Especially, Landis et al. [70] proposed a shear-lag model based on the finite element method in order to calculate the stress profile around a broken fiber and to simulate the damage progress using a Monte Carlo method. They also showed that the finite element shear-lag model can include the influence of matrix axial stress [68].

Although those models are sophisticated, the applications are limited to well-bonded, elastic fiber/matrix composite systems. In this case, the inter-facial shear stress near a broken fiber is quite high, and physically some stress relaxation should occur in real composites. Therefore, a model which considers additional micro-damage mechanisms was recently developed [55, 71, 72]. This pure 3D shear-lag model considers the micro-damage phenomena of inter-facial debonding and inter-facial yielding. Monte Carlo simulations were conducted to obtain the global strength σ_c as a function of the fiber strength and inter-facial properties. The damage progression, the type of inter-facial damage, and the size-scaling of the tensile strengths, were carefully examined [72].

3.5 Creep and time dependent models

Under high steady stresses fiber composites may undergo time dependent deformation resulting in failure called creep rupture which limits their lifetime, and hence, has a high impact on the applicability of these materials as construction elements. Both natural fiber composites like wood [73–76] and various types of fiber reinforced composites [57, 77–79] show creep rupture phenomena, which have attracted continuous theoretical and experimental interest over the past years. Creep failure tests are usually performed under uniaxial tensile loading when the specimen is subjected either to a constant load σ_{o} or to an increasing load (ramp-loading). The time evolution of the damage process is monitored by recording the strain ε (see Fig. 3.4) of the specimen and the acoustic signals emitted by microscopic failure events [57, 77].

The underlying microscopic failure mechanism of creep rupture is very complex depending on several characteristics of the specific types of materials, and is far from being well understood. Theoretical studies encounter various challenges: on the one hand, applications of fiber composites require the development of analytical and numerical models which are able to predict the damage histories of loaded composites in terms of the specific parameters of constituents. On the other hand, creep rupture, similarly to other rupture phenomena, presents a very interesting problem for statistical physics. It is still an open problem to embed creep rupture into the general framework of statistical physics and to understand the analogy between rupture phenomena and phase transitions.

A time-dependent method, which describes the failure of materials under stress, within the fiber bundle paradigm, was early proposed by Coleman in 1957 [10]. In this model a bundle of elements is considered with each element having a prescribed lifetime t_i when subject to an applied stress σ_o . When elements fail, their load is redistributed to other elements of the set according to a prescribed transfer rule. The expressions of the life time

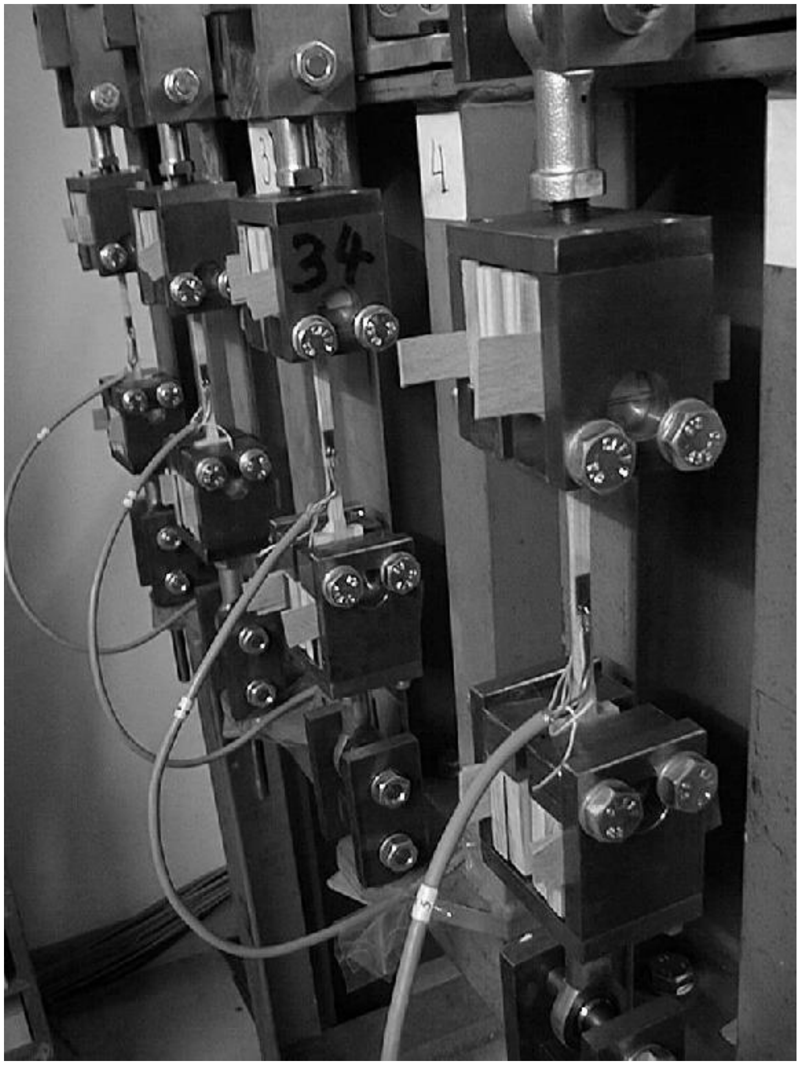

Figure 3.4: Typical experimental setup of creep experiments

distributions of the fibers for the most simple cases of loading histories were deduced. Based on those pioneering ideas some interesting analytical and numerical results have been obtained for the time evolution of the failure [24, 31, 78, 80, 81].

In 1995 Newman et al [31] proposed a phenomenological model for the failure process of a bundle of N independent elements, in global load sharing approximation. So that, the external stress σ_o and the stress on an unbroken fiber σ are related by the following expression

$$\sigma_o = \frac{N}{N_s}\sigma \tag{3.32}$$

where N_s is the number of unbroken fibers. Moreover the rate at which elements fail is approximated as:

$$\frac{dN_s}{dt} = -\nu N_s \tag{3.33}$$

where the hazard rate ν is related to the stress by

$$\nu = \nu_o \left(\frac{\sigma}{\sigma_c}\right)^{\rho}. \tag{3.34}$$

Substituting Eq.(3.32), Eq.(3.33) gives

$$\frac{dN_s}{dt} = -\nu_o \frac{N_o^{\rho}}{N_s^{\rho-1}} \left(\frac{\sigma_o}{\sigma_c}\right)^{\rho} \frac{dt}{N_s^{\rho-1}} dt \tag{3.35}$$

Integrating with the initial condition $N_s = N$ at $t = 0$ we obtain

$$N_s(t) = N_o \left[1 - \nu_o \left(\frac{\sigma_o}{\sigma_c}\right)^{\rho} t\right] \tag{3.36}$$

From this results, the dependence between the external stress σ_o and the time to failure t_f can be analytically deduced as

$$t_f = \frac{1}{\nu_o} \left(\frac{\sigma_c}{\sigma_o}\right)^{\rho}. \tag{3.37}$$

Note, the existence of an unrealistic characteristic time scale $\tau_o = \frac{1}{\nu_o}$. in this phenomenological approach Nevertheless, this relation (3.37) is usually accepted by the experimental community. Moreover, certain local load sharing versions of that model were also considered, and it was found that the life time distribution of the system also strongly depends on the breakdown exponent ρ [22].

Recently, Du and McMeeking [82] developed an useful creep model from the more basic McLean model of creep in continuous fiber composites [83, 84]. They improved McLean's ideas including damage accumulation in the form of fiber fracture as creep strain increases. In a McLean's composite loaded in creep, the matrix undergoes stress relaxation and, in doing so, transfers stress to the fiber reinforcement. The elastic response of the fibers determines the limit of the composites strain. Thus, in the Du and McMeeking model, the creep strain rate is controlled by the rate of matrix stress relaxation and the magnitude of the strain at which the global failure occurs is controlled by the stress supported by the fibers [82].

Guarino et al. [61] have introduced another variant of creep model, taking into account a thermally activated fracture initiation. There are many different ways to introduce such thermally activated rupture. In particular, Phoenix and Tierney [80] derived a breakdown rule based on the inter-atomic potential between atoms as fitted by a Morse potential. The approach of Guarino is based on a different spirit, namely thermal fluctuations are assumed to induce an additional white Gaussian noise in the load carried by the fibers. Based on a numerical study of this model, they obtained results which agree with a number of experimental results [85–88].

Other interesting probabilistic approaches to solve the time dependence of the load transfer in models of fracture have been developed [32, 33, 43–50]. In spite of the fact that these theoretical approaches are so far of the experimental scenario for the real fiber materials [57, 73–79], the possible parallelism existing between phase transitions and fracture in disordered materials have been explored using the fiber bundle models. Their results suggest that fracture process can be seen as a second-order (continuous) phase transition for the global load sharing approximation, whereas for the case of short range interactions the bundle fails suddenly with no prior significant precursor activity signaling the imminent collapse of the system, this case being a first-order like phase transition.

Chapter 4

Bursts in a fiber bundle model with continuous damage

In this chapter we study the constitutive behavior, the damage process, and the properties of bursts in the continuous damage fiber bundle model introduced recently. Depending on its two parameters, the model provides various types of constitutive behaviors including also macroscopic plasticity. Analytic results are obtained to characterize the damage process along the plastic plateau under strain controlled loading, furthermore, for stress controlled experiments we develop a simulation technique and explore numerically the distribution of bursts of fiber breaks assuming infinite range of interaction. Simulations revealed that under certain conditions a power law distribution of bursts arises with an exponent significantly different from the mean field exponent $\frac{5}{2}$. A phase diagram of the model characterizing the possible burst distributions is constructed [36].

4.1 Model

The modeled system is composed of N parallel fibers with identical Young-modulus E_f but with random failure thresholds d_i, $i = 1, \ldots, N$. The failure strength d_i of individual fibers is an independent identically distributed random variable with a probability density $p(d)$ and a cumulative probability distribution $P(d) = \int_0^d p(x)dx$. The fibers are assumed to have linear elastic behavior up to breaking (brittle failure). Under uniaxial loading of the specimen a fiber fails if it experiences a load larger than its breaking threshold d_i. In the framework of the model at the failure point the stiffness of the fiber gets reduced by a factor a, where $0 \leq a < 1$, *i.e.* the stiffness of the fiber after failure is aE_f. In principle, a fiber can fail more than once and the maximum number k_{max} of failures allowed for fibers is a parameter of the model. Once a fiber has failed its damage threshold d_i can either be

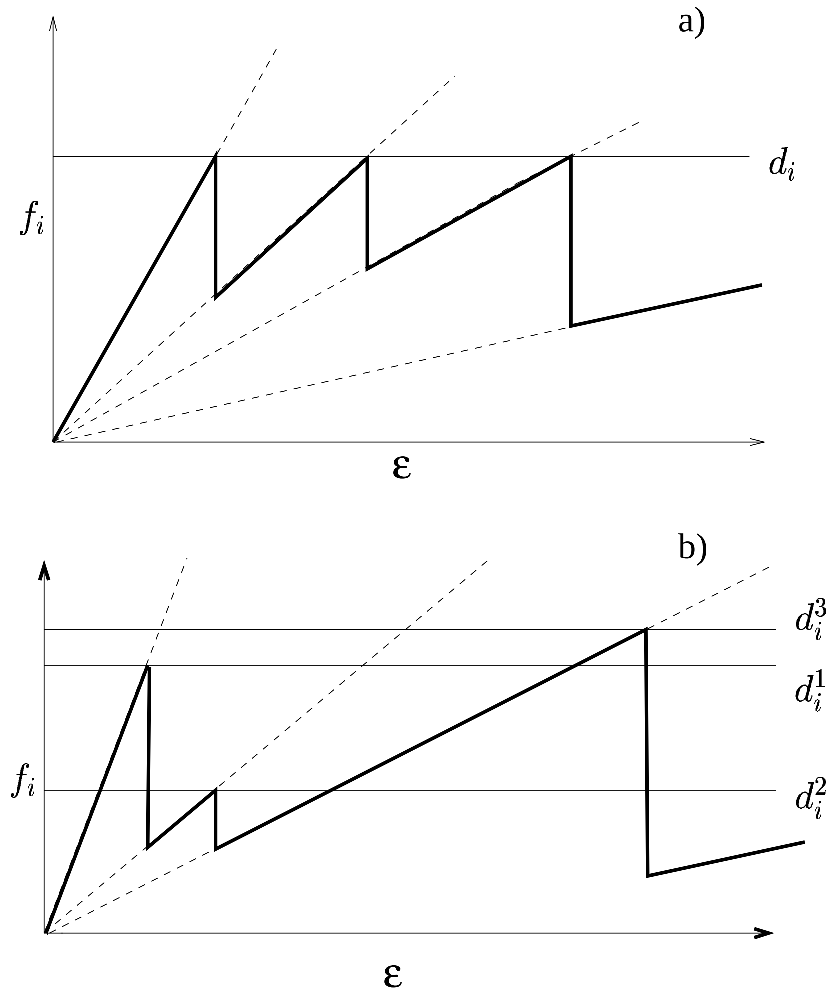

Figure 4.1: The damage law of a single fiber of the continuous damage model when multiple failure is allowed $a)$ for quenched, and $b)$ for annealed disorder. The horizontal lines indicate the damage threshold d_i.

kept constant for the further breakings (quenched disorder) or new failure thresholds of the same distribution can be chosen (annealed disorder), which can model some microscopic rearrangement of the material after failure. The damage law of the model is illustrated in Fig. 4.1 for both types of disorder. The characterization of damage by a continuous parameter corresponds to describe the system on length scales larger than the typical crack size. This can be interpreted such that the smallest elements of the model are fibers and the continuous damage is due to cracking inside fibers. However, the model can also be considered as the discretization of the system on length scales larger than the size of single fibers, so that one element of the model consists of a collection of fibers with matrix material in between. In this case the microscopic damage mechanism resulting in multiple failure of the elements is the gradual cracking of matrix and the breaking of fibers. In the following we refer to the elements of the continuous damage FBM as fibers, but we have the above two possible interpretations in mind.

After failure the fiber discharges a certain amount of load which has to be taken by the other fibers. For the load redistribution we assume an infinite range of interaction among fibers (mean field approach), furthermore, equal strain condition is imposed which implies that stiffer fibers of the system carry more load. At a strain ε the load of fiber i that has failed $k(i)$ times reads as

$$f_i(\varepsilon) = E_f a^{k(i)} \varepsilon, \tag{4.1}$$

where $E_f a^{k(i)}$ is the actual stiffness of fiber i. It is important to note that, in spite of the infinite interaction range, Eq. (4.1) is different from the usual global load sharing where all the intact fibers carry always the same amount of load. In the following the initial fiber stiffness E_f will be set to unity.

4.2 Constitutive laws

This general theoretical framework facilitates to obtain analytic results also for the microscopic failure process. The key quantity is the probability $pb_k(\epsilon)$ that during the loading of a specimen an arbitrarily chosen fiber failed precisely k-times at a strain ϵ, where $k = 0, \ldots, k_{max}$ denotes the failure index, and $k = 0$ is assigned to the intact fibers. $pb_k(\epsilon)$ can be cast in the following form for *annealed disorder*

$$\begin{aligned} & pb_k(\epsilon) = \left[1 - P(a^k\epsilon)\right] \prod_{j=0}^{k-1} P(a^j\epsilon), \\ \text{for} \quad & 0 \leq k \leq k_{max} - 1, \\ \text{and} \quad & pb_{k_{max}}(\epsilon) = \prod_{j=0}^{k_{max}-1} P(a^j\epsilon), \end{aligned} \tag{4.2}$$

and for *quenched disorder*

$$\begin{aligned} & pb_0(\varepsilon) = 1 - P(\varepsilon), \\ & pb_k(\varepsilon) = P(a^{k-1}\varepsilon) - P(a^k\varepsilon), \text{ for } 1 \leq k \leq k_{max} - 1, \\ & \text{and} \quad pb_{k_{max}}(\varepsilon) = P(a^{k_{max}-1}\varepsilon). \end{aligned} \tag{4.3}$$

It can be easily seen that the probabilities Eqs. (4.2,4.3) fulfill the normalization condition

$$\sum_{k=0}^{k_{max}} pb_k(\varepsilon) = 1. \tag{4.4}$$

Average quantities of the fiber ensemble during a loading process can be calculated using the probabilities Eqs. (4.2,4.3). For instance, the average load or stress on a fiber σ at a given strain ε reads as

$$\sigma = \varepsilon \left[\sum_{k=0}^{k_{max}} a^k pb_k(\varepsilon) \right], \tag{4.5}$$

which provides the macroscopic constitutive behavior of the model, and the expression in the brackets can be considered as the macroscopic effective Young modulus of the sample ($E_f = 1$).

Then we can derive the constitutive law for continuous damage FBM and show how the FBMs used in the literature can be recovered in particular limits. We first consider the case in which fibers are allowed to fail only once: the constitutive equation, using Eq. (4.5) with $k_{max} = 1$ reads as

$$\sigma = \varepsilon(1 - P(\varepsilon)) + a\varepsilon P(\varepsilon), \tag{4.6}$$

where $P(\varepsilon)$ and $1 - P(\varepsilon)$ are the fraction of failed and intact fibers, respectively, and the Young-modulus E_f of intact fibers is taken to be unity. In Eq. (4.6) the first term provides the load carried by intact fibers while the second term is the contribution of the failed ones. Note that this particular case together with the parameter choice $a = 0$ (*i.e.* broken fibers carry no load) corresponds to the dry FBM $[1, 2, 9, 10]$, while setting $a = 0.5$ in Eq. (4.6) we recover the so-called micromechanical model of fiber reinforced ceramic matrix composites (CMC's), which has been extensively studied in the literature [5–7]. In CMC's the physical origin of the load bearing capacity of failed fibers is that in the vicinity of the broken face of the fiber the fiber-matrix interface debondings and the stress builds up again in the failed fiber through the sliding fiber-matrix interface.

When the fibers are allowed to fail more than once we have to distinguish between quenched and annealed disorder.

(i) Quenched disorder: When the fibers are allowed to fail twice the constitutive equation, using Eq. (4.5) with $k_{max} = 2$, can be written as

$$\sigma = \varepsilon(1 - P(\varepsilon)) + a\varepsilon \left[P(\varepsilon) - P(a\varepsilon)\right] + a^2\varepsilon P(a\varepsilon), \tag{4.7}$$

where $[P(\varepsilon) - P(a\varepsilon)]$ is the fraction of those fibers which failed only once, and $P(a\varepsilon)$ provides the fraction of fibers which failed already twice. In the general case, when fibers are allowed to fail k_{max} times, where k_{max} can also go to infinity, the constitutive equation can be cast into the form

$$\begin{aligned} \sigma = \varepsilon(1 - P(\varepsilon)) + \sum_{i=1}^{k_{max}-1} & a^i\varepsilon \left[P(a^{i-1}\varepsilon) - P(a^i\varepsilon)\right] \\ & + a^{k_{max}}\varepsilon P(a^{k_{max}-1}\varepsilon). \end{aligned} \tag{4.8}$$

(ii) Annealed disorder: As in the previous case we consider first the case in which fibers are allowed to fail twice, obtaining

$$\sigma = \varepsilon(1 - P(\varepsilon)) + a\varepsilon P(\varepsilon)(1 - P(a\varepsilon)) \\ +a^2\varepsilon P(\varepsilon)P(a\varepsilon), \tag{4.9}$$

where $P(\varepsilon)(1 - P(a\varepsilon))$ is the fraction of fibers which failed only once, and $P(\varepsilon)P(a\varepsilon)$ is the fraction of fibers which failed already twice. Finally, when fibers are allowed to fail k_{max} times, where k_{max} can also go to infinity, the constitutive equation is given by

$$\sigma = \sum_{i=0}^{k_{max}-1} a^i\varepsilon \left[1 - P(a^i\varepsilon)\right] \prod_{j=0}^{i-1} P(a^j\varepsilon) \\ +a^{k_{max}}\varepsilon \prod_{i=0}^{k_{max}-1} P(a^i\varepsilon). \tag{4.10}$$

In Fig. 4.2 we show the explicit form of the constitutive law for quenched disorder for different values of k_{max} in the case of the Weibull distribution

$$P(d) = 1 - e^{-\left(\frac{d}{d_c}\right)^\rho}, \tag{4.11}$$

with disorder parameter $\rho = 2$ and Weibull modulus $d_c = 1$. It is important to remark that the constitutive laws derived above are exact only in the infinite size limit ($N \to \infty$), while fluctuations in the value of the failure stress F_c have been observed and studied for finite size bundles. For this reason, we compare the theoretical results with numerical simulations of bundles of size $N = 128^2$. The agreement between simulations and theory turns out to be satisfactory both for quenched (Fig. 4.2) and annealed disorder.

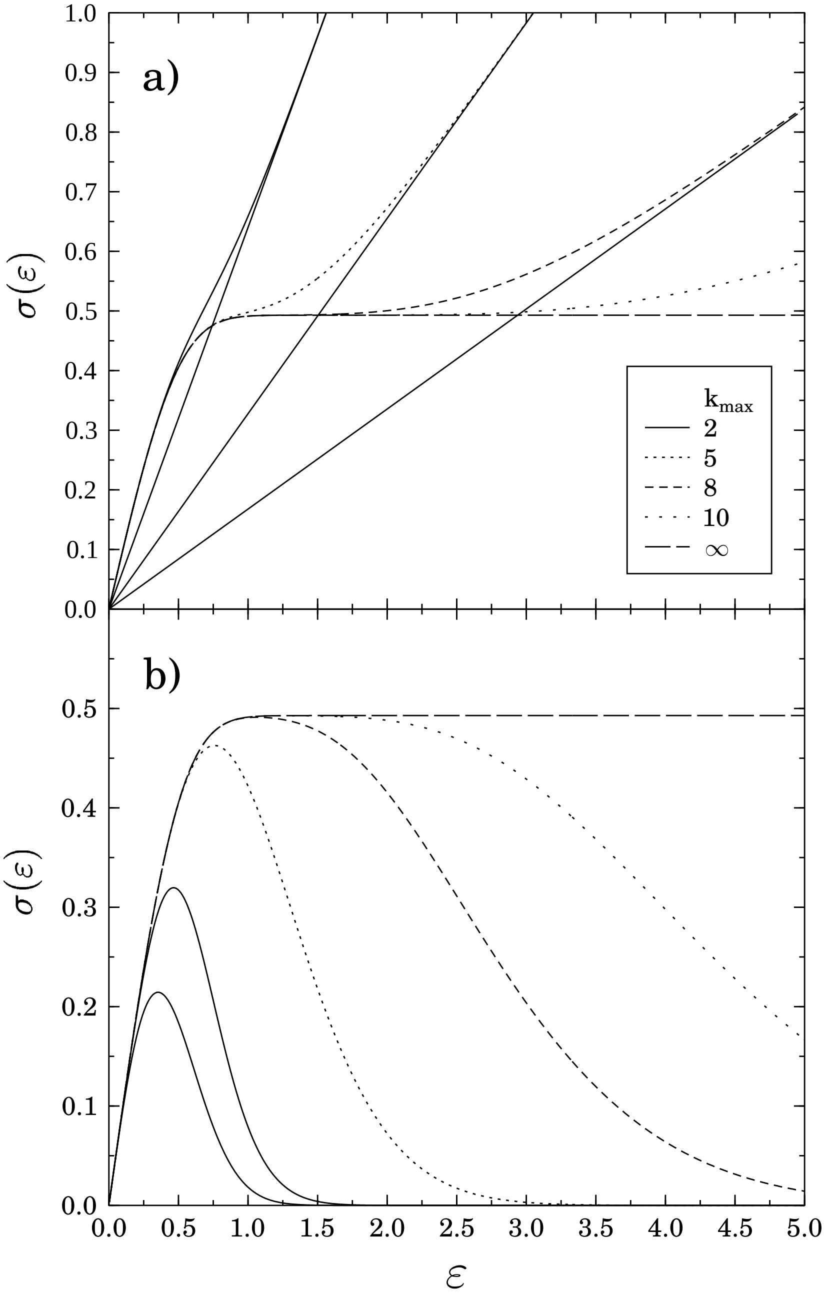

Figure 4.2: Constitutive behavior of the model of quenched disorder $a)$ with $b)$ without residual stiffness at $a = 0.8$ for different values of k_{max} and k^* respectively. In $b)$ the lowest curve presents the constitutive behavior of the dry bundle model for comparison.

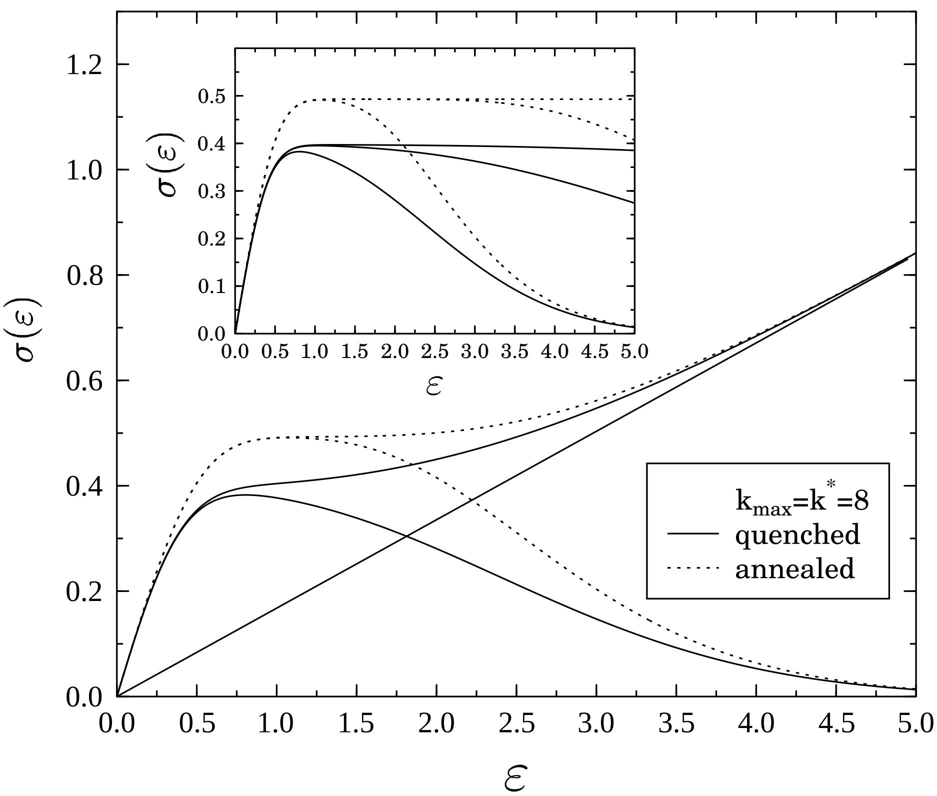

Figure 4.3: Comparison of the constitutive behaviors with annealed and quenched disorder. We show data with and without remaining stiffness. The inset demonstrates how the shape of the constitutive curves changes when increasing k^* with different types of disorders.

In Fig. 4.2 a the fibers have $a^{k_{max}}$ residual stiffness after having failed k_{max} times, which gives rise to hardening of the material, *i.e.* the σ curves asymptotically tend to straight lines with slope $a^{k_{max}}$. Increasing k_{max} the hardening part of the constitutive behavior is preceded by a longer and longer plastic plateau, and in the limiting case of $k_{max} \to \infty$ the materials behavior becomes completely plastic (see Fig. 4.2). A similar plateau and asymptotic linear behavior has been observed in brittle matrix composites, where the multiple cracking of matrix turned to be responsible for the relatively broad plateau of the constitutive behavior, and the asymptotic linear part is due to the linear elastic behavior of fibers that remained intact after matrix cracking [57].

In order to describe macroscopic cracking and global failure instead of hardening, the residual stiffness of the fibers has to be set to zero after a maximum number k^* of allowed failures [17]. In this case the constitutive law can be obtained from the general form

Eqs. (4.8) and (4.10) by skipping the last term corresponding to the residual stiffness of fibers, and by setting $k_{max} = k^*$ in the remaining part. A comparison of the constitutive laws of the dry and continuous damage FBM is presented in Fig. 4.2b for the case of quenched disorder. Annealed disorder yields similar results. One can observe that the dry FBM constitutive law has a relatively sharp maximum, however, the continuous damage FBM curves exhibit a plateau whose length increases with increasing k^*. Note that the maximum value of σ corresponds to the macroscopic strength of the material and in stress controlled experiments the plateau and the decreasing part of the curves cannot be reached. However, by controlling the strain ε, the plateau and the decreasing regime can also be realized. The value of the driving stress corresponding to the plastic plateau is determined by the damage parameter a, while the length of the plateau is controlled by k_{max} and k^*.

In Fig. 4.3, we directly compare the constitutive law for quenched and annealed disorder and confirm that the differences between the cases are very small. In particular, all the basic constitutive behavior are reproduced in the two cases.

It is important to remark that the behavior of the dry FBM model ($a = 0$) under unloading and reloading to the original stress level is completely linear, since no new damage can occur during unloading-reloading sequences and the effect of the matrix material is completely neglected. This also implies that in each damage state the model is completely characterized by the Young modulus defined as the slope of the unloading curve. If the value of the damage parameter is larger than 0 $(a > 0)$ the behavior of the system under unloading and reloading is rather complicated. Due to the sliding of broken fibers with respect to the matrix, hysteresis loops and remaining inelastic strain occur (for examples see Ref. [35] and references therein).

4.3 Damage

The damage state of the model at a certain ε can be characterized by the average number of failures occurred. Based on the probabilities Eqs. (4.2,4.3), we introduce a damage variable $D(\varepsilon)$ as

$$D(\epsilon) = \frac{1}{k_{max}} \sum_{k=1}^{k_{max}} k p b_k(\epsilon), \tag{4.12}$$

which is an integral quantity of the damage process. From the properties of $pb_k(\epsilon)$ it can be seen that D is a monotonically increasing function, and $D \in [0, 1]$. Then the average number of failures can be obtained as $N k_{max} D(\epsilon)$. Fig. 4.4 illustrates the behavior of D for three different values of k_{max}.

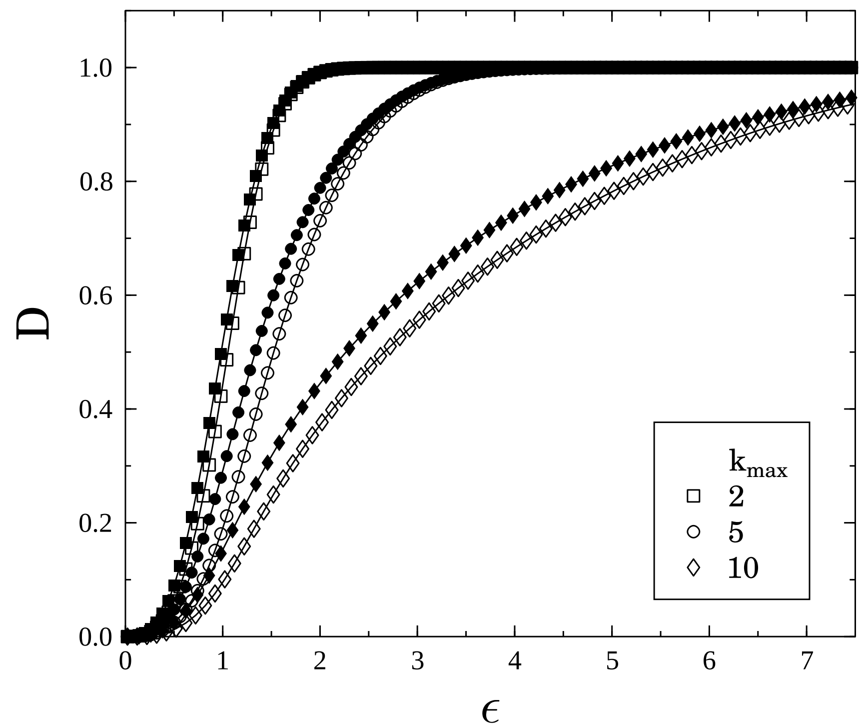

Figure 4.4: The damage variable D for annealed (open symbols) and quenched (filled symbols) disorder for several different values of k_{max}. The damage variable was chosen to be $a = 0.8$.

It can be observed in Fig. 4.4 that the overall behavior of the damage variable D is nearly the same for annealed and quenched disorder, however, there is a significant difference between the microscopic damage processes in the two cases. In spite of the infinite range of interaction among fibers, localization of damage occurs for the case of quenched disorder. It means that weaker fibers tend to break more often than the stronger ones. For quenched disorder, the strain ε_m where the weakest fiber of failure threshold d_m reaches k_{max}, is

$$\varepsilon_m = \frac{d_m}{a^{k_{max}}}. \tag{4.13}$$

Hence, at this loading stage the failure index k of fibers as a function of the damage threshold d can be obtained as

$$k(d) = \frac{1}{\ln a} \ln \frac{d}{d_m} + k_{max}. \tag{4.14}$$

Localization of damage means that k is a decreasing function of d, and it can be seen from

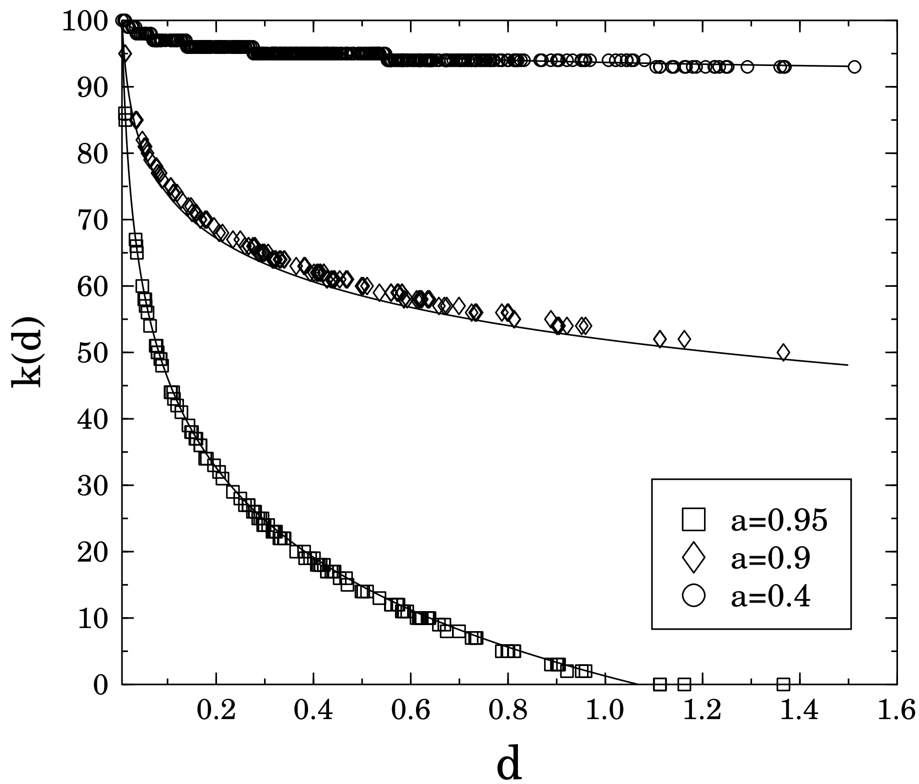

Figure 4.5: The failure index k of fibers as a function of their failure threshold d for several different values of the damage parameter a. The number of fibers was chosen to be $N = 500$. The continuous lines represent the corresponding analytical results of Eq. (4.14).

Eq. (4.14) that the localization gets more pronounced when the damage parameter $a \to 1$. This localization effect is illustrated in Fig. 4.5, where the analytic result Eq. (4.14) is compared to simulations for three different values of a.

4.4 Distribution of bursts

One of the most interesting aspects of the damage mechanism of disordered solids is that the breakdown is preceded by an intensive precursor activity in the form of avalanches of microscopic breaking events [19, 20, 34, 45]. Under a given external load F a certain fraction of fibers fails immediately. Due to the load transfer from broken to intact fibers this primary fiber breaking may initiate secondary breaking that may also trigger a whole avalanche of breakings. If F is large enough the avalanche does not stop and the material fails catastrophically. For the dry FBM it has been shown by analytic means that in the case of global load transfer the size distribution of avalanches follows asymptotically a universal power law with an exponent $-\frac{5}{2}$ [3, 19, 20, 60], however, in the case of local load transfer no universal behavior exists, and the avalanche characteristic size is bounded [3, 19–21].

Introducing a continuous damage law in lattice models, simulations revealed that under strain controlled conditions the system tends to a steady state, which is macroscopically plastic [17], similarly to our case. Due to the long range interaction, the plastic steady state is characterized by power law distributed avalanches of breaks and it has been argued that the underlying damage mechanism displays self organized criticality [17]. In the following we study the distribution of bursts in our CDFBM under strain and stress controlled conditions.

4.4.1 Strain controlled case

Under strain controlled conditions of fiber bundles there is no load transfer from broken to intact fibers since the load carried by each fiber is determined by the externally imposed strain and the local fiber stiffness according to Eq. (4.1). This implies that the number of fibers which break due to an infinitesimal increase of the external strain is completely determined by the statistics of fiber strength, *i.e.* by $p(d)$ and $P(d)$. It has been discussed in Sec. 4.2 that the plastic plateau and the decreasing part of the constitutive law can only be realized in strain controlled experiments. To reveal the nature of ductility arising in our model it turns out to be useful to study the statistics of bursts occurring under strain controlled conditions.

The basic quantity to characterize bursts is the probability $pb_k^{k+1}(\epsilon)d\epsilon$ that a fiber, which has failed k times up to strain ϵ imposed externally, will fail again under an infinitesimal strain increment $d\epsilon$. From Eqs. (4.2,4.3) $pb_k^{k+1}(\epsilon)$ can be cast in the form for *annealed disorder*

$$\begin{aligned} pb_k^{k+1}(\varepsilon) &= \prod_{j=0}^{k-1} P(a^j\varepsilon) \sum_{i=0}^{k} \frac{p(a^i\varepsilon)a^i}{P(a^i\varepsilon)}, \\ k &= 0, \ldots, k_{max}-1, \end{aligned} \tag{4.15}$$

and for *quenched disorder*

$$pb_k^{k+1}(\varepsilon) = p(a^k\varepsilon)a^k, \qquad k = 0, \ldots, k_{max}-1, \tag{4.16}$$

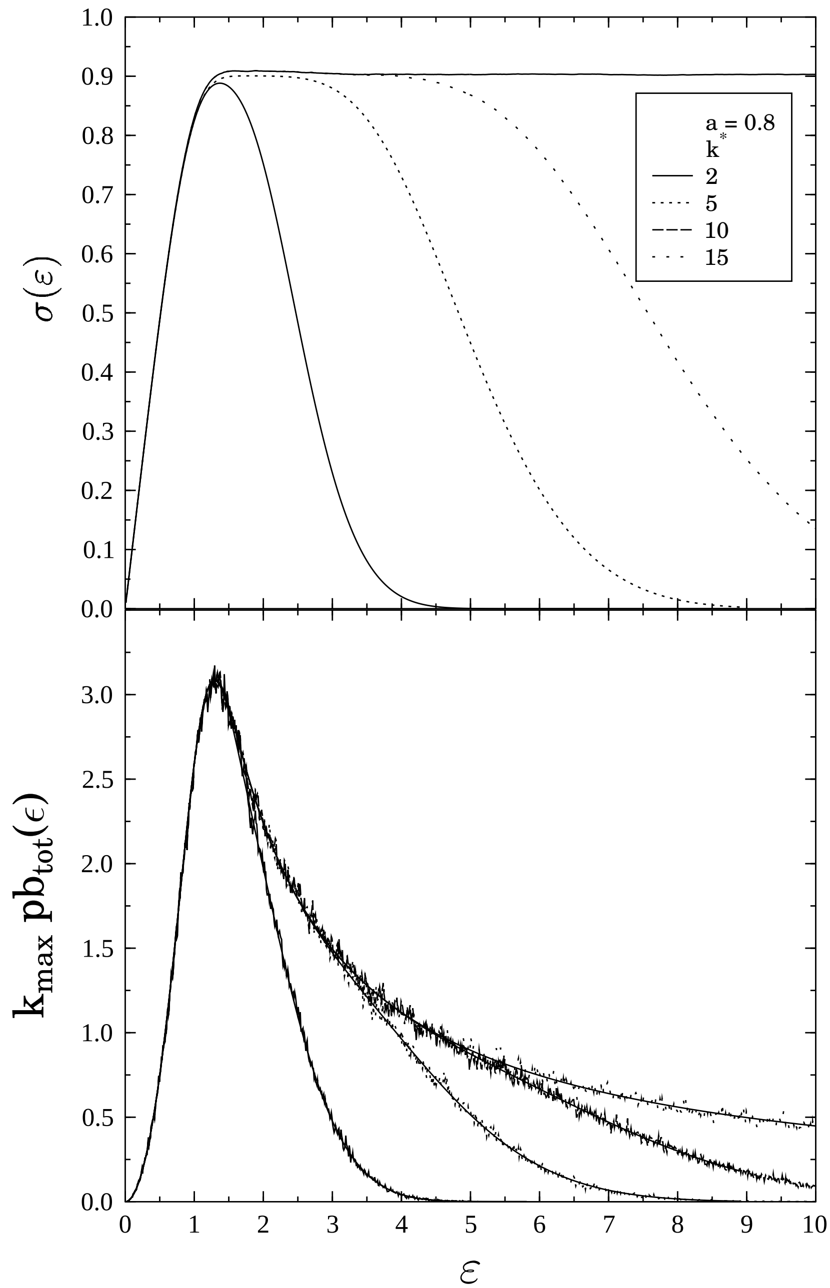

Figure 4.6: $k_{max}pb_{tot}$ as a function of ε for annealed disorder, comparison of simulations and analytic results of Eq. (4.15) (continuous lines). The integral of the functions is always equal to k^*. In the upper part of the figure the corresponding constitutive curves are also presented for comparison.

and the total probability of fiber breaking can be obtained by summing over k

$$pb_{tot}(\epsilon) \;=\; \frac{1}{k_{max}} \sum_{k=0}^{k_{max}-1} pb_k^{k+1}(\epsilon). \tag{4.17}$$

The number of fiber failures occurring in the strain interval $[\epsilon, \epsilon + d\epsilon]$ dN_e can be obtained as

$$dN_e = N k_{max} pb_{tot}(\epsilon) d\epsilon. \tag{4.18}$$

This is a very important characteristic quantity of the microscopic damage process since it can be monitored experimentally by means of acoustic emission techniques. The behavior of pb_{tot} is shown in Fig. 4.6 for the softening case with several values of k^*, where also the corresponding constitutive curves are presented. It can be seen that pb_{tot} has a maximum where the plastic regime of the constitutive curve starts, and it is a decreasing function of ϵ in the whole plastic region. Due to the stiffness reduction of the system caused by the subsequent failures, in the plastic regime the same increase of strain results in smaller and smaller load increments on fibers, and hence, pb_{tot} and the number of failures decreases. It also implies that the breaking activity, which can be measured by acoustic emission techniques, decreases along the plateau in agreement with experimental results [56].

It follows from the above argument that decreasing the value of the damage parameter a while k_{max} is kept fixed, the length of the plastic plateau, preceding the decreasing or hardening part of the constitutive behavior, increases since larger strain is required to achieve successive failure. This is demonstrated in Fig. 4.7, where one can also see that for small a the constitutive curve develops distinct maxima. In order to clarify the occurrence of these maxima in the plastic plateau, in Fig. 4.7 we also plotted pb_k^{k+1} for three different values of k at $a = 0.4$. With decreasing a the length of the plastic plateau increases, however, the consecutive maxima of pb_k^{k+1} get more and more separated giving rise to visible maxima in the plateau. The broader the disorder distribution, the smaller is the value of a where the maxima of σ appear.

The energy dissipation rate is also a very important aspect of the ductile regime of the model. The energy dissipation rate $E_{dis}(\epsilon)$ is defined so that the energy dissipated due to the failure of fibers in the strain interval $[\epsilon, \epsilon + d\epsilon]$ can be obtained as $E_{dis}(\epsilon)d\epsilon$

$$E_{dis}(\epsilon) = \sum_{k=0}^{k_{max}-1} \left[\frac{1}{2}\epsilon^2 a^k (1-a)\right] pb_k^{k+1}(\epsilon), \tag{4.19}$$

where the expression in the brackets provides the energy dissipated by the failure of a fiber which has already failed k-times. In Fig. 4.8 the energy dissipation rate $E_{dis}(\epsilon)$ is plotted for two different values of k_{max}. Comparing Fig. 4.8 to the corresponding constitutive curves in Fig. 4.2 can observe that in the plastic regime $E_{dis}(\epsilon)$ is constant.

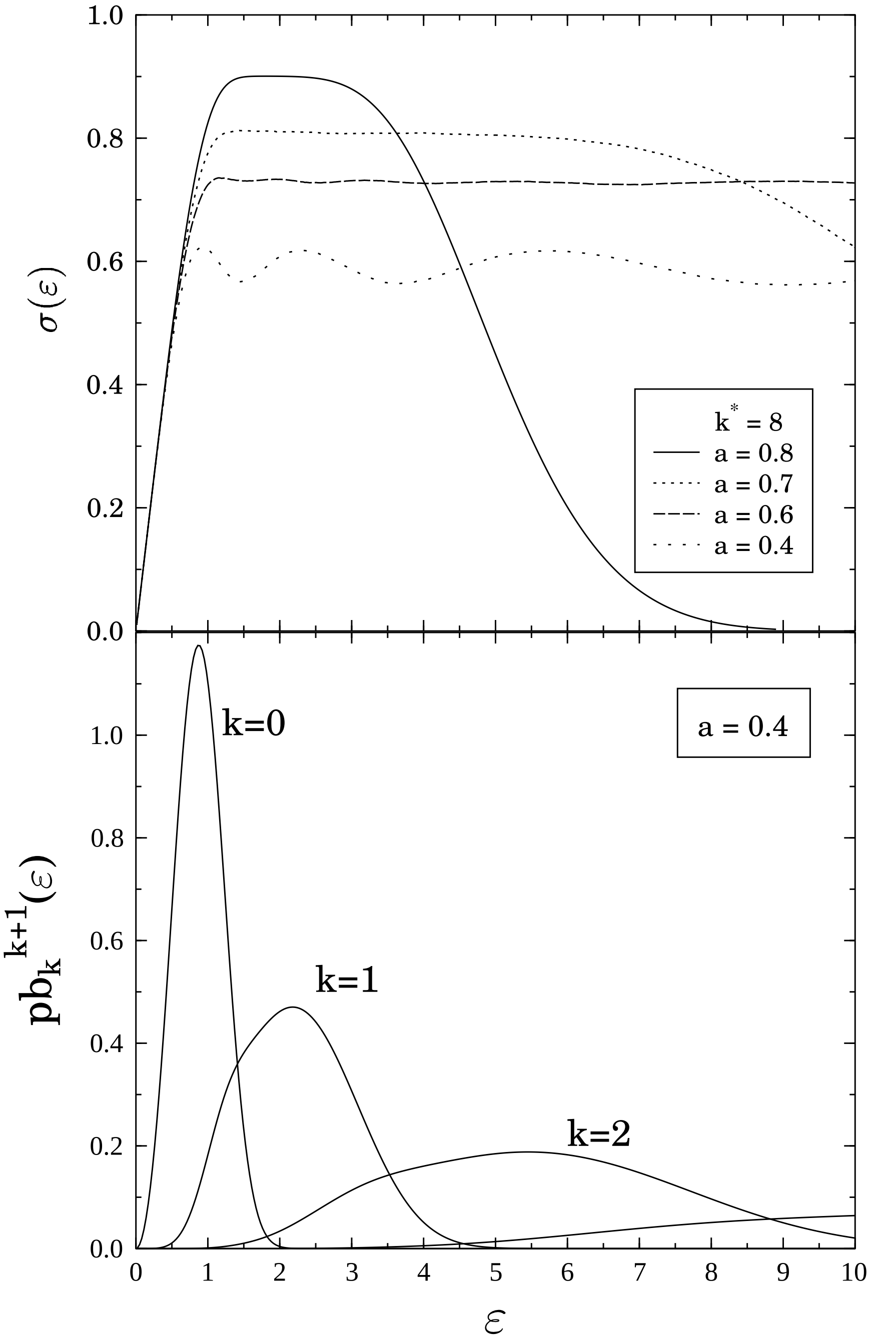

Figure 4.7: $a)$ The constitutive behavior varying the damage threshold at a fixed k^*. $b)$ $pb_k^{k+1}(\varepsilon)$ for $a = 0.4$.

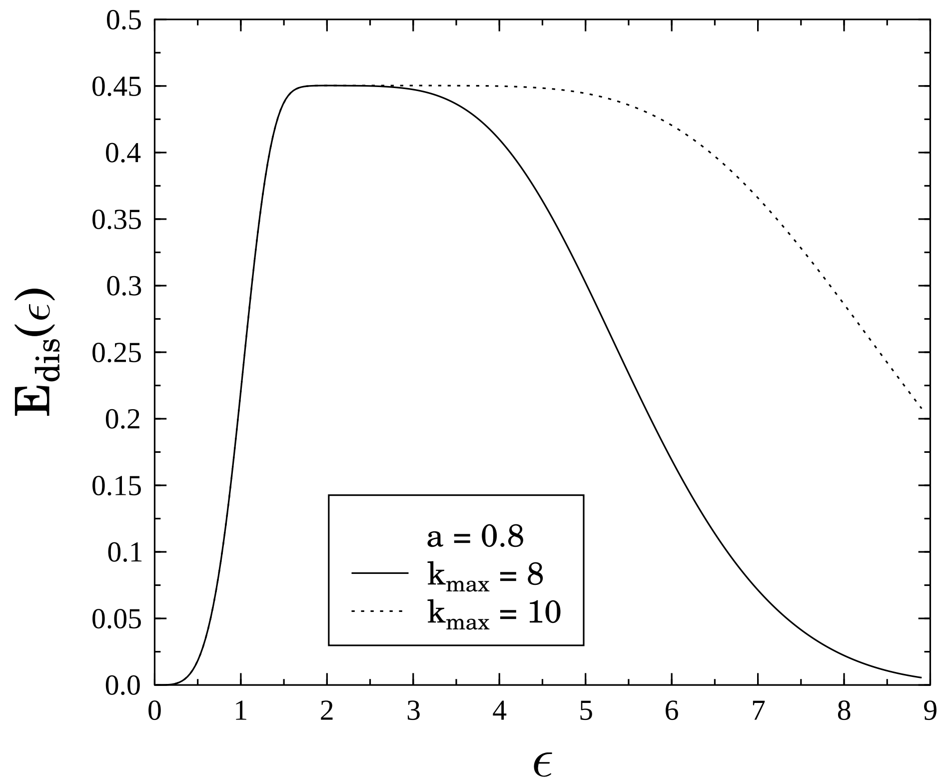

Figure 4.8: The energy dissipation rate for two different values of k_{max}.

4.4.2 Stress controlled case

Under stress controlled loading conditions the microscopic dynamics of the damage process is more complicated than in the strain controlled case, since the failure of each fiber is followed by a redistribution of load, which can provoke further fiber breakings resulting in an avalanche of failure events. Studying the statistics of avalanches under quasi-static loading of a specimen, important information can be gained about the dynamics of damage, which can be then compared to the results of acoustic emission experiments. Due to the difficulties of the analytic treatment, we develop a simulation technique and explore numerically the properties of bursts in our continuous damage fiber bundle model. The interaction of fibers, *i.e.* the type of load redistribution is crucial for the avalanche activity. A very important property of CDFBM is that in spite of the infinite range of interaction the load on intact fibers is not equal, but stiffer fibers carry more load, furthermore, for quenched disorder damage localization occurs, which might also affect the avalanche activity.

To implement the quasi-static loading of a specimen of N fibers in the framework of CDFBM, the local load on the fibers f_i has to be expressed in terms of the external driving F. Making use of Eq. (4.1) it follows that

$$F = \sum_{i=1}^{N} f_i = \epsilon \sum_{i=1}^{N} a^{k(i)}, \tag{4.20}$$

and hence, the strain and the local load on fibers can be obtained as

$$\epsilon = \frac{F}{\sum_{i=1}^{N} a^{k(i)}}, \qquad f_i = F \frac{a^{k(i)}}{\sum_{i=1}^{N} a^{k(i)}}, \tag{4.21}$$

when the external load F is controlled. The simulation of the quasi-static loading proceeds as follows: in a given stable state of the system we determine the load on the fibers f_i from the external load F using Eq. (4.21). The next fiber to break i^* can be found minimizing $\frac{d_i}{f_i}$. Let us define

$$r = \min_{i^*} \frac{d_{i^*}}{f_{i^*}}, \qquad r > 1, \tag{4.22}$$

To ensure that the local load of a fiber is proportional to its stiffness, the external load has to be increased in a multiplicative way, so that

$$F \to rF \tag{4.23}$$

is imposed, and the failure index of fiber i^* is increased by one

$$k(i^*) \to k(i^*) + 1. \tag{4.24}$$

After the breaking of fiber i^*, the load f_i carried by the fibers has to be recalculated making use of Eq. (4.21), which provides also the correct load redistribution of the model. If there are fibers, whose load exceeds the local breaking threshold, they fail, *i.e.* their failure index is increased by 1 and the local load is again recalculated until a stable state is obtained. A fiber cannot break any longer if its failure index k has reached k^* or k_{max} during the course of the simulations. This dynamics gives rise to a complex avalanche activity of fiber breaks, which is also affected by the type of disorder. The size of an avalanche S is defined as the number of breakings initiated by a single failure due to an external load increment.

Simulations revealed that varying the two parameters of the model k_{max}, a, or k^*, a and the type of disorder, the CDFBM shows an interesting variety of avalanche activities, characterized by different shapes of the avalanche size distributions.

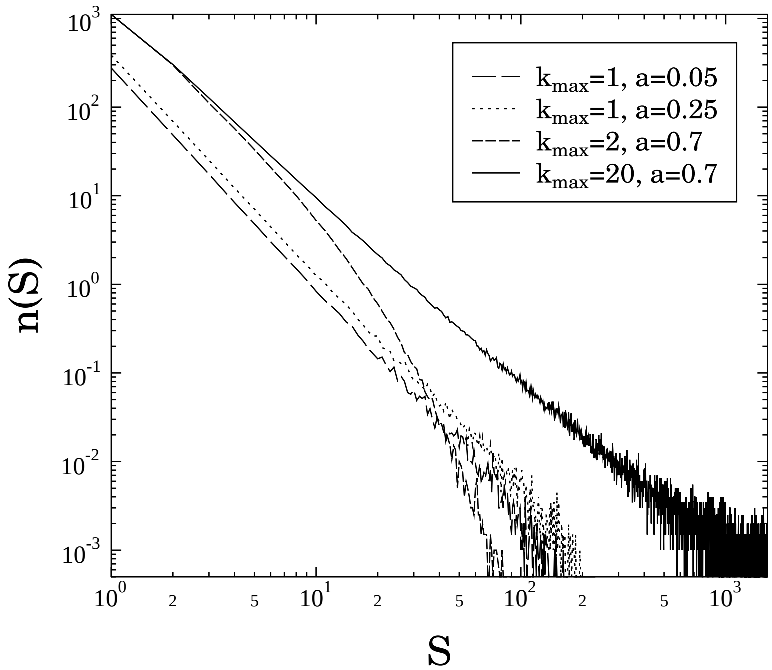

Figure 4.9: Avalanche size histograms for different values of k_{max} and a when fibers have remaining stiffness and the disorder is annealed. The number of fibers was $N = 1600$ and averages were made over 2000 samples. The number of avalanches n of size S are shown to demonstrate also how the total number of avalanches changes.

In Fig. 4.9 the histograms $n(S)$ of the avalanche sizes S are shown which were obtained for a system of remaining stiffness and annealed disorder with Weibull parameters $m = 2$, $d_c = 1$. Since in the limiting case of $a \to 0$ the CDFBM recovers the global load sharing dry fiber bundle model, in Fig. 4.9 the curves with small a and $k_{max} = 1$ are power laws with an exponent $\alpha = 5/2$ in agreement with the analytic results [3, 19, 20, 60]. Increasing the value of a at a fixed k_{max} only gives rise to a larger number of avalanches, *i.e.* parallel straight lines are obtained on a double logarithmic plot, but the functional form of $n(S)$ does not change. However, when a exceeds a critical value a_c ($a_c \approx 0.3$ was obtained with the Weibull parameters specified above) the avalanche statistics drastically changes. At a fixed $a > a_c$ when k_{max} is smaller than a specific value $k_c(a)$, the avalanche sizes show exponential distribution, while above $k_c(a)$ the distribution takes a power law form with an exponent $\beta = 2.12 \pm 0.05$.

Based on the above results of simulations a phase diagram is constructed which summarizes the properties of avalanches with respect to the parameters of the model. Fig. 4.10 demonstrates the existence of three different regimes. If the damage parameter a is smaller than a_c, the dynamics of avalanches is close to the simple Dry Bundle Model

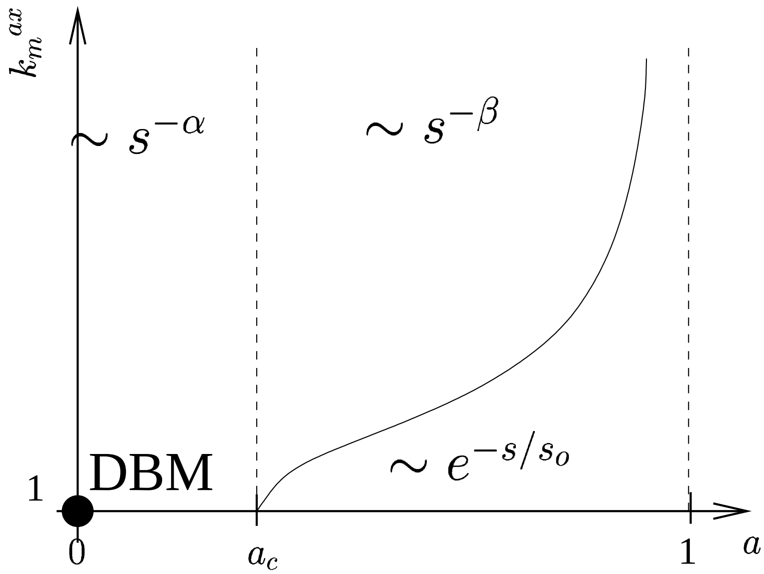

Figure 4.10: Phase diagram for the continuous damage model with remaining stiffness for both types of disorder. The functional form of the avalanche statistics is given in the parameter regimes. The location of the Dry Bundle Model (DBM) in the parameter space is also indicated.

characterized by a power law of the mean field exponent $\alpha = -\frac{5}{2}$. However, for $a > a_c$ the avalanche size distribution depends on the number of failures k_{max} allowed. The curve of $k_c(a)$ in the phase diagram separates two different regimes. For the parameter regime below the curve, avalanche distributions with an exponential shape were obtained. However, the parameter regime above $k_c(a)$ is characterized by a power law distribution of avalanches with a constant exponent $\beta = 2.12 \pm 0.05$ significantly different from the mean field exponent $\alpha = -\frac{5}{2}$ [3, 19, 20, 60]. It is important to emphasize that the overall shape of the phase diagram is independent on the type of disorder (annealed or quenched), moreover, the specific values $a_c \approx 0.3$ and $k_c(a)$ depend on the details of the disorder distribution $p(d)$.

A very different behavior was obtained for the system when fibers do not have remaining stiffness after k^* number of failures. Simulations revealed that in this case the avalanche statistics strongly depends on the type of disorder. When the disorder is quenched the size distribution of avalanches follows always the dry bundle results for the whole domain of parameters, *i.e.* $N(S)$ shows power law behavior with an exponent $\alpha = -\frac{5}{2}$. When $k^* > 1$ the larger number of breakings results in more avalanches but the overall distribution does not change. Nevertheless, when the disorder is annealed the system shows a more complex behavior. When a falls below a certain critical value a_c the results are similar to DBM independently of the value of k^*, however, for $a > a_c$ a novel

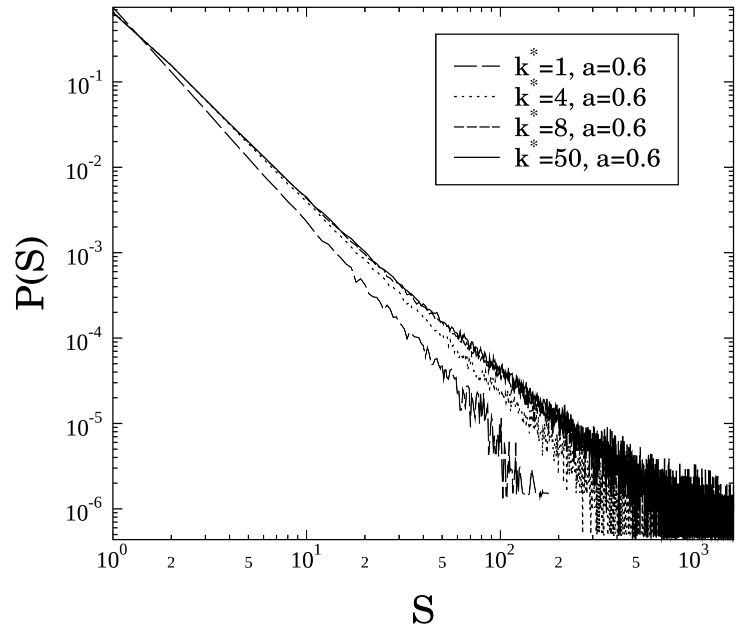

Figure 4.11: Avalanche size distributions for different values of k^* at a fixed $a > a_c$ when fibers have no remaining stiffness and the disorder is annealed.

avalanche dynamics appears (for the present values of the Weibull parameters $a_c \approx 0.35$ was obtained). In Fig. 4.11 the avalanche distributions are shown for an a value above a_c, varying the value of k^*. It is very important to emphasize that the curves in all the cases can be well fitted with a power law, however, the value of the exponent depends on k^*. Two extreme cases can be distinguished: for $k^* = 1$ the system recovers the DBM avalanche dynamics. On the other hand, for $k^* > k_c(a)$ the exponent of the power laws is $\beta = 2.12 \pm 0.05$, similarly to the case of remaining stiffness. Below $k_c(a)$ the exponents τ vary as a function of k^* between the mean field exponent α and β. The phase diagram of Fig. 4.12 summarizes the properties of avalanches with respect to the parameters of the model. It is well known that the breakdown of the reinforced composites is preceded by intense precursors in the form of avalanches. It has been observed that the acoustic emission (AE) response to an increasing external stress takes place in bursts distributed over a wide range of scales. Examples are found in the fracturing of wood [61], and concrete [63]. Those experiments are usually performed increasing the external traction slowly until the material (wood, concrete or fiberglass) macroscopically breaks. The acoustic energy is released and its amplitude shows a net increase as the material approaches the breakdown point. The integrated distribution of burst energies has often been found to follow a power law with an exponent between 1 and 2 [61, 63], which is good agreement with our numerical results.

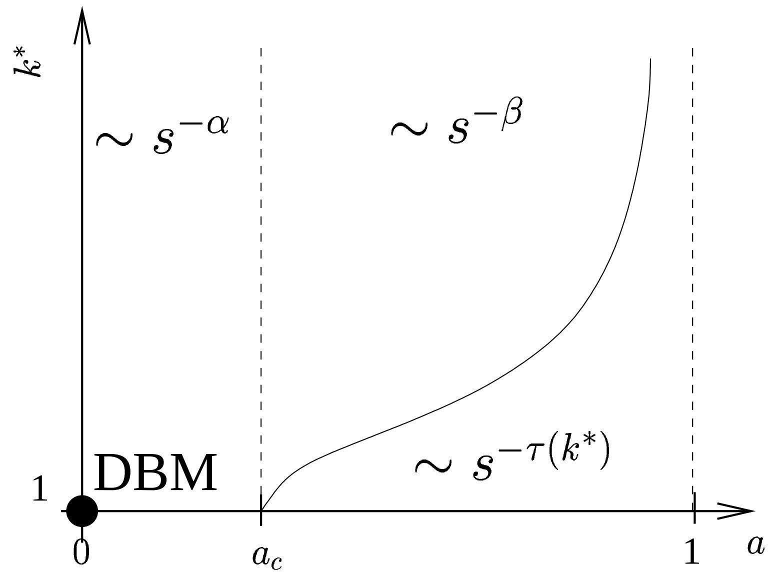

Figure 4.12: Phase diagram for the continuous damage model without remaining stiffness for annealed disorder. The functional form of the avalanche statistics is given in the parameter regimes. The location of the Dry Bundle Model (DBM) in the parameter space is also indicated.

On the other hand, based on Refs. [19] the different types of avalanche size distributions can also be understood up to some extent in terms of the constitutive curves of Sec. 4.2. Checking Fig. 4.3 and Figs. 4.9, 4.11 one can recognize that if the constitutive curve has a single quadratic maximum the corresponding avalanche size distribution of CDFBM follows the mean field results, while other types of avalanche statistics arise when this condition does not hold.

4.5 Conclusions

A detailed analytical and numerical study of the continuous damage fiber bundle model was presented. The model is an extension of the classical fiber bundle model by introducing a continuous damage law, and allowing for multiple failure of fibers with quenched and annealed disorders. A simple general derivation of the constitutive behavior of the model is provided, which also facilitates to obtain analytic results for the microscopic damage process. Varying its parameters, the model provides a broad spectrum for the description of materials ranging from strain hardening to perfect plasticity, and hence, the model can be relevant to describe the damage process of various types of materials [56, 57, 61, 63]. It is a remarkable feature of the model that multiple failure of brittle elements can result in a macroscopically plastic state, which has also been observed experimentally in materials where the damage mechanism is the gradual multiple failure of ingredients. We also focused on the microscopic damage process to understand the emergence of the plastic plateau under strain controlled loading, and the resulting avalanche activity under stress controlled loading of the continuous damage fiber bundle model. Analytic results are obtained to characterize the damage process along the plateau under strain controlled loading, furthermore, for stress controlled experiments a simulation technique was developed and the distribution of avalanches of fiber breaks was explored numerically. Simulations showed that depending on the parameters of the model the distribution of bursts of fiber breaks can be exponential or power law. Based on extensive computer simulations, a phase diagram characterizing the possible avalanche distributions is constructed in terms of the two parameters of the model. One of the most appealing outcomes is that the model has a broad parameter regime where the avalanche statistics shows a power law behavior with an exponent significantly different from the well know mean field exponent, in spite of the infinite range of interaction among fibers. The results obtained have relevance to understand the acoustic emission measurements performed on various elasto-plastic materials [61, 63].

Chapter 5

Evolution of percolating force chains in compressed granular media

In a granular packing the forces are transfered from grain to grain through their contacts which one can consider as nearly point-like. In this way the forces go along lines which can branch at a grain generating a force network. These force networks can be experimentally visualized by means of photoelasticity using grains made of photoelastic material, and putting them between crossed polarizers and shining light through the setup. When the packing is loaded and a certain grain is stressed, it rotates the optical axis and lights up. In this way the force network becomes visible as a beautiful lightened pattern as figure 5.1 shows. One can even observe in these photoelastic experiments that while the external stress is increased, more and more force lines appear and that each force line undergoes an erratic transformation before reaching a stationary state at high enough load in which all the grains light up equally [89]. In this chapter the generation and evolution of percolating force chains is studied experimentally and theoretically in granular packings subjected to an uniaxial external load. The macroscopic constitutive behavior and the acoustic signals emitted by microscopic restructuring events compressing an ensemble of spherical glass bead confined in a cylinder were measured. Based on an analogy of force lines percolating through the system and fibers of a fiber composite we propose a novel theoretical approach, namely, an inversion of the Continuous Damage Model of fiber bundles to describe the stress transmission through granular assemblies. The model naturally captures the emergence and gradual hardening of force chains and provides analytic solutions for the constitutive behavior and acoustic activity [90–92].

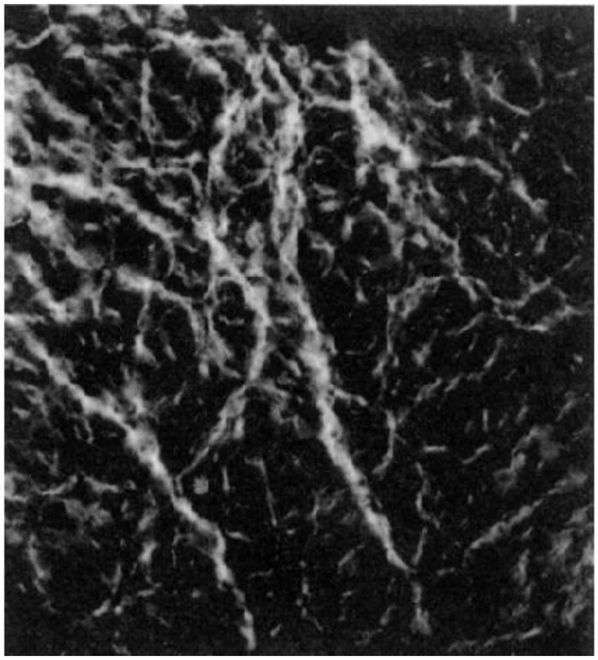

Figure 5.1: An image of the force chains in a granular media as viewed between two crossed circular polarizers. The particles, 3-mm Pyrex spheres are surrounded by an index-matching fluid. The force is exerted on a piston that covers the top surface [89].

5.1 Compression of a Granular Media

Recently, the behavior of granular materials has been extensively studied under various conditions due to their scientific and technological importance. Huge experimental and theoretical efforts have been devoted to obtain a better understanding of the global behavior of granular media in terms of microscopic phenomena which occur at the level of discrete particles [89, 93–98]. Subjecting a confined granular packing to an uniaxial compression a rather peculiar constitutive behavior can be observed: for small strains a strong deviation from the linear elastic response can be found implying that the system drastically hardens in this regime [93, 98]. Linear elastic behavior can only be achieved asymptotically at larger deformations when the system gets highly compacted. When the external load is decreased again the system shows an irreversible increase in its effective stiffness, furthermore, under cyclic loading hysteretic behavior is obtained.

Microscopically, inside a compressed granular packing, stresses are transferred by the contact of particles. Under gradual loading conditions the particles get slightly displaced changing their contacts and the local load supported by them, which can be experimentally visualized using photoelastic materials for grains. These experiments revealed that in a compressed granular system the stresses are transmitted along the direction of the exter-

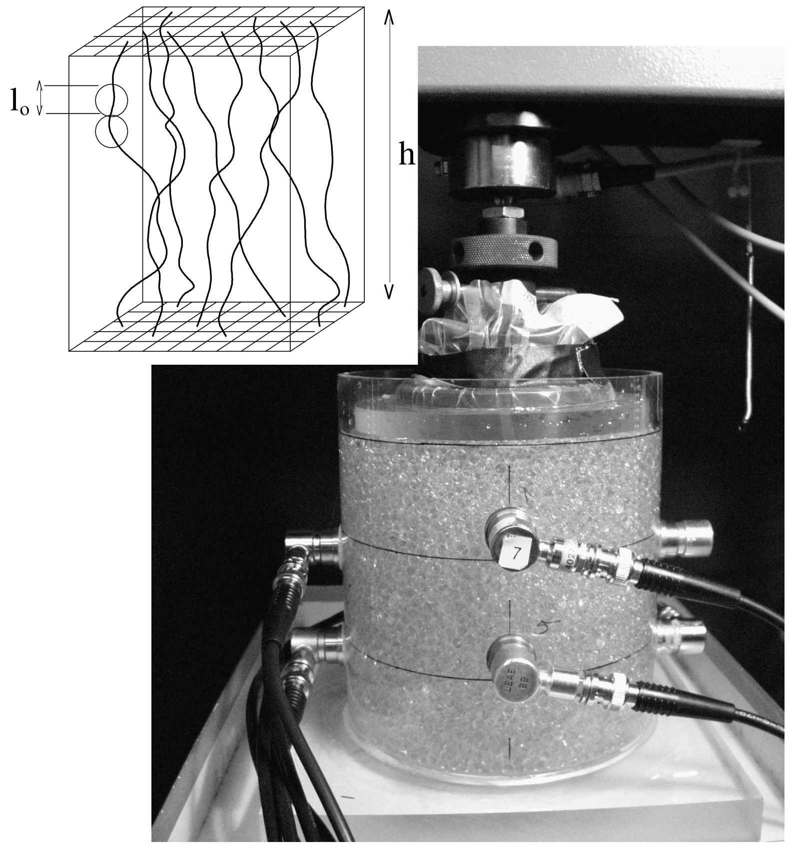

Figure 5.2: Experimental set up and sketch of the array of force chains used in the model. The eight acoustic emission sensors can be observed on the container

nal load by force chains which can branch at the grains and form a complex network [89]. Particles lying between lines of the force network do not support any load and can even be removed from the packing without changing its mechanical properties. Increasing the external load, more and more force lines appear and they all undergo erratic changes until the system reaches a saturated state when all the particles hold typically the same load and the system behaves as a bulk material. The creation and restructuring of percolating force chains implies relative displacements of particles which can be followed experimentally by recording the acoustic waves emitted, however, up to now no such experiments have been performed systematically. Theoretically, this problem has been mainly studied by means of contact dynamics simulations using spherical or cylindrical particles, and cellular automata [95–98]. Computer simulations also revealed the generation and evolution of force chains in compressed granular materials, however, the statistics of microscopic restructuring events, the emergence of the array of force chains and their relation to the macroscopic constitutive behavior remained unclarified.

5.2 Experiment Description

In collaboration with the *Institute of Construction Materials* (IWB) at University of Stuttgart, the evolution of effective force chains percolating through a granular system under uniaxial compression was experimentally investigated. The actual experiments were performed by the group of Dr. Christian Große.

In the experiments a cylindrical container made of PMMA was filled with glass beads of 5 mm diameter and water. The cylinder has a thickness of 5 mm and a diameter of 140 mm. An uniaxial compression test was carried out applying monotonically increasing displacements at the top level of the glass beads. Experiments were performed under strain controlled conditions at a fixed strain rate, *i.e.* moving the traverse at a constant speed of some mm/minute. The examples of the nonlinear elastic response of the system can be observed in Fig. 5.3 where the measured force is presented as a function of relative displacement of the cylinder top.

To obtain information about microscopic processes, the acoustic waves emitted due to sudden relative displacements of particles were monitored. Eight acoustic sensors were placed at the container wall to record the signals emitted during the compression of the beads, as can be seen in Fig. 5.2. The position of the sensors was chosen in a way that subsequently a 3D localization would be carried out using the sensor data of the acoustic emissions. Usually, the acoustic emission signal energy is relatively weak and a proper coupling of the sensors is required. To enhance the data quality in regard to the signal-to-noise ratio the space between the beads was saturated with water. The water pressure was kept constant during the course of the experiments by making holes in the upper side of the cylinder. An eight channel (two with 10 MHz and six with 1 MHz) transient recorder was used as an analogue-digital converter to enable the storing of the acoustic emission waveforms and a signal-based data. This implies a sampling rate of 1 ms or 100 ns.

Typically several hundred signals were recorded during the experiment. The inset of Fig. 5.4 shows the automatically extracted peak amplitudes of the burst signals versus time. The energy is defined as the integral of the acoustic emission signal amplitude following the onset time. The energy values of the acoustic emissions are summed up in intervals of 30 seconds to elucidate the time dependent evaluation of acoustic emission activity. More details of acoustic emission data analysis and especially signal-based techniques can be found in [99–102]. The statistics of restructuring events is characterized by the distribution $D(s)$ of the height s of peaks, which is presented in Fig. 5.4 on a double logarithmic plot. It can be seen that $D(s)$ shows a power law behavior over two orders of magnitude, the exponent of the fitted straight line is $\delta = 1.15 \pm 0.05$. The data in Fig. 5.4 are obtained from the eight recorders so that the event size distribution presented is an average over the event size distributions detected by each recorder independently. In this way the influence of the position of the recorders is reduced.

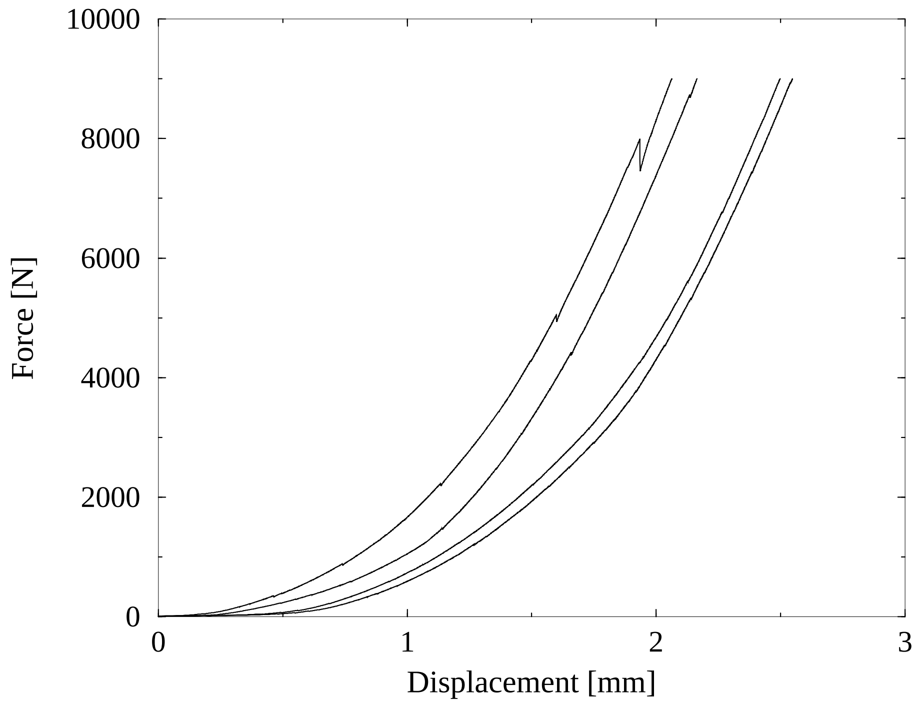

Figure 5.3: Experimental constitutive behavior for different strain rate between $0.1 mm/min$ and $1.0 mm/min$

5.3 Model

We propose a model for the hardening of the individual force lines during compression by using an analogy to the fiber models used in rupture mechanics to describe the failure of fiber-reinforced composites. Our theoretical approach is named an inverted fiber bundle model. Under applied external load the constitutive behavior of the fiber bundle models are linear for small stresses (see Chapter 3). With increasing stress, the weakest elements reach their breaking threshold values and the nonlinearity appears. So that, the microscopic damage evolves inside the sample and after each breaking event the fiber becomes softer. Our model for hardening force networks inverts this situation. The individual lines of the network are considered as fibers which instead of rupturing under tension do harden under pressure due to contact rearrangements.

Fiber bundles are composed of parallel fibers of identical elastic properties but stochastically distributed breaking thresholds. A fiber fails during the loading process when the local load on it exceeds its breaking threshold. Fiber failures are followed by a redistribution of load on the remaining intact fibers according to the range of interaction in the system. The so-called Continuous Damage Model (CDM) introduced in section 4, is

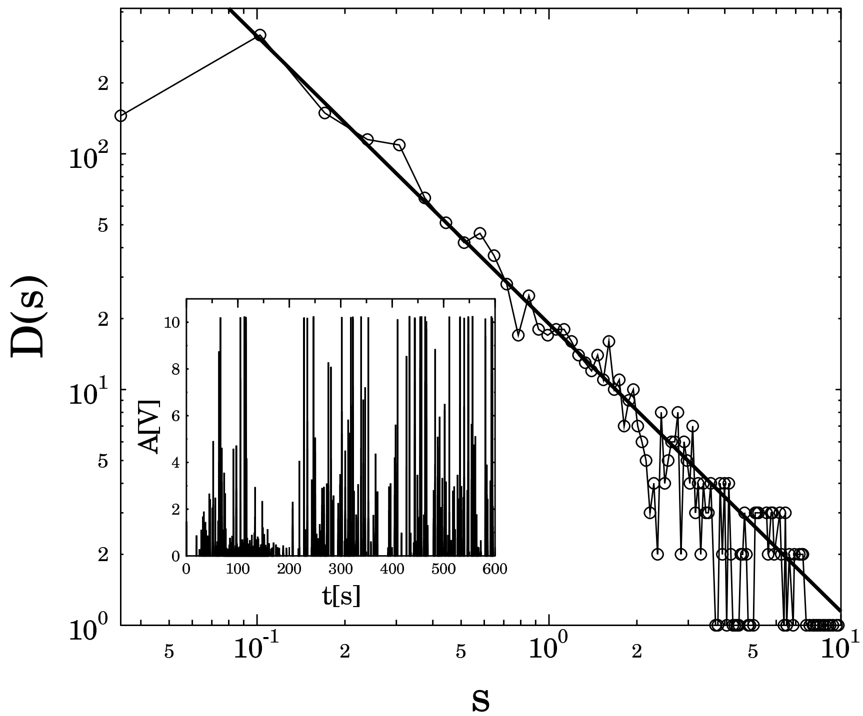

Figure 5.4: The statistics of acoustic signals. A power law of an exponent $\delta = 1.15 \pm 0.05$ was fitted to the size distribution of the signals of the inset.

particularly suited to model granular materials since it captures gradual stiffness changes of elements of the model. In our model of compressed packings, force lines formed by particles are represented by an array of lines organized in a square lattice as illustrated in the inset of Fig. 5.2. A randomly distributed rearrangement threshold d is assigned to each line of the array from a cumulative probability distribution $P_0(\frac{d}{d_c})$, where d_c denotes the characteristic strength of force lines.

During the compression process, when the local load on a line exceeds its threshold value d the line undergoes a sudden restructuring as a result of which it becomes stiffer and straighter. The lines' stiffness increases in a multiplicative manner, *i.e.* the stiffness is multiplied by a factor $a > 1$ at each restructuring so that the constitutive equation of a single line after suffering k restructurings reads as $\sigma = E_o a^k \varepsilon^\alpha$. Here E_o denotes the stiffness characterizing single particle contacts, and the exponent α takes into account possible non-linearities of a single contact like for Hertz law $\alpha = 1.5$. After each rearrangement the force chain gets a new threshold value (annealed disorder) from a distribution of the same functional form, but the characteristic strength d_c of the distribution is increased in a multiplicative way so that after k rearrangement events the disorder distribution takes

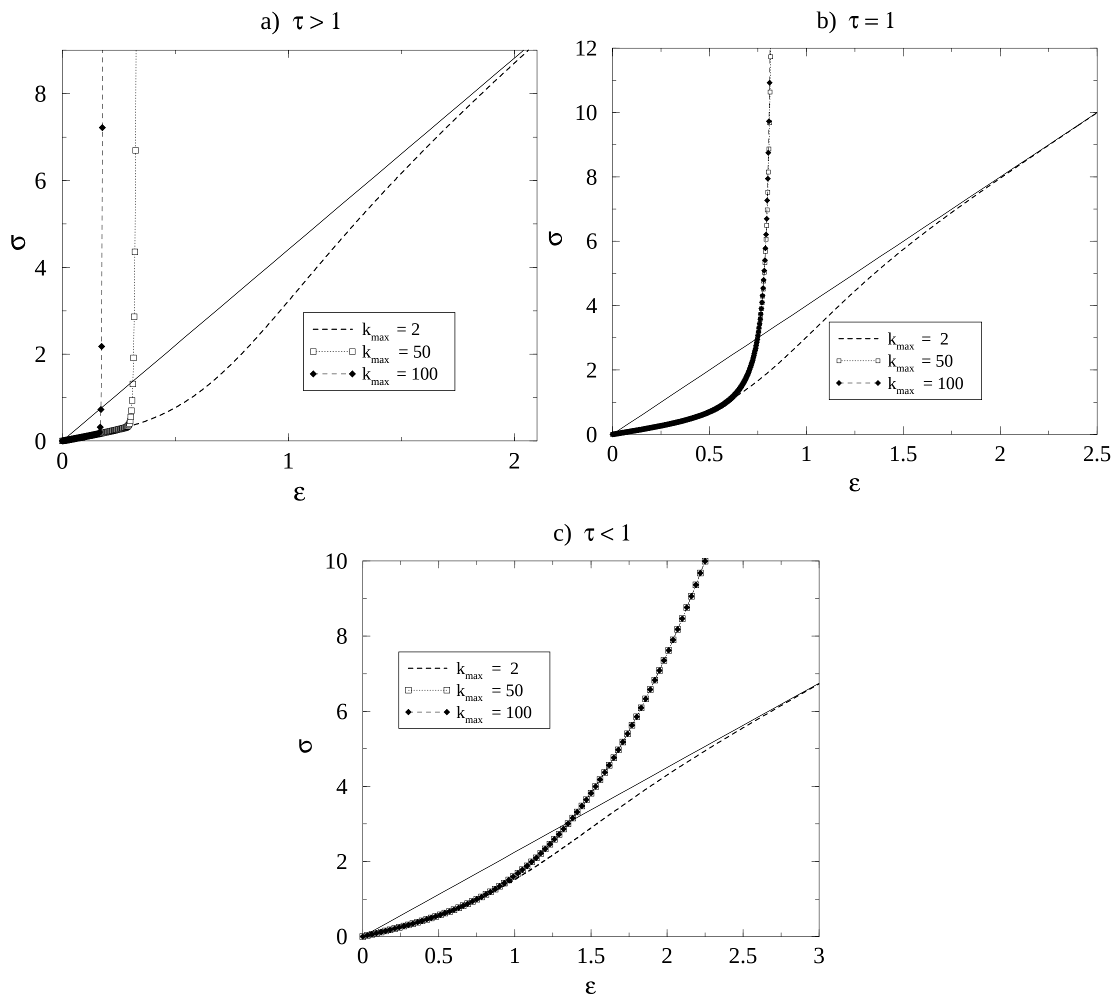

Figure 5.5: Constitutive behavior of the model for different values of k_{max} and τ. The cumulative Weibull distribution with $\rho = 2$ and $d_c = 1$ was used.

the form

$$P_k(\frac{d}{d_c}) = P_0(\frac{d}{d_o q^k}). \tag{5.1}$$

The corresponding distribution density reaches as

$$p_k(\varepsilon) = \frac{dP_k(\varepsilon)}{d\varepsilon}. \tag{5.2}$$

The maximum value of possible restructurings k_{max} is proportional to the number of contacts, and therefore, to $\frac{h}{l_o}$ (see inset of Fig. 5.2). The ratio $\tau = \frac{a}{q}$ is a very important parameter of the model, it decides whether the force chain becomes more fragile ($\tau > 1$) or more ductile ($\tau < 1$) as a result of restructuring.

Following the derivation of the constitutive behavior of the CDFBM of fiber bundles (see Sec. 4) the relation between the stress σ and the strain ϵ is given by

$$\sigma(\varepsilon) = \sum_{i=0}^{k_{max}-1} a^i E_o \varepsilon^\alpha [1 - P_i(a^i\varepsilon)] \prod_{j=0}^{i-1} P_j(a^j\varepsilon) + a^{k_{max}} E_o \varepsilon^\alpha \prod_{i=0}^{k_{max}-1} P_i(a^i\varepsilon). \tag{5.3}$$

The first part of Eq. (5.3) contains the elements which have undergone $i < k_{max}$ restructurings characterized by the local stiffness $E_o a^i$. The second part includes the elements which have already reached k_{max} and the local stiffness $E_o a^{k_{max}}$.

When the particles are elastic $a^{k_{max}}$ is a finite value related to the stiffness of an individual particle as $E_p = a^{k_{max}} E_o$. In this cases after all the fibers reach the allowed restructuring event number k_{max} the system will have the same constitutive behavior as a single contact.

The nonlinear stress-strain curves observed in the figures 5.5 $a)$, $b)$ and $c)$ are in good qualitative agreement with previous experimental and numerical works [93, 95, 96]. The superposition of the curves for $\tau \leq 1$ and big values of k_{max} supports that the solution for $k_{max} = \infty$ will have the same shape. Moreover for $\tau \geq 1$ the shape of the curves suggests the existence of a finite and non-zero critical value of strain ε_c.

For the case $\tau = 1$ the stress and the threshold stress increase with exactly the same prefactor. Therefore the cumulative distribution for restructuring the kth time is independent on k and consequently the same for all the fibers and only depends on the strain value $P_k(a^k\varepsilon) = P_0(\varepsilon)$. For that case the constitutive law Eq. (5.3) takes de form

$$\sigma(\varepsilon) = \varepsilon^\alpha (1 - P_0(\varepsilon)) \sum_{i=0}^{k_{max}-1} a^i P_0(\varepsilon)^i + a^{k_{max}} \varepsilon^\alpha P_0(\varepsilon)^{k_{max}}. \tag{5.4}$$

It can be seen from Eq. (5.4) that if the maximum number k_{max} of possible restructuring events goes to infinity the stress σ has finite values only for $aP_0(\varepsilon) < 1$. In this case the summation can be performed in the first term, while the second term tends to zero, and the constitutive equation takes the form

$$\sigma(\varepsilon) = E_o \varepsilon^\alpha \left[1 - P_0(\varepsilon)\right] \frac{1}{1 - aP_0(\varepsilon)}. \tag{5.5}$$

It follows that the stress σ diverges when ε approaches a critical value ε_c, where ε_c satisfies the equation $P_0(\varepsilon_c) = 1/a$. Expanding $P_0(\varepsilon)$ into a Taylor series at ε_c

$$P_0(\varepsilon) = P_0(\varepsilon_c) + p_0(\varepsilon_c)(\varepsilon_c - \varepsilon) + \ldots, \tag{5.6}$$

and assuming linear contact ($\alpha = 1$) the behavior of σ in the vicinity of ε_c reads as:

$$\sigma(\varepsilon) \sim (\varepsilon_c - \varepsilon)^{-1}, \tag{5.7}$$

with

$$\varepsilon_c = \frac{1}{a}. \tag{5.8}$$

This result is also valid for other distributions, while the critical value ε_c changes. For a cumulative Weibull distribution

$$P_k(d) = 1 - e^{-(\frac{d}{d_o^k})^\rho}, \tag{5.9}$$

a value of critical strain

$$\varepsilon_c = \left[\ln\left(\frac{a}{a-1}\right)\right]^{\frac{1}{\rho}} \tag{5.10}$$

was obtained.

It means that the stress σ shows a power law divergence when ε approaches the critical value ε_c. The value of the exponent is universal; it does not depend on the form of disorder distribution $P_0(\varepsilon)$, while the value of ε_c depends on it. It is interesting to note that in Ref. [97] the same power law divergence with an exponent 5.7 was found in large scale molecular dynamics simulations of a hard sphere system. Unfortunately, this divergence in the vicinity of ε_c could not be studied with the present experimental setup.

When the number of force lines is fixed it is possible to obtain analytic results also for the statistics of restructuring events. Under strain controlled loading of a fiber bundle the load on a fiber is determined by its local stiffness and the strain imposed externally. Applying the CDM to compressed granular systems the same assumption is made, *i.e.* there is no load redistribution among existing force lines, hence, the restructuring of a force line does not affect other elements of the system. Restructuring occurs during the compression process when the local load on a force line exceeds its threshold value. If the new threshold value, assigned to the force line after rearrangement, is smaller than the local load, the force line undergoes successive restructurings until it gets stabilized. The number of steps to reach the new stable state defines the size s of the restructuring events. The number of restructuring events $N_{k,s}$ of size s starting in force chains which have already suffered k restructurings can be deduced as

$$\frac{N_{k,s}(\varepsilon)}{N_o} = p_0(\varepsilon) P_0^{s+k-1}(\varepsilon)\left[1 - P_0(\varepsilon)\right], \tag{5.11}$$

for $s + k \leq k_{max} - 1$, and

$$\frac{N_{k,s}(\varepsilon)}{N_o} = p_0(\varepsilon) P_0^{k_{max}-1}(\varepsilon), \tag{5.12}$$

for $s + k = k_{max}$

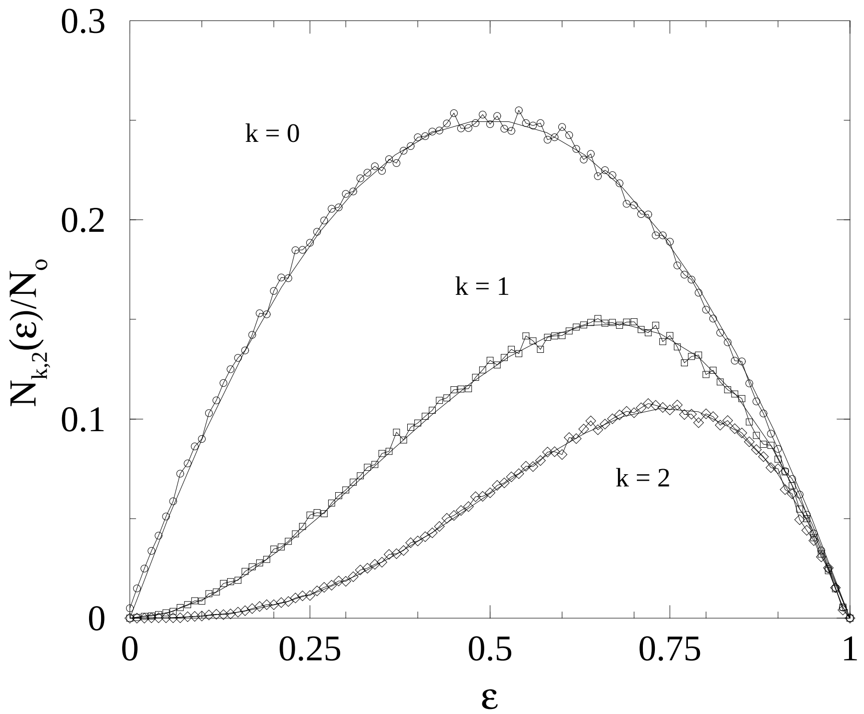

Figure 5.6: Conditional probability for the appearance of an event of size $i = 2$ if the line of force had already k reordering events. Both numerical and analytical results are shown.

This conditional probability is normalized by the total number of elements N_o and is shown in Fig. 5.3 for severals values of k. The number of events of size s, *i. e.* $D(s)$ is deduced taking into account the whole compression process and all the starting configurations. Hence, this magnitude can be calculated as

$$D(s) = \sum_{k=0}^{k_{max}-s} \int_0^{\varepsilon^*} \frac{N_{k,s}(\varepsilon)}{N_o} d\varepsilon + \int_0^{\varepsilon^*} \frac{N_{k_{max}-s,s}(\varepsilon)}{N_o} d\varepsilon. \tag{5.13}$$

Here ε^* denotes the strain value for which all the force chains have reached the maximum number k_{max} of reordering events, thus $P_0(\varepsilon^*) = 1$ follows. Finally, substituting Eqs. (5.11,5.12) into Eq. (5.13)

$$D(s) = \sum_{k=0}^{k_{max}-s} \int_0^1 P^{s+k-1}(1-P)dP + \int_0^1 P^{k_{max}-1} dP, \tag{5.14}$$

and performing the calculations yields

$$D(s) = s^{-1}. \tag{5.15}$$

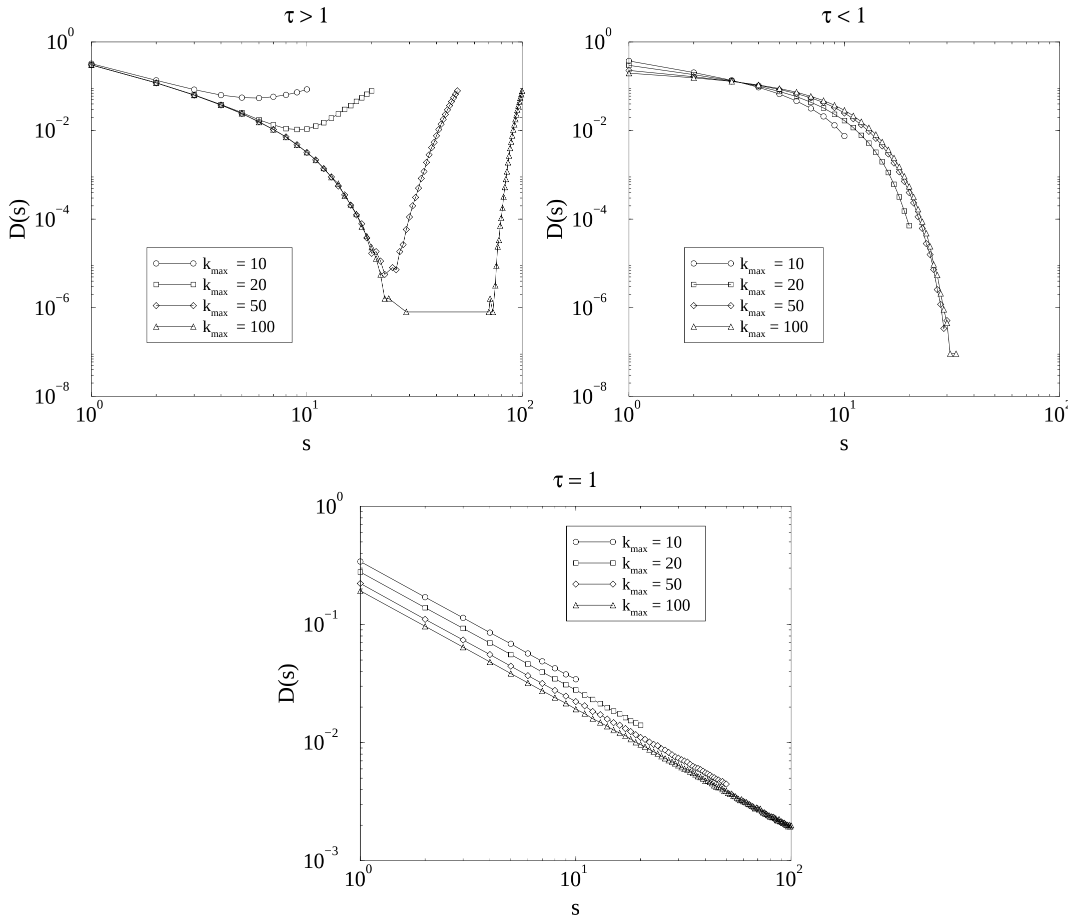

Figure 5.7: Distributions of local avalanches for different values of τ.

The distribution of microscopic restructuring events exhibits an universal power law behavior with an exponent 1, which is completely independent on the disorder distribution.

The numerical results obtained applying the algorithm of the continuous damage model (see Chapter 4) show how the statistics of the process is governed by the value of τ. Our results reveal the existence of different local avalanche regimes which was deduced checking the shape of the local avalanche size distributions. In Fig. 5.7 the results obtained for different values of τ are shown. The condition $\tau > 1$ (see Fig. (5.7) a)) implies whether one element of the system reaches the restructuring threshold value with high probability in the next step it will reach again the new restructuring threshold value. When the element reached the maximum value of k_{max} the local avalanches stop. This results in a peak at the value $s = k_{max}$ in the local avalanche distribution which coincides with the cut off value $S_c = k_{max}$.

The system exhibits the inverse behavior for $\tau < 1$. In those conditions whether one element of the system reaches the restructuring threshold value, the probability to reach the new restructuring threshold value in the next step is very low. This effect is reflected by the shape of the local avalanche size distribution and its maximum at $s = 1$, Fig. 5.7 b). In this case the results for different k_{max} imply that the local avalanche size distribution for hard particles ($k_{max} = \infty$) will have the same shape and a finite cut off S_c.

In the case $\tau = 1$, for all the values of k_{max} the avalanche size distributions have a power law shape with an universal exponent $\beta = -1$. Only the statistics of the events changes with the increase of k_{max}.

The normalized total number of restructuring events $\frac{N_e}{N_o}$ is presented in the Fig. 5.8 for different system sizes. The collapse of the curves shows that the results are independent on the transversal area of the sample. Moreover, the numerical results suggest the existence of a logarithmic dependence between the total number of events and k_{max}, in the case $\tau = 1$. Integrating the equation (5.15), $\frac{N_e}{N_o}$ is deduced as

$$\frac{N_e}{N_o} = \sum_{s=1}^{k_{max}} \frac{1}{s} \sim \int_1^{k_{max}} \frac{ds}{s} = \ln k_{max}. \tag{5.16}$$

As it was already pointed out, the maximum number of restructuring events k_{max} is related to the height of the container h and the particle size l_o as $k_{max} \sim \frac{h}{l_o}$. In this manner, with the assumption of $\tau = 1$, the above result Eq. 5.16 could be used to argue about the type of relationship between the total number of events N_e and the geometrical size of the particles l_o and the container h, since it holds

$$\frac{N_e}{N_o} \sim \ln F(\frac{h}{l_o}). \tag{5.17}$$

At the time of writing this thesis, experiments with different ratios $\frac{h}{l_o}$ were being accomplished. Moreover, it can be seen in Fig. 5.8 that for $\tau > 1$ a saturation of the total number of events N_e appears, and for $\tau < 1$ it diverges with increasing k_{max} .

5.4 Application

Experiments and discrete element simulations [89, 98] have revealed that the number of effective force chains increases during the compression process until it reaches a saturation value. To capture this effect in our model, for the number of elements we prescribe the form

$$N(\varepsilon) = N_o G(\varepsilon), \tag{5.18}$$

where N_o denotes the saturation number of chains, and the profile $G(\varepsilon)$ has the property $G(\varepsilon) \to 1$ with increasing ε. Hence, the number of force lines dN emerging due to an

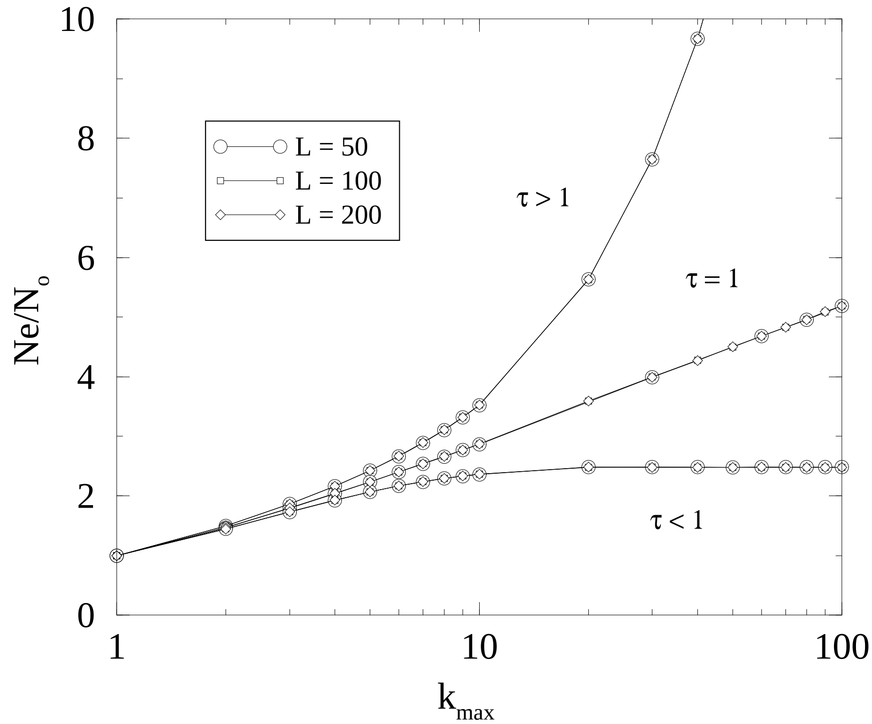

Figure 5.8: Total number of restructuring events for different values of τ and different system sizes

infinitesimal deformation increment from ε to $\varepsilon + d\varepsilon$ is

$$dN = N_o g(\varepsilon) d\varepsilon, \tag{5.19}$$

where

$$g(\varepsilon) = dG(\varepsilon)/d\varepsilon. \tag{5.20}$$

As shown before, following the derivation of the constitutive behavior of the CDFBM of fiber bundles (see Chapter 4), the macroscopic constitutive equation of the compressed granular system for $\tau = 1$ can be cast into the form

$$\begin{aligned}\sigma(\varepsilon) &= E_o \sum_{i=0}^{k_{max}-1} \int_0^{\varepsilon} a^i (\varepsilon - \varepsilon_o)^{\alpha} g(\varepsilon_o) P_0^i(\varepsilon - \varepsilon_o) \left[1 - P_0(\varepsilon - \varepsilon_o)\right] d\varepsilon_o \\ &+ \int_0^{\varepsilon} a^{k_{max}} (\varepsilon - \varepsilon_o)^{\alpha} g(\varepsilon_o) P_0^{k_{max}}(\varepsilon - \varepsilon_o) d\varepsilon_o. \end{aligned}\tag{5.21}$$

The first part of Eq. (5.21) contains the elements which have undergone $i < k_{max}$ restructurings characterized by the local stiffness $E_o a^i$. The second part includes the elements which have already reached k_{max} and the local stiffness $E_o a^{k_{max}}$. Eq. (5.21) takes also

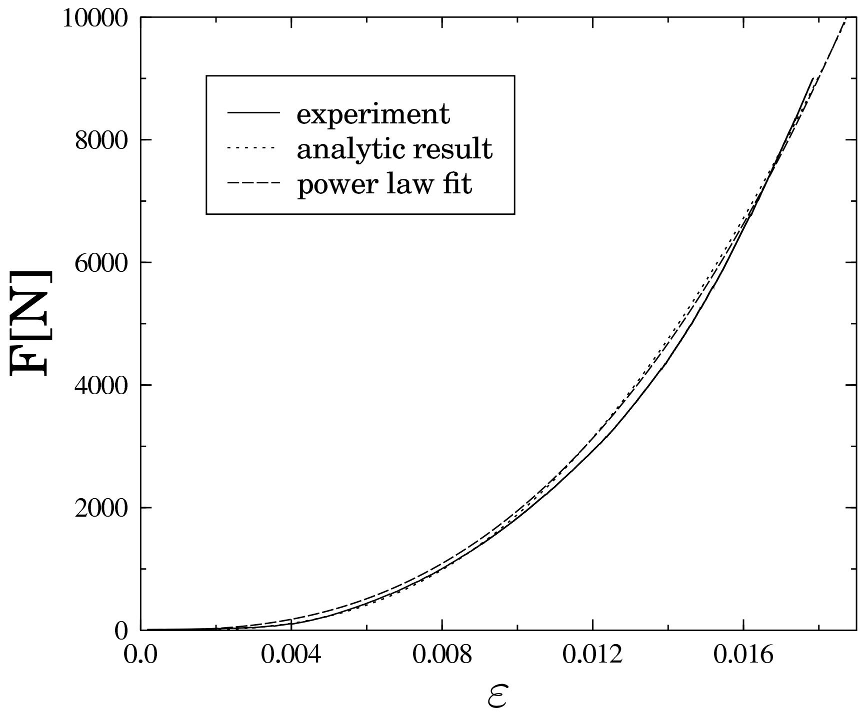

Figure 5.9: Constitutive behavior for small strain values measured experimentally and comparison to the theoretical results.

into account that the local strain of force lines $\varepsilon - \varepsilon_o$ is different from the externally imposed strain value ε since it also depends on the initial strain ε_o. The integral is performed over the whole loading history to take into account all the generated lines. For explicit calculations we imposed an exponential form

$$N(\varepsilon) = N_o(1 - e^{-\frac{\varepsilon}{\beta}}) \tag{5.22}$$

for the number of chains.

The best fit obtained to the experimental data is presented in Fig. 5.9 where the force $F = N_o\sigma$ is plotted against deformation ε. It can be seen that using Eq. (5.21) a good fit was achieved with physically reasonable parameter values. A power law of an exponent 2.6 was obtained as a good fit to the measured data in a reasonable agreement with former experiments of Ref. [93]. The maximum possible number of percolating force chains N_o that can emerge in the system was estimated as the ratio of the total area of the container A_o to the cross section of a single particle A_p, *i. e.* we choose $N_o = \frac{A_o}{A_p} = 784$. An uniform distribution of the restructuring thresholds and a big value of k_{max} were used. The value of the other parameters are $E_o = 4600\frac{N}{m^2}$, $d_o = 3N$, $\beta = 0.01$ and $a = q = 1.01$. The value of a falls close to one meaning that a single restructuring gives rise only to a slight increase of stiffness of a force chain. Model calculations revealed that the zero

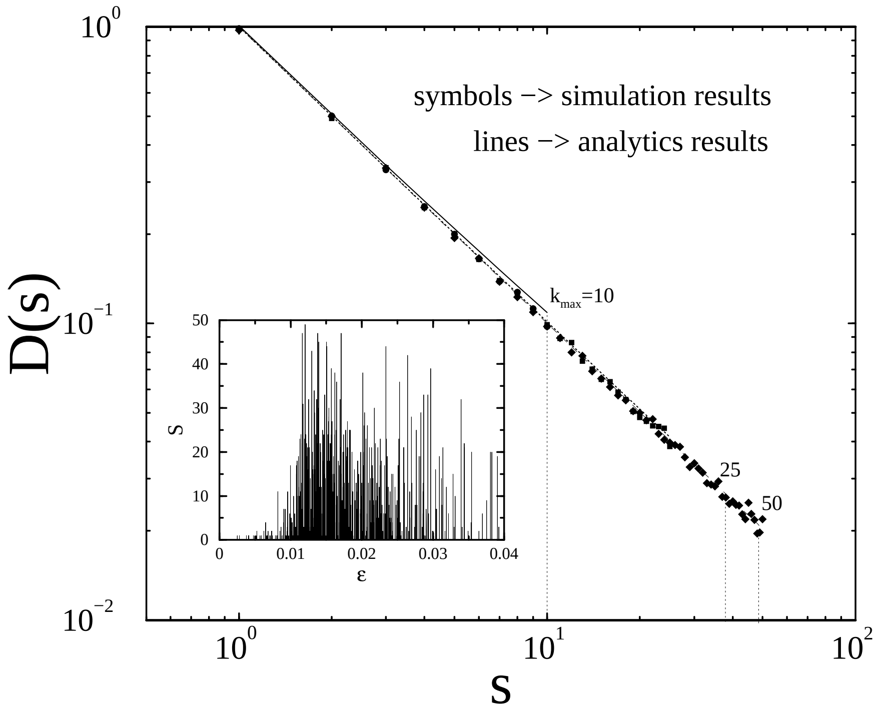

Figure 5.10: Event sizes s occurring during the loading history ε, and their size distribution $D(s)$ on a double logarithmic plot.

derivative at the starting part of the constitutive curve is due to the gradual creation of load bearing force chains [95, 96]. The small value of β implies that the generation of new force chains stops at a relatively small strain value, and hence, the later rapid increase of F as a function of ε is mainly caused by the hardening of the existing force lines occurring due to restructurings.

Numerical simulations revealed that the universal power law behavior also holds when the gradual creation of force chains is taken into account, *i.e.* when the system is described by the full Eq. (5.21). The statistics of restructuring events obtained by Monte Carlo simulations taking also into account the gradual emergence of force lines is presented in Fig. 5.10. The power law behavior of the analytic prediction is verified. It is important to emphasize that the theoretical results on event statistics (see Fig. 5.10) are in a very good quantitative agreement with the experimental findings (see Fig. 5.4).

Note, that the functional form and the value of the exponent of $D(s)$ in the analytic calculations is mainly the consequence of the locality of restructurings due to the absence of load redistribution. Hence, entire restructuring events of size s can occur on a single force line before any of the other force lines is modified. The excellent agreement observed indicates that this is likely the microscopic mechanism responsible for the power law statistics of acoustic signals observed experimentally. At the time of writing this thesis, the localization of the acoustic emission sources was being experimentally accessed.

5.5 Conclusion

The evolution of effective force chains percolating through a compressed granular system was investigated. The experiments were made by compressing an ensemble of spherical particles in a cylindrical container monitoring the macroscopic constitutive behavior and the acoustic signals emitted by microscopic rearrangements of particles. We have presented a simple model of parallel force lines which harden under load due to restructuring events. If the increase of stiffness and the increase in the restructuring threshold stress are equal, the model can be solved analytically. So that, we applied the continuous damage model of fiber bundles to describe the evolution of the array of force chains during the loading process. The model provides a nonlinear constitutive behavior in good quantitative agreement with the experimental results. The stress σ shows a power law divergence when ε approaches the critical value ε_c. The value of the exponent is universal; it does not depend on the form of disorder distribution $P_0(\varepsilon)$, while the value of ε_c depends on it. Unfortunately, this divergence in the vicinity of ε_c could not be studied with the present experimental setup. The rearrangement of granular materials results in a spontaneous release of acoustic energy radiating waves similar to that observed in other brittle materials under load. The amplitude distribution of acoustic signals was found experimentally to follow a power law with an exponent $\delta = 1.15 \pm 0.05$ which is in a good agreement with the analytic solution of the model $D(s) = s^{-1}$. We argue that this is a consequence of the locality of restructurings due to the absence of load redistribution.

Chapter 6

A fracture model with variable range of interaction

In this chapter, it presents a fiber bundle model where the interaction among fibers is modeled by an adjustable stress-transfer function which can interpolate between the two limiting cases of load redistribution, the global and the local load sharing schemes is introduced. By varying the range of interaction several features of the model are numerically studied and a crossover from mean field to short range behavior is obtained. The properties of the two regimes and the emergence of the crossover in between are explored by numerically studying the dependence of the ultimate strength of the material on the system size, the distribution of avalanches of breakings, and of the cluster sizes of broken fibers [38].

6.1 Model

The fracture of heterogeneous systems is characterized by a highly localized concentration of stresses at the crack tips that makes possible the nucleation of new cracks at these regions such that the actual crack grows leading to the final collapse of the system. In elastic materials, the stress redistribution follows a power law,

$$\sigma_{add} \sim r^{-\gamma}, \tag{6.1}$$

where σ_{add} is the stress increase on a material element at a distance r from the crack tip. In fiber-reinforced composites the stress is transfered from the broken elements to the unbroken ones through the matrix. In the neighborhood of a single fiber embedded in an infinite matrix , the stress profile can also be approximated by Eq. 6.1. Moreover,

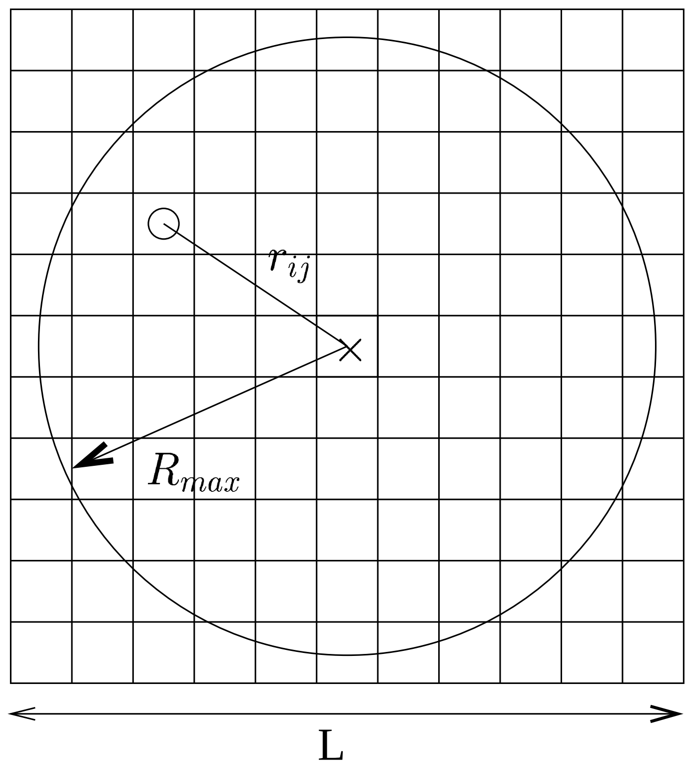

Figure 6.1: Illustration of the model construction. $\times$ indicates a fiber, which is going to break, and $\circ$ is an intact fiber in the square lattice.

the global and local load sharing approaches, introduced before and widely used in fiber bundle models of fracture, are covered by Eq. 6.1 as the limiting cases $\gamma \to 0$, and $\gamma \to \infty$, respectively.

Motivated by the above statements we introduce a fiber bundle model where the load sharing rule takes the form of Eq. (6.1). Suppose a set of N parallel fibers each one having statistically distributed strength taken from a cumulative distribution function $P(\frac{\sigma}{\sigma_o})$ and identified by an integer i, $1 \leq i \leq N$ on a square lattice. Thus, to each fiber i a random threshold value $\sigma_{i_{th}}$ is assigned. The system is driven by increasing quasistatically the load on it, which is performed by locating the fiber which minimizes $\sigma_i - \sigma_{i_{th}}$ and adding this amount of load to all the intact fibers in the system. This provokes the failure of at least one fiber which transfers its load to the surviving elements of the set. This may provoke other fractures in the system which in turn induce tertiary ruptures and so on until the system fails or reaches an equilibrium state where the load on the intact fibers is lower than their individual strengths. In this later case, the slow external driving is applied again and the process is repeated up to the macroscopic failure of the material. The number of broken fibers between two successive external drivings is the size of an avalanche s, and the number of parallel updates of the lattice during an avalanche is called its lifetime T.

We now focus on the load transfer process following fiber failures. We suppose that, in general, all intact fibers have a nonzero probability of being affected by the ongoing failure event, and that the additional load received by an intact fiber i depends on its distance r_{ij} from fiber j which has just been broken. Furthermore, elastic interaction is assumed between fibers such that the load received by a fiber follows the power law form of Eq. (6.1). Hence, in our discrete model the stress-transfer function $F(r_{ij}, \gamma)$ takes the form

$$F(r_{ij}, d) = \frac{r_{ij}^{-\gamma}}{Z}, \tag{6.2}$$

where γ is our adjustable parameter, Z is given by the normalization condition

$$Z = \sum_{i \in I} r_{ij}^{-\gamma}, \tag{6.3}$$

the sum runs over the set I of all intact elements and r_{ij} is the distance of fiber i to the rupture point (x_j, y_j), *i.e.*,

$$r_{ij} = \sqrt{(x_i - x_j)^2 + (y_i - y_j)^2} \tag{6.4}$$

in 2D. Periodic boundary conditions are assumed so that the largest r value is $R_{max} = \frac{\sqrt{2}(L-1)}{2}$, where L is the linear size of the system. We note here that the assumption of periodic boundary conditions is made for simplicity. In principle, an Ewald summation procedure would be more accurate. The model construction is illustrated in Fig. 6.1. It is easy to see that in the limits $\gamma \to 0$ and $\gamma \to \infty$ we recover the two extreme cases of load redistribution in fiber bundle models: the global load sharing and the local load sharing, respectively. We should note here that, strictly speaking, for all γ the range of interaction covers the whole lattice. However, when changing this exponent, one moves from a very localized *effective* range of interaction to a truly global one as γ approaches zero. So, we will refer henceforth to a change in the *effective* range of interaction.

In summary, during an avalanche of failure events, an intact fiber i receives at each time step τ the load borne by failing elements j. Consequently, its load increases by an amount,

$$\sigma_i(t+\tau) = \sigma_i(t+\tau-1) + \sum_{j \in B(\tau)} \sigma_j(t+\tau-1) F(r_{ij}, \gamma), \tag{6.5}$$

where the sum runs over the set $B(\tau)$ of elements that have failed in a time step τ. Thus,

$$\sigma_i(t_0 + T) = \sum_{\tau=1}^{T} \sigma_i(t_0 + \tau) \tag{6.6}$$

is the total load element i receives during an avalanche initiated at t_0 and which ended at $t_0 + T$. In this way, when an avalanche ends, the external field is applied again and another avalanche is initiated. The process is repeated until no intact elements remain in the system and the ultimate strength of the material σ_c, is defined as the maximum load the system can support before its complete breakdown.

Unfortunately, the complete analytical approach to the general model introduced here is not possible. There are a few cases where this task can be achieved such as the global load sharing model where the load acting on surviving elements for a given external force F is known [1–3, 19, 20]. The main difficulty is that in order to analytically solve the problem, one needs to know the transition probabilities for all the possible paths leading the system from the state in which all the elements are intact to the state in which they have failed. This calculation eventually becomes impossible for large system sizes. So, a first step is to learn from Monte Carlo simulations which, furthermore, allows us to better understand the physical mechanisms of fracture and to study models difficult to handle analytically as well as to guide our search for analytical calculations.

6.2 Monte Carlo simulation of the failure process

We have carried out large scale numerical simulations of the model described above in two dimensions. The fibers are identified with the sites of a square lattice of linear size L with periodic boundary conditions. The failure process is then simulated by varying the effective range of interaction between fibers by controlling γ, and recording the avalanche size distribution, the cluster size distribution and the ultimate strength of the material for several system sizes. Each numerical simulation was performed over at least 50 different realizations of the disorder distribution.

Figure 6.2 shows the ultimate macroscopic strength of a bundle of single fibers which have a cumulative Weibull threshold distribution $P(\frac{\sigma}{\sigma_o}) = 1 - e^{-\left(\frac{\sigma}{\sigma_o}\right)^{\rho}}$. In that case a disorder parameter $\rho = 2$ and a characteristic strength $\sigma_o = 1$ were used. Different values of the parameter γ were explored and the calculation was made for several system sizes from $L = 33$ to $L = 257$. Clearly, two distinct regions can be distinguished. For small γ, σ_c is independent, within statistical errors, of both the effective range of interaction and the system size. At a given point $\gamma = \gamma_c$ a crossover is observed, where γ_c falls in the vicinity of $\gamma = 2$. The region $\gamma > \gamma_c$ might eventually be further divided into two parts, the first region characterized by the dependence of the ultimate strength of the bundle on both the system size and the effective range of interaction; and a second region where σ_c only depends on the system size. This would mean that there might be two transition points in the model, for which the system displays qualitatively and quantitatively different behaviors. For $\gamma \leq \gamma_c$ the ultimate strength of the bundle behaves as in the limiting case of global load sharing, whereas for $\gamma \geq \gamma_c$ the local load sharing behavior seems to prevail. Nevertheless, the most important feature is that when decreasing the effective

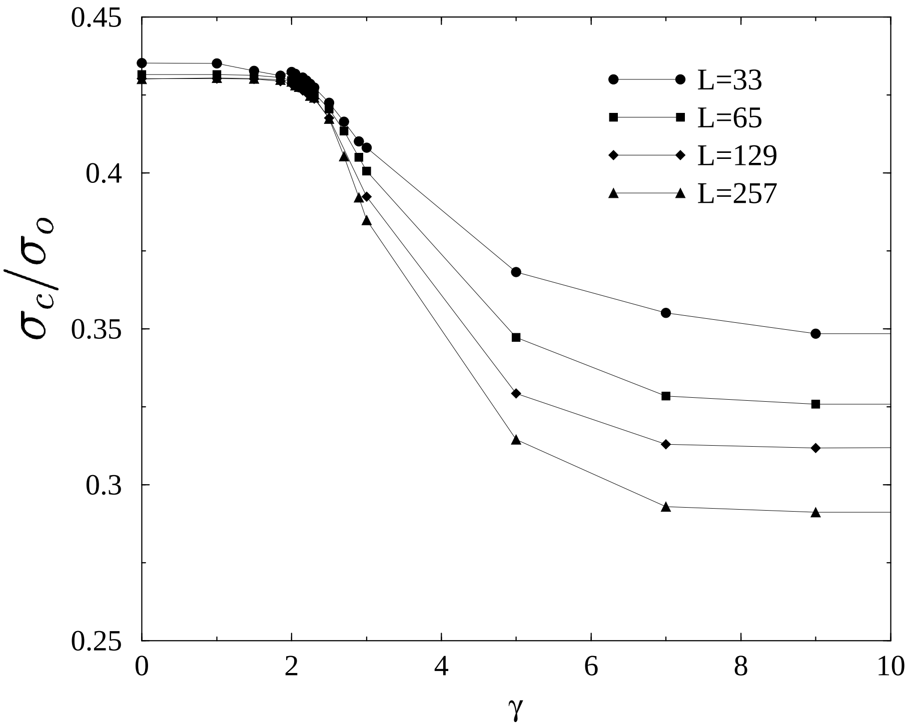

Figure 6.2: Variation of the material strength with N for several values of γ. Note that when γ increases the critical load vanishes in the thermodynamic limit, whereas, for small γ it has a nonzero value independent on the system size.

range of interaction in the thermodynamic limit, for $\gamma > \gamma_c$, the critical load is zero. This observation is further supported by Fig. 6.3, where we have plotted the evolution of σ_c as a function of $\frac{1}{\ln N}$ for different values of the exponent γ. Here, the two limiting cases are again clearly differentiated. For large γ all curves decrease when $N \to \infty$ as

$$\sigma_c(N) \sim \frac{\alpha}{\ln N} + C. \tag{6.7}$$

This qualifies for a genuine short range behavior as found in LLS models where the same relation was obtained for the asymptotic strength of the bundle [19, 103]. It is worth noting that in the model we are analyzing, the limiting case of local load sharing corresponds to cases in which short range interactions are considered to affect the nearest and the next-nearest neighbors. In the transition region, the maximum load the system can support also decreases as we approach the thermodynamic limit, but in this case much slower than for $\gamma \gg \gamma_c$. It has been pointed out that for some modalities of stress transfer, which can be considered as intermediate between GLS and LLS, σ_c decreases for large system sizes following the relation $\sigma_c \sim \frac{1}{\ln(\ln N)}$ as in the case of hierarchical load transfer models [31]. In our case, we have fitted our results with this relation but we have not obtained a single collapsed curve because the slopes continuously vary until the LLS limit

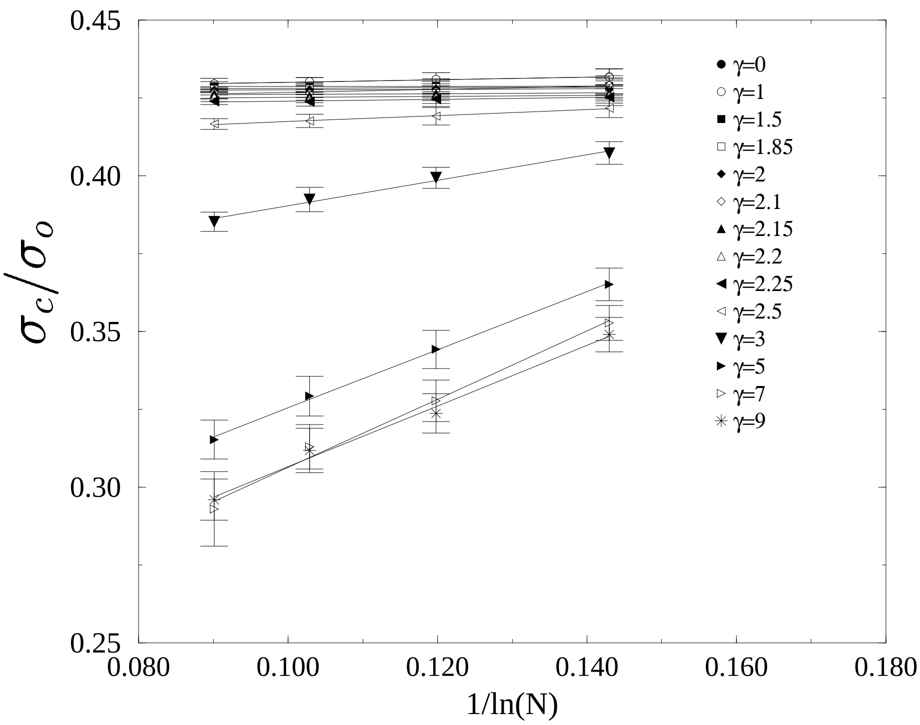

Figure 6.3: Ultimate strength of the material for different system sizes as a function of the effective range of interaction γ. A crossover from mean field to short range behavior is clearly observed.

is reached. Finally, the region where the ultimate stress does not depend on the system size shows the behavior expected for the standard GLS model, where the critical load can be exactly computed as $\frac{\sigma_c}{\sigma_o} = (\rho e)^{-1/\rho}$ for the Weibull distribution. The numerical values obtained for different values of ρ are in excellent agreement with this later expression. To determine the position of the crossover point more accurately we also analyzed the behavior of α characterizing the strength α of the logarithmic size effect in Eq. (6.7), as a function of γ (see Fig. 6.4). The fracture process can also be investigated by looking at the precursory activity before the complete breakdown. The statistical properties of rupture sequences are characterized by the avalanche size distribution which from the experimental point of view could be related to the acoustic emissions generated during the fracture of materials. Figure 6.5 shows the avalanche size distribution for different values of γ. Again, we observe that for decreasing effective range of interaction (increasing γ) there is a crossover in the distribution of avalanche sizes. The upper curves can be very well fitted by a power law

$$P(m) \sim m^{-\tau}, \tag{6.8}$$

with $\tau \approx -\frac{5}{2}$, the value obtained for long range interactions [3, 19, 20]. As soon as the localized nature of the interaction becomes dominant $\gamma > \gamma_c$, the power law dependence

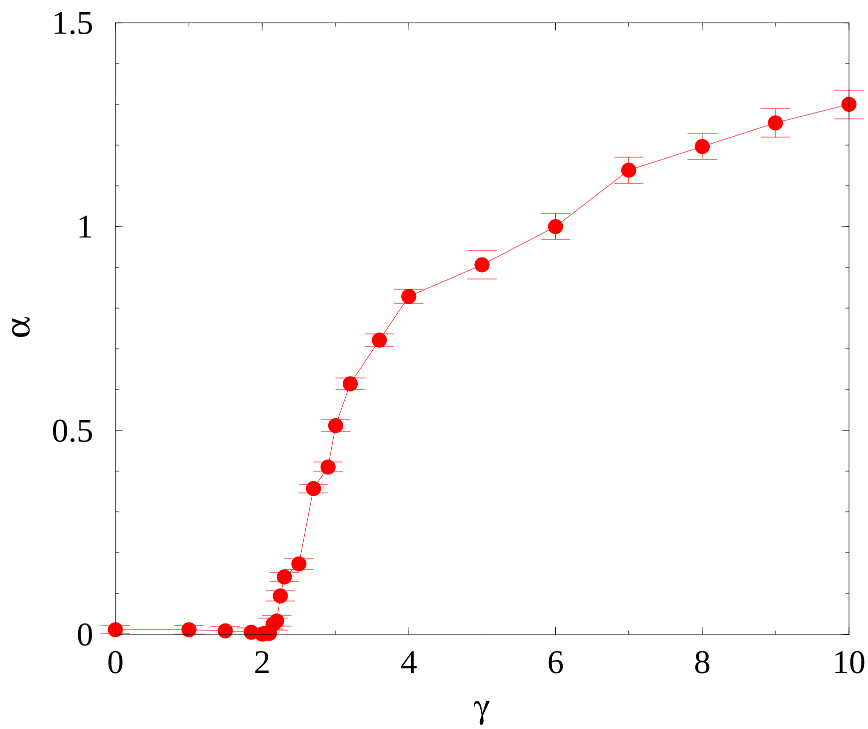

Figure 6.4: The parameter α of Eq. (6.7) (logarithmic size effect), is presented as a function of γ. A clear change close to $\gamma_c = 2$ is observed

of the avalanche size distribution with the exponent $\tau \approx -\frac{5}{2}$ does not apply anymore. The lack of a characteristic size is a fingerprint of a highly fluctuating activity that could be related to the very nature of the long range interactions. The avalanche size distribution is a measure of causally connected broken sites and the spatial correlations in this limit are ruled out. All the intact elements have a nonzero chance to fail independent on the (spatial) rupture history, and any given element could be near to its rupture point regardless on its position in the lattice. This is not the case when γ is large enough and the short range interaction prevails. Now, the spatial correlations are important and concentration of stress takes place in the fibers located at the perimeter of an already formed cluster. Fibers far away from the clusters of broken elements have significantly lower stresses and thus the size of the largest avalanche is reduced as well as the number of failed fibers belonging to the same avalanche, leading to a lower precursory activity.

A further characterization of what is going on in the fracture process can be carried out by focusing on the properties of clusters of broken fibers. The clusters formed during the evolution of the fracture process are sets of spatially connected broken sites on the square lattice. We consider the clusters just before the global failure and they are defined taking into account solely nearest neighbor connections. It is important to note that the case of

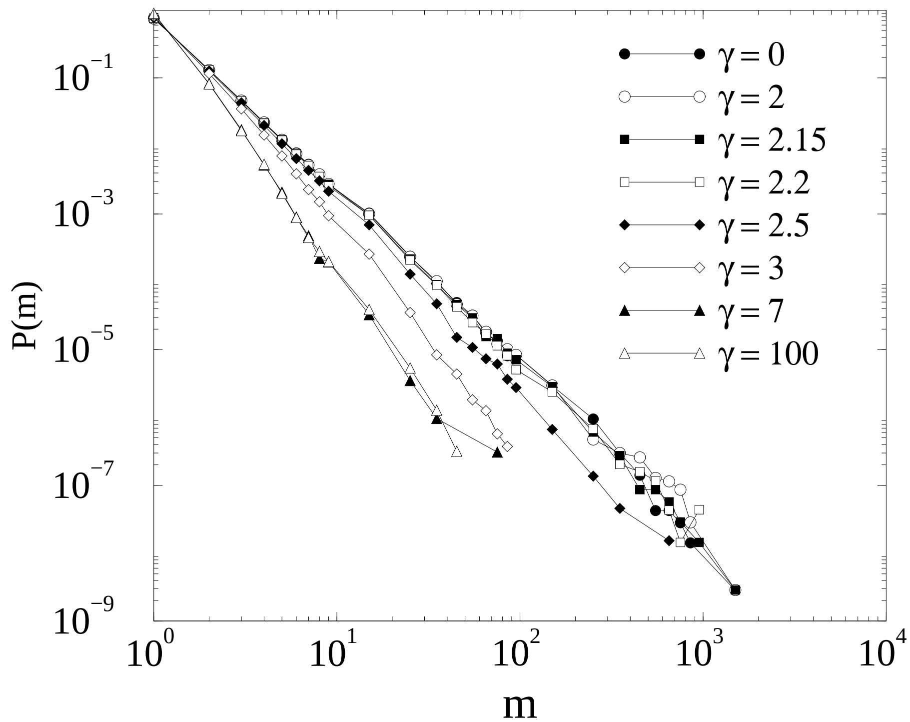

Figure 6.5: Avalanche size distributions for different values of the exponent of the stress-transfer function γ. The upper group of curves can be very well fitted with a straight line with a slope $\tau = -\frac{5}{2}$ ($L = 257$).

global load sharing does not assume any spatial structure of fibers since it corresponds to the mean field approach. However, in our case it is obtained as a limiting case of a local load sharing model on a square lattice, which justifies the cluster analysis also for GLS. Fig. 6.6 illustrates how the cluster structure just before complete breakdown changes for various values of γ.

In the limiting case of global load sharing the breaking of fibers is a completely random nucleation process, there is no correlated crack growth in the system, and the fiber failure which results in the catastrophic avalanche occurs at a random position in the system. As long as this microscopic damage mechanism holds when changing the exponent γ, the system will behave in a global load sharing manner. On the other hand, when the load sharing is very localized, at the beginning of the failure process we get random nucleation of microcracks but later, correlated growth of clusters of broken fibers occurs. It then follows that along the perimeter of the clusters there is a high stress concentration and the final avalanche is driven by a fiber located at the perimeter of one of the clusters (the dominant one). At the fibers far away from the perimeter, the stress concentration is significantly lower, and the stress distribution is very inhomogeneous. In the case of

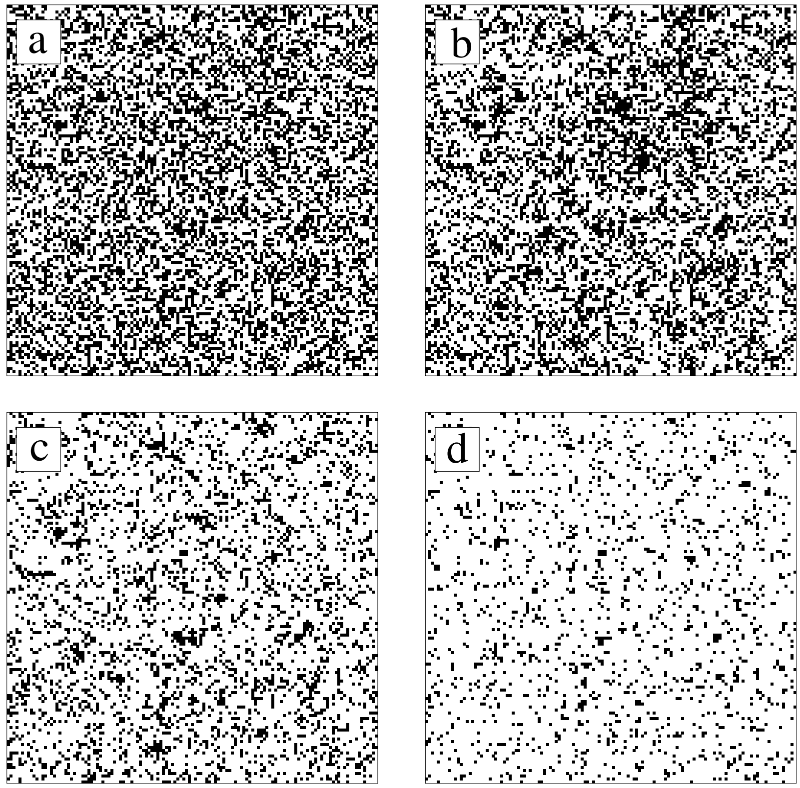

Figure 6.6: Snapshots of the clusters just before the complete breakdown of the material. The change in the structure of the clusters can be seen. The values of γ are: *a)* $\gamma = 0$, *b)* $\gamma_c = 2.2$, *c)* $\gamma = 3$, and *d)* $\gamma = 9$.

localized load sharing this mechanism gives rise also to the logarithmic size effect as obtained also for the random fuse model [104].

We have also recorded the cluster size distribution as a function of the effective range of interaction. Figure 6.7 shows the size distribution $n(s_c)$, of the two-dimensional clusters for several values of the exponent of the load sharing function. The distributions have clearly two groups as found for other quantities also. In the limit where the long range interaction dominates, the clusters are randomly distributed on the lattice indicating that there is no correlated crack growth in the system as well as that the stress is not concentrated in regions. The cluster structure of the limiting case of $\gamma = 0$ can be mapped to percolation clusters on a square lattice generated with the probability $0 < P(\sigma_c) < 1$, where σ_c is the fracture strength of the fiber bundle. However, the value of $P(\sigma_c)$ depends on the Weibull index ρ and is normally different from the critical percolation probability $p_c = 0.592746$ of the square lattice. $P(\sigma_c) = p_c$ is obtained for $\rho = 1.1132$, hence, for physically relevant ρ values used in simulations the system is below p_c at complete breakdown. This argument also justifies the exponential-like shape of the cluster size distributions of GLS in Fig. 6.7. This picture radically changes when the short range interaction prevails. In this case, the stress transfer is limited to a neighborhood of the failed elements and there appear regions where a few isolated cracks drive the rupture of the material by growth and coalescence. Thus, the probability of the existence of a weak region somewhere in the system is high and a weak region in the bundle may be responsible for the failure of the material. The differences in the structure of clusters also explain the lack of a critical strength when N goes to infinity in models with local rearrangement of stress. Since in the GLS model the clusters are randomly dispersed across the entire lattice, the system can "store" more damage or stress, whereas for LLS models a small increment of the external field may provoke a runaway event ending with the macroscopic breakdown of the material. Up to now, the change of the behavior of the system was observed for a certain value of γ analyzing various measured quantities. All these numerical results suggest that the crossover between the two regimes occurs in the vicinity of $\gamma = 2$. Further support for the precise value of γ_c can be obtained by studying the change in the cluster

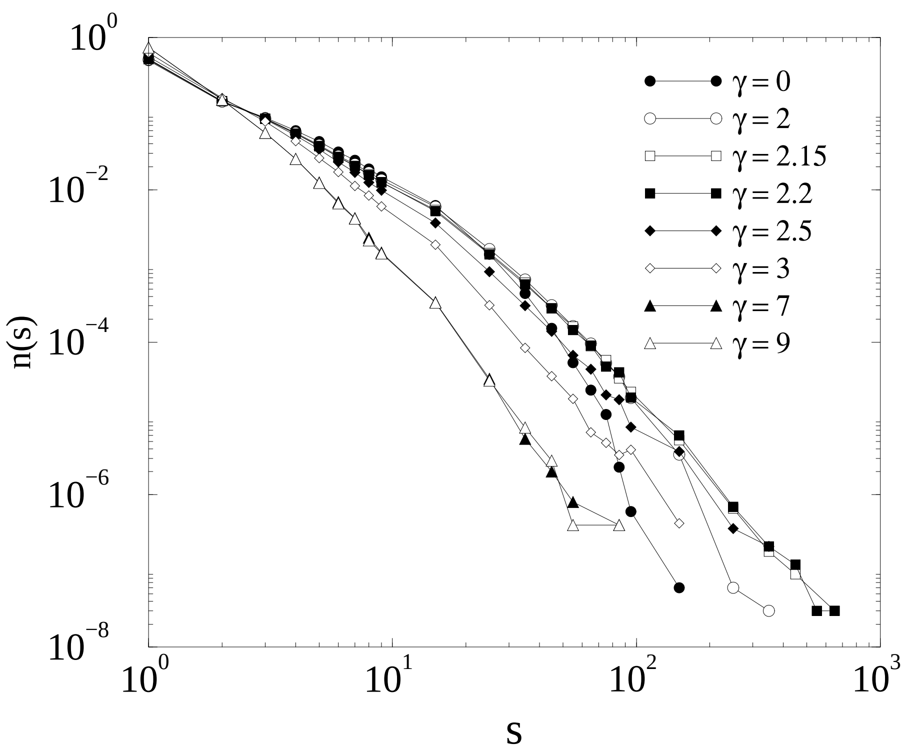

Figure 6.7: Cluster size distributions for different values of the stress-transfer function exponent γ. Clearly, two different groups of curves can be distinguished as also found for other quantities ($L = 257$).

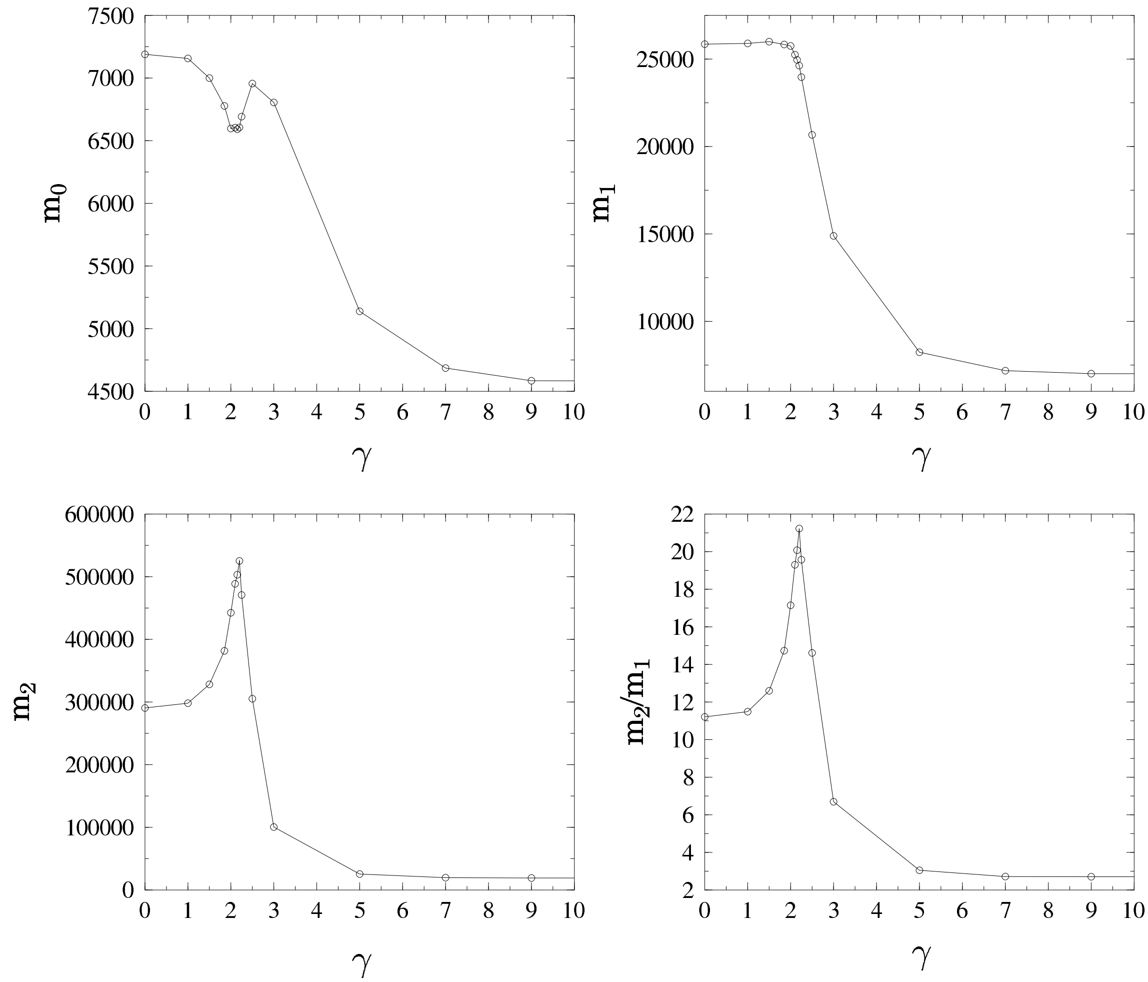

Figure 6.8: Moments of the cluster size distribution as a function of γ (see text for details on the definition of m_k). A sharp maximum is observed at $\gamma = \gamma_c \sim 2.2$ for the average cluster size $\langle s_c \rangle = \frac{m_2}{m_1}$.

structure of broken fibers. The moments of $n(s_c)$ defined as

$$m_k \equiv \int s_c^k n(s_c) ds \tag{6.9}$$

where m_k is the kth moment, describe much of the physics associated with the breakdown process. We will use these moments to quantitatively characterize the point where the crossover from mean field to short range behavior takes place. The zero moment $n_c = m_o$ is the total number of clusters in the system and is plotted in Fig. 6.8a as a function of the parameter γ. Figure 6.8b represents the variation of the total number of broken sites N_c (the first moment $N_c = m_1$) when γ increases. It turns out that up to a certain value of the effective range of interaction, N_c remains constant and then it decreases fast until a second plateau seems to arise. Note that the constant value of N_c for small γ is in agreement with the value of the fraction of broken fibers just before the breakdown of the material in mean field models. This property clearly indicates a change in the evolution of the failure process and may serve as a criterion to calculate the crossover point. However, a more abrupt change is observed in the average cluster size $\langle s_c \rangle$ at varying γ. According to the moments description, the average cluster size is equal to the second moment of the cluster distribution divided by the total number of broken sites, *i.e.* $\langle s_c \rangle = m_2/m_1$. It can be seen in Fig. 6.8d that $\langle s_c \rangle$ has a sharp maximum at $\gamma = 2.2 \pm 0.1$, and thus the average cluster size drastically changes at this point, which again suggests the crossover point to be in the vicinity of $\gamma_c = 2$.

We now discuss the finite size scaling (FSS) of the avalanche size and the cluster size distributions. For local load sharing one expects that the cutoff in the avalanche distribution does not scale with L while for global load sharing the cutoff should scale with the size of the system. We have plotted in Fig. 6.9 the avalanche size distribution for several system sizes. As can be observed, the FSS hypothesis is verified for the values of the exponent γ corresponding to the global (Fig. 6.9b) and the local (Fig. 6.9a) load sharing cases. Figure 6.9c shows the moment analysis for five different system sizes in the range $2.0 \leq \gamma \leq 2.5$. It can be seen that the position of the maximum of the m_2/m_1 curves is always at $\gamma = 2.2 \pm 0.1$, it does not scale with the system size. The value of γ_c defined as the maximum of m_2/m_1 (see Fig.6.9c) does not scale with L, and it turns out that its value will asymptotically (when $N \to \infty$) remain constant. We shall discuss this issue in more details elsewhere. This test of scaling can also be used to obtain accurately the critical value of γ when the size of the system goes to infinity. Our numerical results point out that again $\gamma_c = 2.2 \pm 0.1$ as it was obtained by the moment analysis. Furthermore, one could be tempted to infer that the critical point γ_c varies as the size of the system increases.

From all the studies it turned out that a consistent interpretation of the numerical results can be given assuming that the crossover occurs in the vicinity of $\gamma_c = 2.0$ but stronger statement cannot be drawn due to the limited precision of calculations.

6.3 Conclusion

We have studied a fracture model of the fiber bundle type where the interaction among fibers is considered to decay as a power law of the distance from an intact element to the rupture point. Two very different regimes are found as the exponent of the stress-transfer function varies and a crossover point is identified at $\gamma = \gamma_c$. The strength of the material for $\gamma < \gamma_c$ does not depend on the system size and γ qualifying for mean-field behavior, whereas for the short range regime, the critical load decreases with the system

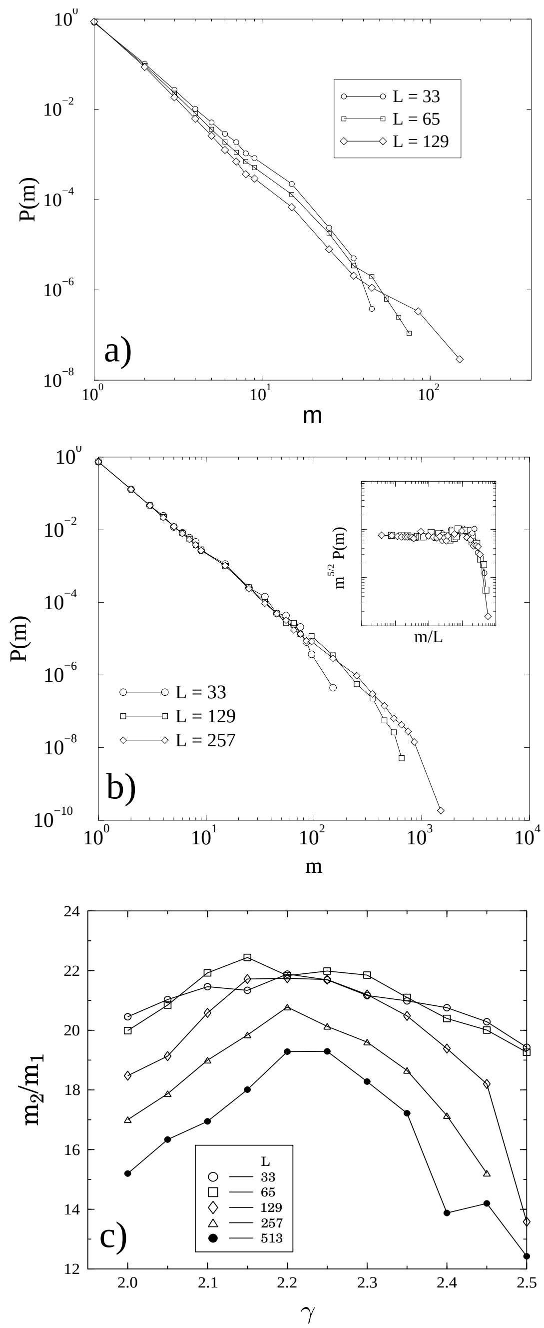

Figure 6.9: Finite size scaling analysis. $a)$ Scaling of the cutoff with the system size for the local load sharing case, $b)$ Scaling of the cutoff with the system size for the global load sharing case, and $c)$ Average cluster size, $\langle s_c \rangle = \frac{m_2}{m_1}$, for different system sizes. Note that in $c)$ the position of γ_c does not change.

size as $\sigma_c \sim 1/\ln(N)$. The behavior of the model at both sides of the crossover point was numerically studied by recording the avalanche and the cluster size distributions. The numerical results suggest that the crossover point falls in the vicinity of $\gamma_c = 2.0$. An interesting aspect to be explored in future work is whether there is or not a second transition point in the model when the γ-dependence of σ_c seems to disappear (see Fig. (6.2))

Chapter 7

Size dependency of tension strength in natural fiber composites

7.1 Introduction

Scale effects of wood strength are well known with respect to tension loading perpendicular to fiber direction. In this weak plane of wood, exhibiting the most brittle failure mode of splitting, the pronounced scale effect of the stressed volume can be modeled adequately by a simple weakest link approach for a purely serial system [105]. However, recent investigations showed that the purely serial system approach is not fully applicable for realistic length scales but that the stress redistribution effects of partial parallel systems have to be taken into account.

In case of bending and tension parallel to fiber direction scale effects of width and depth have been reported in several studies [106]. However, modeling of wood loaded parallel to fiber as a parallel system of fibers has not yet been performed to our knowledge. Existing models mostly treat all scale effects in view of some modified weakest link approach thereby silently neglecting the effects of stress redistribution after the initial fracture of the weakest fiber [107].

This chapter reports on a combined experimental and theoretical study on the size dependency of tension strength of clear wood. The fracture behavior of the tested softwood specimens was found to be rather brittle with low precursory activity and a statistical variation of the strength. A significant dependency of the mean strength of the material on the cross-sectional size of the specimens was obtained. The range of load redistribution in clear wood subjected to tension parallel to fiber was assessed by the theoretical concept of fiber bundle models for fiber composites [40].

7.2 Experiment description

In collaboration with the *Otto-Graf-Institute* (FMPA) at University of Stuttgart, the size dependency of tension strength of clear wood at loading parallel to fiber direction was experimentally accessed. The actual experiments were performed by the group of Dr. Simon Aicher.

The tested material was soft-wood of the species spruce (picea abies) being the most important wooden building material for load bearing timber structures in Europe. In order to investigate the size effect of tension strength parallel to fiber direction, two sets of specimens were manufactured with cross-sections varying by a factor of 10. The specimens with the smaller cross-section will be denoted ”small” specimens and those with the large cross-section will be denoted ”large” specimens. In order to minimize uncontrolled variability of material parameters of the natural wood several aspects had to be taken care of:

1. All specimens were cut from one single log.
2. The specimens were selected to be free of macroscopic defects such as knots.
3. The most crucial parameter for the tension strength of the mainly unidirectional fiber composite wood is the angle between fiber direction, or longitudinal direction ”L”, and applied tension load. Due to low tension strength perpendicular to the fiber the off-axis strength decreases by about 50 percent at fiber deviations of 10^o [108]. Within a typical rectangularly sawn scantling the deviation between nominal longitudinal direction of the stem and local fiber direction may vary considerably between 0^o and about 15^o. Whereas a non-destructive evaluation of the fiber deviation is technically quite demanding, the fracture surfaces of *splitted* wood indicate the fiber direction in a straightforward manner. Therefore the specimen raw material has been split to obtain straight grained wood pieces and the specimens were then cut parallel to the split surfaces.
4. As an additional measure of scatter reduction the specimens have been matched as twin-pairs consisting of one large and one small specimen each cut from adjacently located wood segments. Thereby each pair showed the highest possible conformity with respect to strength relevant parameters such as density or year ring width.

The specimen shape has been chosen with respect to three major aspects, being:

- the anisotropy of the material with high tension strength parallel to fiber *vs.* low compression strength perpendicular to fiber direction;

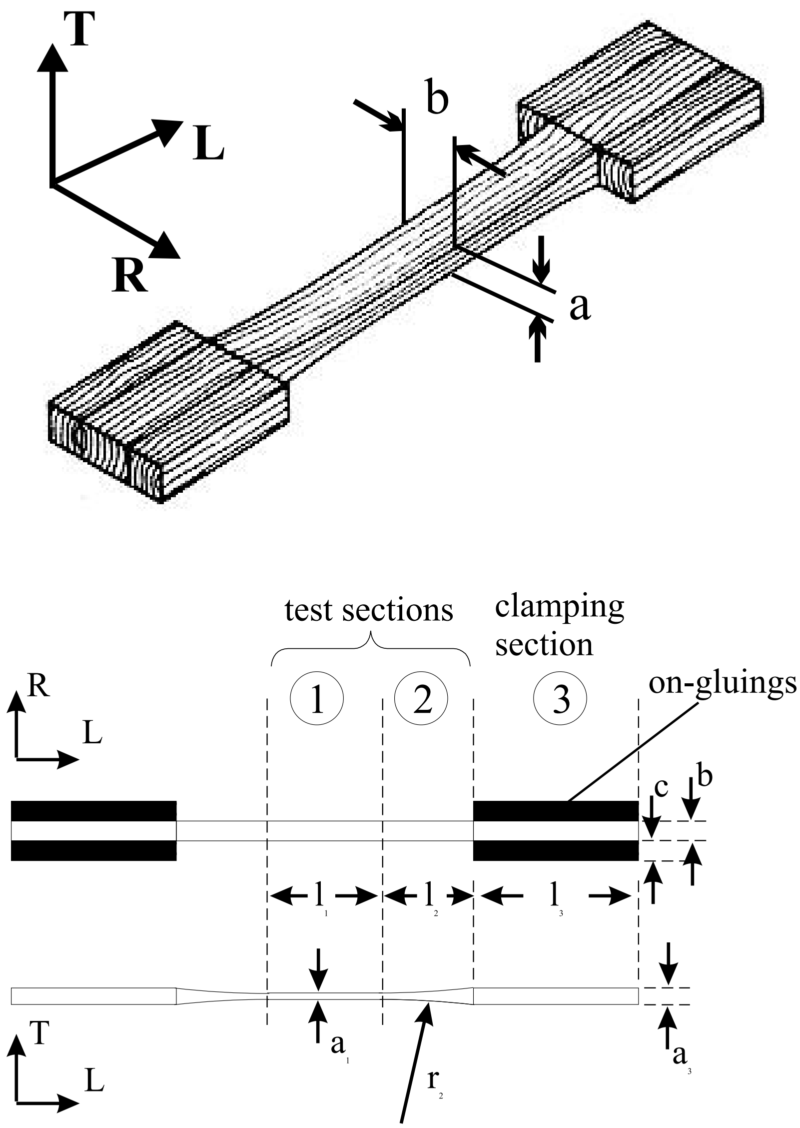

Figure 7.1: Specimen geometry and the used notations

- the low shear strength of the annual ring interface between high-density late wood and low-density early wood and
- the necessity of scalability. Figure 7.1 shows the employed specimen shape and the dimensional notations.

The dimensions of the small and large specimens are given in table 7.1.The specimen shape is characterized by a rectangular cross-section with a shoulder shaped reduction of the thickness a_i parallel to the tangential growth direction T (following the annual rings).

Nom. Dim.	a_1	a_3	r_2	b	l_1	l_2	l_3	c	$A = a_1 b$
small	2	5	200	6	35	27.5	50	6	12
large	6	15	700	20	110	80	150	20	120

Table 7.1: Nominal dimensions of the small and large tension specimens (in mm)

In detail the specimen shape shows a straight section (1) of length l_1 with a constant minimal cross-section $a_1 b$, a curved shoulder section (2) of length l_2 and radius r_2 and, (3) the straight clamping section with cross section $a_3 b$ and length l_3. The specimen's width b parallel to radial growth direction R (perpendicular to the annual rings) has been chosen constant in order to minimize shear and transverse tension stresses perpendicular to the weak annual ring interfaces.

In order to enlarge the clamping area in sections (3), thereby reducing the necessary compression stresses for load application in width direction, on-gluings of width c and depth a_3 were adhered both-sided to the ends of the specimens. All dimensions between the small and the large specimens were scaled by a factor of about $10^{\frac{1}{2}}$ in order to achieve geometrically similar shapes and a scale factor of 10 between the cross-sections of the small and the large specimens.

The load was applied to both, the small and large specimens by means of clamping. In case of the small specimens a screw clamp has been used with a nominally equally distributed compression stress at the clamping faces. In case of the large specimens hydraulic clamps were applied which allowed continuously decreasing compression stresses towards the edge of the on-gluings. Both clamping arrangements yield, compared to usual wedge type clamping devices, relatively smooth stress distributions at the transition from the clamping section to the test section.

The sets of small and large specimens consisted of 23 specimens each. The experiments were performed as stroke,(*i.e.* global deformation) controlled ramp-load tests with a constant cross-head displacement rate of the test machine. The stroke rate was chosen based on pre-testing of additional specimens such that fracture was obtained within 180 ± 60 seconds. In case of the small specimens the tests were conducted in a screw-driven test machine, whereas for the large specimens a servo-hydraulic type machine has been used. Figures (7.2a,7.2b) show photographs of a small and large specimen, installed in the respectively employed clamping arrangements of the different testing machines. In case of the large specimens, the mean strain of the straight section has been recorded with a strain gauge based extensiometer, too Fig.(7.2b). However, as the strain was only measured for the large specimens the quantitative evaluation of the test results focuses solely on the strength results.

a) b)

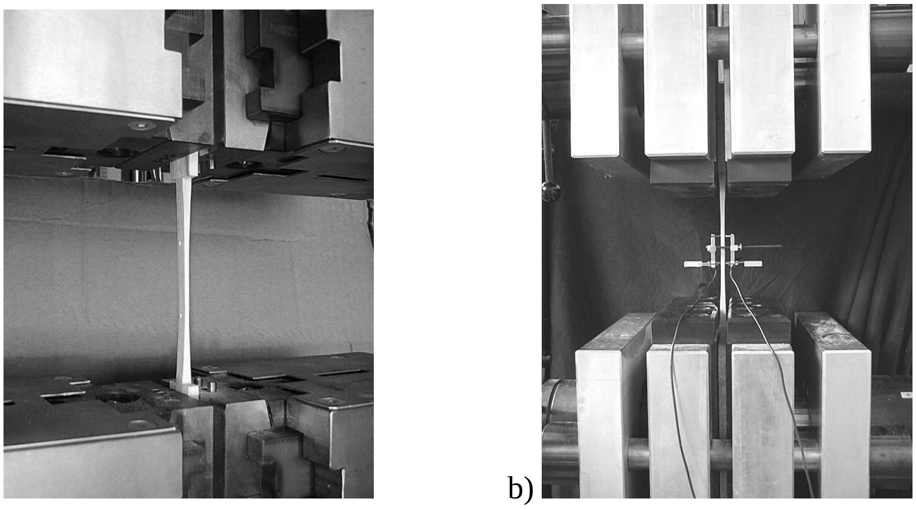

Figure 7.2: Views of experimental setups for small (a) and large (b) tension specimens mounted in the different test machines

7.3 Experimental results

The fracture of the tension specimens occurred throughout within the test sections, *i. e.* predominantly in the straight section (1) and partly in the shoulder-shaped section (2). No failure occurred within the clamping section. Two typical views of broken small and large specimens are shown in Figs. (7.3a, 7.3b). The fracture surfaces were throughout influenced by the inhomogeneity of the annual rings: Distinct blunt tension ruptures can be observed in the early wood layers and then local shear failure planes along the early wood-late wood interfaces yielding pronouncedly stepped fracture surfaces. During the tension test it was not possible to follow the succession of fracture processes, however, quite often some cracking sound and dust presumably from a crack, yet not visible for blank eye could be observed prior to failure. Moreover, some of the stress-strain curves, recorded in case of the large specimens, showed pre-peak load drops with load recovery, which additionally indicated, that some kind of damage or crack evolution stop mechanism acted during loading. Figure (7.4) shows a measured curve of global stress vs. global strain within the straight cross-section (1) of one large specimen exhibiting a pre-peak load drop. The ultimate failure occurred throughout as an unstable, brittle fracture. For all tests the maximum load was recorded and the strength was calculated on the basis of the individually measured minimal cross-sections. The mean values and standard deviations of the tension strength σ_c and the mean values of the effective cross-sections $A = a_1 b$ are summarized in Table 7.2 separately for both test sets. The small specimens exhibited an 8.2 percent higher mean tension strength as compared to the large specimens. Thus, the results indicate a size effect of tension strength parallel to fiber of wood on the mean value level. However, also the scatter of the results is higher for the small specimens

a) 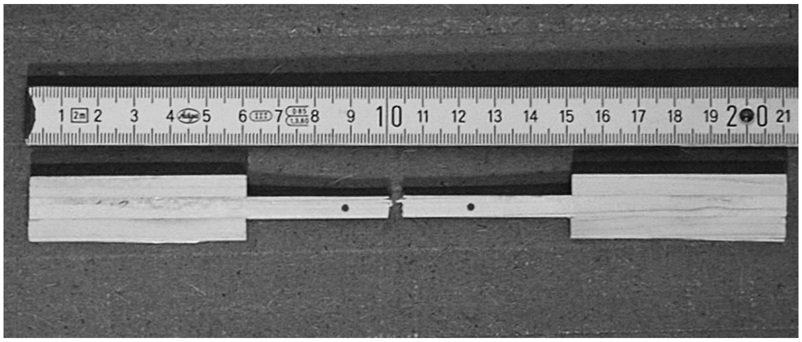

b) 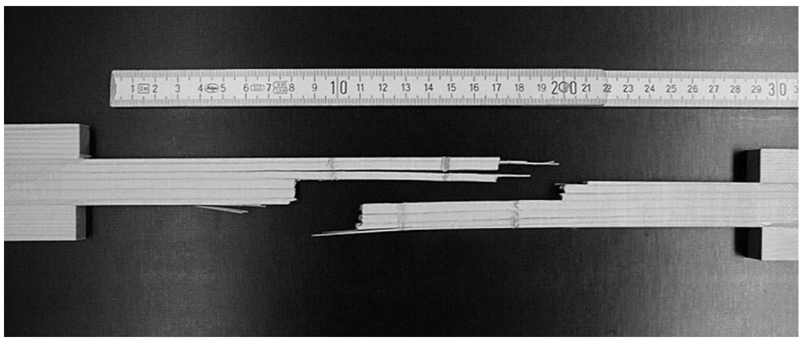

Figure 7.3: Views of typical failure appearance of small a) and large b) specimens

compared to the test set with the large cross-sections. Thus, the size effect seems to be smaller for the lower values of the strength distribution.

The cumulative frequencies of both strength data sets are plotted in Fig. 7.5. Hereby the empiric cumulative frequency H_i of each individual strength value σ_c has been estimated based on ranking of the results in increasing order of the strength values according to

$$H_i = \frac{n_i}{N+1}, \tag{7.1}$$

whereby n_i and N denote the rank number and the total number of specimens in both samples, respectively. For both sets of strength values a two-parameter Weibull distribution

$$P(\sigma_c) = 1 - \exp\left[-\left(\frac{\sigma_c}{\sigma_o^b}\right)^\rho\right] \tag{7.2}$$

has been fitted. In Eq. (7.2) quantity σ_o^b denotes the stress scale parameter and ρ is the Weibull shape parameter which characterizes the amount of disorder in the sample being determined by the coefficient of variation. The numerical result for the Weibull parameters, σ_o^b and ρ, obtained by least square fitting are given in table 7.2; the respective

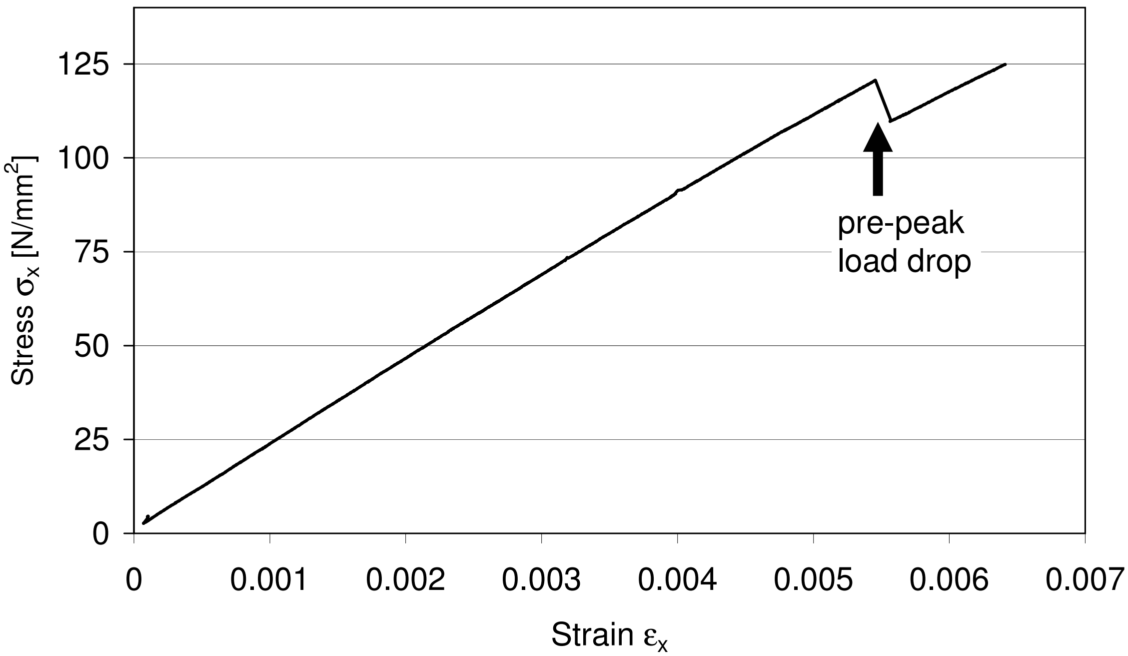

Figure 7.4: Typical stress-strain behavior obtained for a large specimen

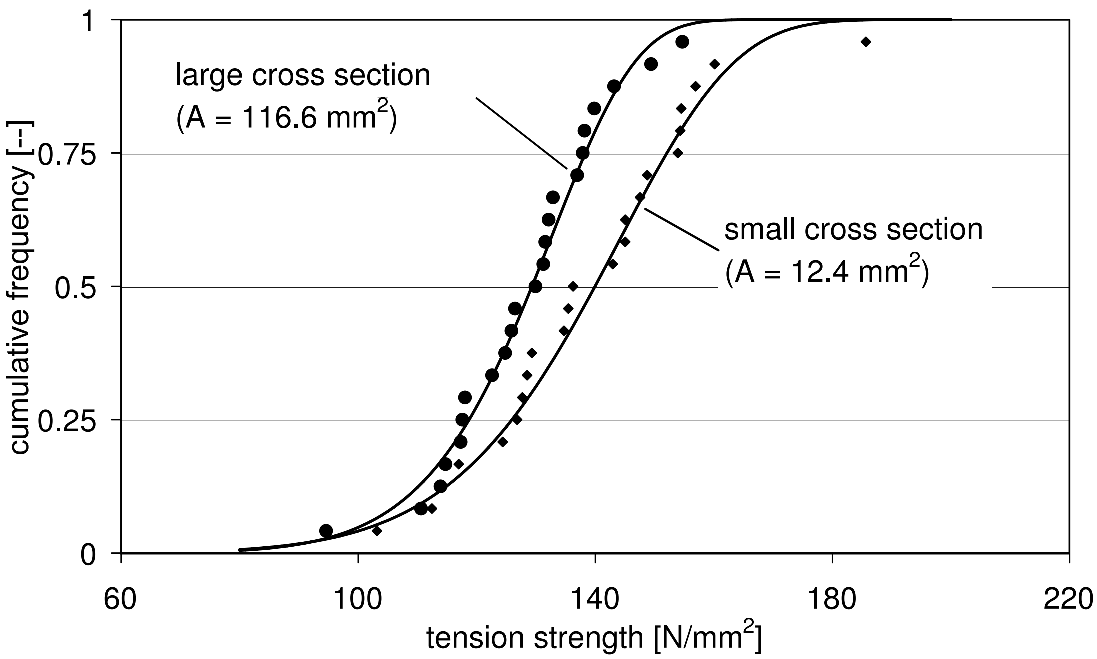

Figure 7.5: Strength cumulative distribution from specimens with different sizes

Specimen Size	Cross-Section $[mm^2]$	Number of Fibers	$\overline{\sigma}_c \pm \Delta\sigma_c$ $[\frac{N}{mm^2}]$	σ_o^b $[\frac{N}{mm^2}]$	ρ
small	12.4	~ 5000	138.5 ± 18.7	146.2	8.3
large	116.6	~ 50000	128.0 ± 13.6	134.0	10.3

Table 7.2: Summary of results of the tension tests

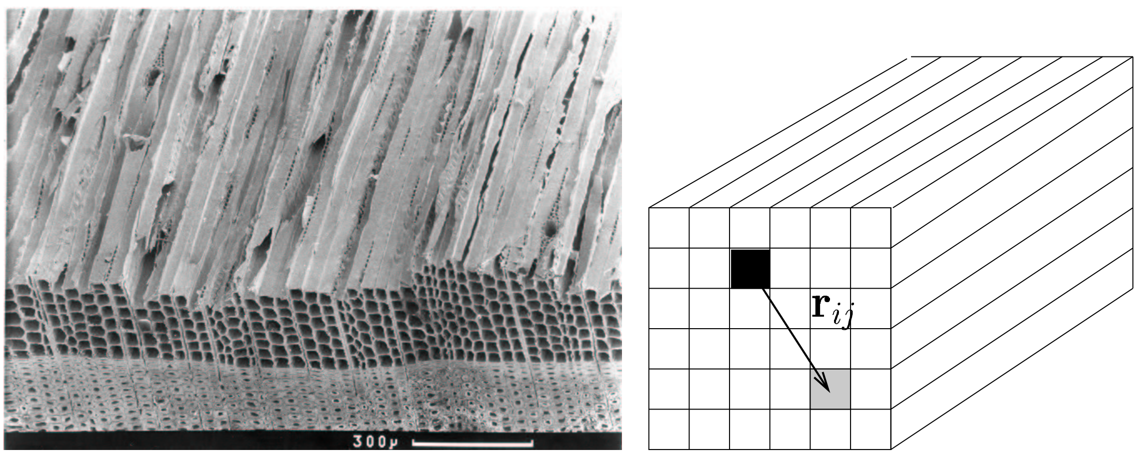

Figure 7.6: The structure of softwood (*left*) and illustration of the model build-up (*right*). The wood fibers are arranged on a regular square lattice for which fiber bundle models can provide an adequate description.

cumulative distribution functions are plotted in Fig. 7.5 together with the empirical data .

7.4 Modeling of damage development

For a realistic modeling of the damage process of natural fiber composites under an uniaxial load, the local stress distribution should be calculated in the whole volume of the sample. Even limiting the number of independent variables needed to describe the internal microstructure of the specimen, an accurate prediction of the ultimate strength is a computationally demanding task. Hence, in general, the modeling of fiber composites is based on certain idealizations about the geometry of the fiber arrangement and the stress redistribution following fiber failures in the specimen. One of the most important type of models of fiber composites are the so-called Fiber Bundle Models (FBM) and they properties have been described in Chapter 3.

Then, if global load sharing is assumed in the case of a small number of fibers, it can be shown analytically that the global strength of a bundle of Weibull fibers approximately follows a Weibull distribution [25, 59, 80, 103]. The Weibull strength distribution then implies a decrease of the average strength according to a power law when the number of fibers is increased. Finally, approaching very large system sizes the strength distribution slowly converges to a normal distribution with a constant value of the average strength.

Contrary, when the load sharing mechanism is assumed to be completely localized, then the approximated strength distribution takes again the Weibull form, whereby the parameters, describing the macroscopic distribution, are different from the microscopic ones. The Weibull shape parameter of the bundle, ρ, is related to that of the single fibers as

$$\rho = N_c \rho_s \tag{7.3}$$

where N_c denotes the size of the critical cluster of broken fibers. The Weibull distribution of global strength implies again a power law size dependence of the average strength which asymptotically turns into a slower logarithmic decrease [80, 103].

A wood sample may be modeled by an array of parallel fibers arranged approximately on a regular square lattice. This is in agreement with the morphology of the real material at the micro-scale (see Fig. 7.6). The amount of matrix material between fibers is rather low, less than 1% of the total volume of the sample. The macroscopic strength of fiber composites is mainly determined by the strength distribution of individual fibers and the interaction of fibers governing the load redistribution. Recently, the strength distribution of single wood fibers extracted from softwood materials has been studied extensively [8].Experiments showed that the rupture of wood fibers is caused by the flaws of various sizes existing along fibers. The distribution of fiber strength values is controlled by the size distribution of flaws. It was found that the strength values σ_c of single wood fibers with a fixed length can be well described by a two-parameter Weibull distribution of the form of Eq. (7.2), with the stress scale parameter σ_o and the Weibull shape parameter ρ_s, which characterizes the amount of disorder in single fibers. It was found that the value of ρ_s for single fibers always ranges between 1 and 2 indicating the presence of high disorder in wood fibers due to the pre-existing flaws [8].

In the above reported experiments on wood samples hardly any precursory breaking activity could be observed. The constitutive curves were practically linear up to the failure point and the final rupture occurred in a rather brittle manner suggesting a very localized load redistribution. The strong locality of load redistribution is further supported by the macroscopic Weibull shape parameters of $\rho \approx 8 - 10$, which are much larger than the corresponding range of single fibers according to [8]. Assuming completely local load sharing it follows from Eq. (7.3) that the size N_c of the critical cluster in softwood is in the range of $4 - 10$; so when a cluster of N_c broken fibers is formed, the sample becomes instable and fails abruptly. If the empiric data follow a Weibull distribution, which cannot be proved , the size effect can approximately be given in the power-law form $\sigma_o^b \sim N^{-\frac{1}{\rho}}$, where $\overline{\sigma}_c$ denotes the average strength of a sample of N fibers, which is in reasonable agreement with the experimental results (see Tab. 7.2). The discrepancy between the calculated value of $(\frac{N_2}{N_1})^{\frac{1}{\rho}} = 1.25.$ and the value of $\frac{\sigma_{o1}^b}{\sigma_{o2}^b} = 1.08.$ *vs* the empiric data should result from the fact, that the extreme LLS case is an approximation, and not an exact model for wood at tension loading parallel to fiber direction.

7.5 Application of the fiber bundle model with variable range of interaction

In order to get a deeper insight into the damage process of wood at uniaxial loading in fiber direction the new fiber bundle model introduced in chapter 6 was applied. The model is composed of N parallel fibers having statistically distributed strength drawn from a cumulative distribution function $P(\frac{\sigma}{\sigma_o})$. Thus, to each fiber i a random strength value is assigned. All intact fibers have a nonzero probability of being affected by the ongoing damage process. In that model approach the interaction among fibers is modeled by an adjustable stress-transfer function 6.2. Varying the parameters of the model an interpolation can be performed between the two limiting cases of load redistribution, the global and the local load sharing schemes.

In section 7.3 a significant dependency of the average failure strength of the specimens on the size of their cross- section was obtained experimentally. Based on the empirical results, an estimate of an effective exponent γ, characterizing the load redistribution in softwood, was provided in the framework of a model with variable range of interaction (Chapter 6.2).

It is plausible that real materials are not characterized by the extreme cases of global or local load sharing. A real specimen with N fibers should have a normalized strength value $\frac{\sigma_c(N)}{\sigma_o}$ which falls between the bounds of the GLS and LLS approaches. The normalization constant σ_o is the characteristic stress value of the cumulative strength distribution of

Weibull Disorder Parameter	Weibull Scaling Parameter $[\frac{N}{mm^2}]$	Slope	Load-Sharing Parameter
$\rho_s = 1$	$384.7 < \sigma_o < 520.1$	$0.8 < \alpha < 1.1$	$6 < \gamma < 10$
$\rho_s = 2$	$322.8 < \sigma_o < 426.5$	$0.9 < \alpha < 1.3$	$5 < \gamma < 10$

Table 7.3: Load sharing parameters estimated from the strength values obtained from test samples with different sizes.

single elements. As in the present case σ_o is unknown, it has been used as a free fit parameter.

For an estimation of upper and lower boundaries of σ_o first the limits of GLS and LLS were calculated. Numerical results, using a cumulative Weibull distribution with the disorder parameter $\rho_s = 2$, are shown in the Figs. (6.2),(6.3). In can be seen that in the global case, due to the independence of the system size, the $\frac{\sigma_c}{\sigma_o}$ vs $\frac{1}{\log N}$ plot results a line parallel to the $\frac{1}{\log N}$ axis,

$$\frac{\sigma_c}{\sigma_o} = (\rho_s e)^{-\frac{1}{\rho_s}}. \tag{7.4}$$

Note that given by Figs. (6.2) and (6.3) this value is $\frac{\sigma_c}{\sigma_o} = 0.429$. This parallel line is the upper bound for the strength data of the test series with smaller number of fibers $N = 5000$. Using its corresponding strength value (shown in Tab. 7.2) yields the lower bound of $\sigma_o = 322.8 \frac{N}{mm^2}$.

In the same manner the limiting case of LLS ($\gamma = 9$), *i.e.* a line

$$\frac{\sigma_c}{\sigma_o} = 0.97\frac{1}{\log N} + 0.21, \tag{7.5}$$

gives a lower bound of normalized strength, for the empirical test series with higher number of fibers $N = 50000$, and thereby yields the upper bound of $\sigma_o = 426.5 \frac{N}{mm^2}$.

In this way it is possible to fit the experimental results presented in section 7.3 with the model using the fit parameter σ_o. The slope α of the fitted curves can be calculated, enabling a numerical estimation of the value γ.

In Tab. 7.3 the results of the limit case considerations are compiled including the ranges of σ_o, the derived slopes α and finally the resulting values for the load sharing exponent γ. In the fitting procedure, two extreme values of the Weibull shape parameter ρ_s, previously determined by Thuvander *et al*, have been used [8].

Using the fitted values of α and the results of Chapter 6 the value of the exponent that characterizes the load sharing type in wood was approximately obtained (see Tab.7.3). Those results suggest, that in case of tension loading parallel to the fiber direction, the load redistribution after the failure of a single fiber falls in the regime where the behavior of the system can be well described by assuming almost completely localized load sharing. This result is in agreement with the general arguments of the previous section.

7.6 Conclusions

The size effect of tension strength of softwood loaded parallel to fiber direction has been assessed experimentally and theoretically. The macroscopic constitutive behavior of the specimens was rather brittle and the strength values showed a statistical variation which could be well fitted in terms of a Weibull distribution. It was revealed that the average strength is a decreasing function of the cross-sectional specimen size. In order to provide a theoretical interpretation of the experimental results with respect to the size effect and the modeling of the load sharing mechanism, the wood material was modeled as a natural fiber composite with extremely small volume fraction of matrix material. Comparing the strength distribution of single fibers and that of the macroscopic samples it was deduced that the load redistribution among wood fibers is short ranged giving rise to a low precursory activity preceding final failure and small clusters of broken fibers. For qualitative characterization of the load sharing it has been assumed that the load-transfer function has a power law form and its effective exponent has been estimated. The experimental and theoretical results are in satisfactory agreement.

Additional research is needed in order to confirm the results in a more quantitative manner including experiments with intermediate size scales. Moreover, some aspects of the damage evolution of wood tension loading parallel to fiber are not yet well described by the used FBMs.

Chapter 8

Creep rupture of viscoelastic fiber bundles

In this chapter a novel method to deal with the real time dependence in the breakdown process of the fiber materials is presented. Here we develop a fiber bundle model whose fibers have viscoelastic behavior and the macroscopic damage mechanism leading to creep rupture is the strain dependent breaking of the fibers during the time evolution of the deformation of the system. Both limit cases global and local load sharing have been treated. Moreover, a variable range of interaction model has also been applied [37, 39]. This type of model is relevant for the study of composites whose viscoelastic properties are concentrated on the fibers, *i.e.* viscoelastic fibers embedded in a brittle matrix.

8.1 Model

In order to work out a theoretical description of creep failure of viscoelastic fiber composites we improve the classical fiber bundle model which has proven very successful in the study of fracture of disordered materials (see Chapter 3).

The model consists of N parallel fibers having viscoelastic constitutive behavior. For simplicity, the pure viscoelastic behavior of fibers is modeled by a Kelvin-Voigt element which consists of a spring and a dashpot in parallel (see Fig. 8.1) and results in the constitutive equation

$$\sigma_{\mathrm{o}} = \beta\dot{\varepsilon} + E\varepsilon, \tag{8.1}$$

where β denotes the damping coefficient, and E the Young's modulus of fibers, respectively. Eq. (8.1) provides the time dependent deformation $\varepsilon(t)$ of a fiber at a fixed external

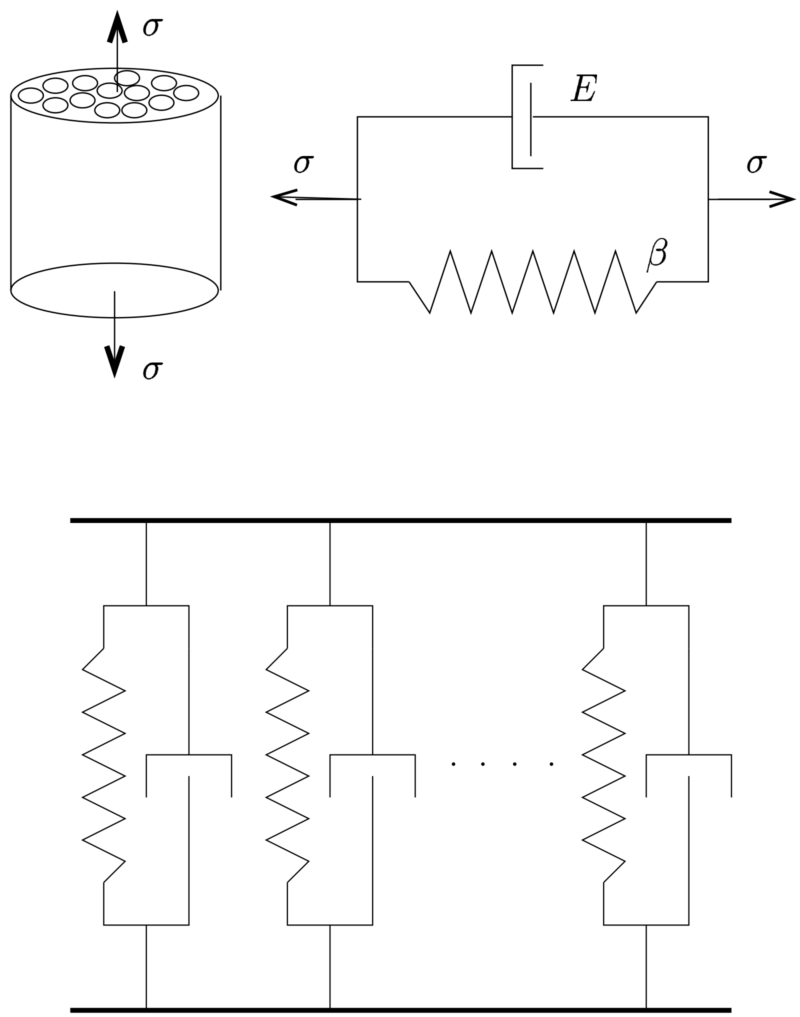

Figure 8.1: The viscoelastic fiber bundle: intact fibers are modeled by Kelvin-Voigt elements. After fiber breaking the corresponding element is removed from the model.

load σ_o

$$\varepsilon(t) = \frac{\sigma_o}{E}\left[1 - e^{-Et/\beta}\right] + \varepsilon_o e^{-Et/\beta}, \tag{8.2}$$

where ε_o denotes the initial strain at $t = 0$. It can be seen that $\varepsilon(t)$ converges to σ_o/E for $t \to \infty$, which implies that the asymptotic strain fulfills Hook's law. If no failure occurs, Eq. (8.2) would fully describe the time evolution of the system. To incorporate breaking in the model we introduce a strain controlled failure criterion for fibers: a fiber fails during the time evolution of the system if its strain exceeds a damage threshold ε_d, which is an independent identically distributed random variable of fibers with probability density $p(\varepsilon_d)$ and cumulative distribution $P(\varepsilon_d) = \int_0^{\varepsilon_d} p(x)dx$.

Due to the validity of Hook's law for the asymptotic strain values, the formulation of the failure criterion in terms of strain instead of stress implies that under a certain steady load the same amount of damage occurs as in the case of stress controlled failure, however, the breaking of fibers is not instantaneous but distributed over time. When a fiber fails its load has to be redistributed to the intact fibers, according to the interaction law of the fibers.

8.1.1 Global load sharing

Analytic model

Assuming global load sharing (see Chapter 3), the time evolution of the system under a steady external load σ_o is finally described by the equation

$$\frac{\sigma_{\mathrm{o}}}{1 - P(\varepsilon)} = \beta\dot{\varepsilon} + E\varepsilon, \tag{8.3}$$

where the viscoelastic behavior of fibers is coupled to the failure of fibers in a global load sharing framework. Eq. (8.3) is a first order differential equation for $\varepsilon(t)$ which has to be solved at fixed σ_o values.

For the behavior of the solutions of Eq. (8.3) two distinct regimes can be distinguished depending on the value of the external load σ_{o}: When σ_{o} is below a given critical stress value σ_{c} Eq. (8.3) has a stationary solution ε_s, which can be obtained by setting $\dot{\varepsilon} = 0$ in Eq. (8.3)

$$\sigma_{\mathrm{o}} = E\varepsilon_s[1 - P(\varepsilon_s)]. \tag{8.4}$$

It means that until this equation can be solved for ε_s at a given external load σ_{o}, the solution $\varepsilon(t)$ of Eq. (8.3) converges to ε_s when $t \to \infty$, and no macroscopic failure occurs. However, when σ_{o} exceeds the critical stress value σ_c no stationary solution exists, furthermore, $\dot{\varepsilon}$ remains always positive, which implies that for $\sigma > \sigma_c$ the strain of the system $\varepsilon(t)$ monotonically increases until the system fails globally at a given time t_f. Below t_f is called time to global failure or lifetime indifferently.

In the regime $\sigma_{\mathrm{o}} \leq \sigma_{\mathrm{c}}$ Eq. (8.4) also provides the asymptotic constitutive behavior of the fiber bundle which can be measured by controlling the external load σ_{o} and letting the system relax to ε_s. It follows from the above argument that the critical value of the load σ_c is the static fracture strength of the bundle which can be determined from Eq. (8.4) as

$$\sigma_c = E\varepsilon_c[1 - P(\varepsilon_c)], \tag{8.5}$$

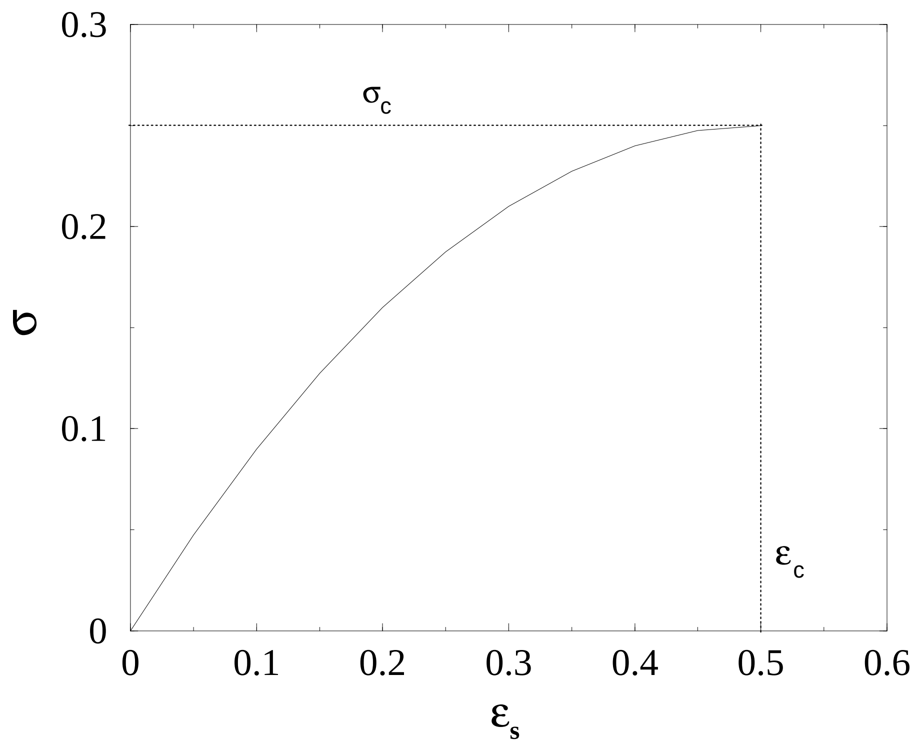

Figure 8.2: Relation between the critical stress σ_c and strain ε_c. An uniform cumulative distribution $P(\varepsilon) = \varepsilon$ has been used.

where ε_c is the solution of the equation [1, 2]

$$\left. \frac{d\sigma_{\mathrm{o}}}{d\varepsilon_s} \right|_{\varepsilon_{\mathrm{c}}} = 0. \tag{8.6}$$

Since $\sigma_{\mathrm{o}}(\varepsilon_{\mathrm{s}})$ has a maximum of σ_{c} at ε_{c}, in the vicinity of ε_{c} it can be approximated as

$$\sigma_{\mathrm{o}} \approx \sigma_{\mathrm{c}} - A(\varepsilon_{\mathrm{c}} - \varepsilon_s)^2, \tag{8.7}$$

where the multiplication factor A depends on the probability distribution $P(\varepsilon)$. A complete description of the system can be obtained by solving the differential equation Eq. (8.3). After separation of variables the integral arises

$$t = \beta \int d\varepsilon \frac{1 - P(\varepsilon)}{\sigma_{\mathrm{o}} - E\varepsilon \left[1 - P(\varepsilon)\right]} + C, \tag{8.8}$$

where the integration constant C is determined by the initial condition $\varepsilon(t = 0) = 0$.

The creep rupture of the viscoelastic bundle can be interpreted so that for $\sigma_{\mathrm{o}} \leq \sigma_{\mathrm{c}}$ the system suffers only a partial failure which implies an infinite lifetime $t_f = \infty$ and the emergence of a macroscopic stationary state, while above the critical load $\sigma_\mathrm{o} > \sigma_\mathrm{c}$ global failure occurs at a finite time t_f, which can be determined by evaluating the integral Eq. (8.8) over the whole domain of definition of $P(\varepsilon)$.

In order to characterize the creep rupture transition occurring at σ_c we studied how the system behaves when σ_o approaches σ_c form below and above.

Below the critical point $\sigma_\mathrm{o} \leq \sigma_\mathrm{c}$ the bundle relaxes to the stationary deformation ε_s through a decreasing breaking activity. To find the characteristic time scale of this relaxation process the behavior of $\varepsilon(t)$ has to be analyzed in the vicinity of ε_s. It is useful to introduce a new variable δ as

$$\delta(t) = \varepsilon_s - \varepsilon(t). \tag{8.9}$$

The governing differential equation of δ can be obtained from Eq. (8.3) by expanding it around ε_s

$$\frac{d\delta}{dt} = -\frac{E}{\beta}\left[1 - \frac{\varepsilon_s p(\varepsilon_s)}{1 - P(\varepsilon_s)}\right]\delta. \tag{8.10}$$

The solution of Eq. (8.10) has the form

$$\delta \sim \exp\left[-t/\tau\right], \tag{8.11}$$

where τ is the characteristic time scale of the relaxation process

$$\tau = \frac{\beta}{E}\frac{1}{\left[1 - \dfrac{\varepsilon_s p(\varepsilon_s)}{1 - P(\varepsilon_s)}\right]}. \tag{8.12}$$

We now study how the relaxation time τ changes when the external driving approaches the critical point σ_c from below. Based on Eq. (8.7) it can be simply shown that

$$\tau \sim (\sigma_c - \sigma_\mathrm{o})^{-1/2}, \quad \text{for} \quad \sigma_o < \sigma_\mathrm{c}, \tag{8.13}$$

which means that approaching the critical point from below the relaxation time of the system diverges according to a universal power law with an exponent $-\frac{1}{2}$ independent on the form of disorder distribution. Note that a similar power law divergence of the number of successive relaxation steps was found in Refs. [32, 33] for a dry fiber bundle subjected to a constant load.

Below the critical point the creep rupture of the viscoelastic bundle can be interpreted so that for $\sigma_\mathrm{o} \leq \sigma_\mathrm{c}$ the life time (or the time to failure) of the bundle is infinite $t_f = \infty$, while above the critical load $\sigma_\mathrm{o} > \sigma_\mathrm{c}$ global failure occurs at a finite time t_f, which can be determined by evaluating the integral Eq. (8.8) over the whole domain of definition of

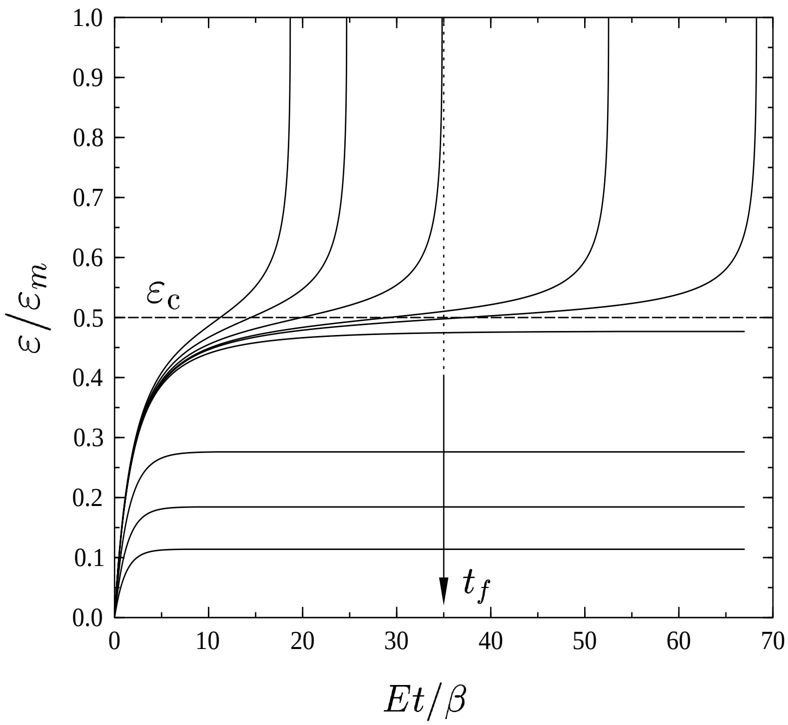

Figure 8.3: The analytic solution $\varepsilon(t)$ given by Eqs. (8.19,8.20) for several values of σ_o below and above σ_c. The critical strain ε_c and the time to failure t_f for one example are indicated.

$P(\varepsilon)$. From the theoretical and experimental point of view it is very important how t_f depends on the external load above σ_c. When σ_o is in the vicinity of σ_c, *i.e.*

$$\sigma_o = \sigma_c + \Delta\sigma_o, \tag{8.14}$$

where

$$\Delta\sigma_o << \sigma_c, \tag{8.15}$$

we can expect that the curve of $\varepsilon(t)$ falls very close to ε_c after a very long time and the breaking of the system occurs suddenly. Hence, the total time to failure, *i.e.* the integral in Eq. (8.8), is dominated by the region close to ε_c when $\Delta\sigma_o$ is small. Making use of the power series expansion Eq. (8.7) the integral in Eq. (8.8) can be rewritten as

$$t_f \approx \beta \int d\varepsilon \frac{1 - P(\varepsilon)}{\Delta\sigma_o - A(\varepsilon_c - \varepsilon)^2}, \tag{8.16}$$

which has to be evaluated over a small ε interval in the vicinity of ε_c. After performing

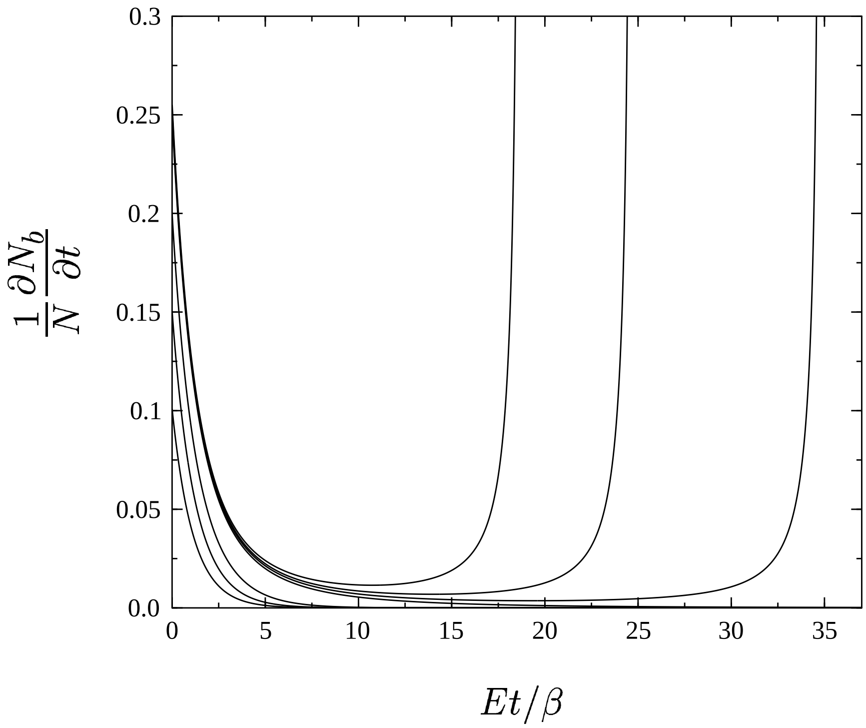

Figure 8.4: The analytic solution for the breaking rate Eq. (8.24) for several values of σ_o below and above σ_c

the integration it follows

$$t_f \approx (\sigma_o - \sigma_c)^{-1/2}, \qquad \text{for} \qquad \sigma_o > \sigma_c. \tag{8.17}$$

Thus, t_f has a power law divergence at σ_c with a universal exponent $-\frac{1}{2}$ independent of the specific form of the disorder distribution $p(\varepsilon)$.

For the purpose of explicit calculations we considered the case of a uniform distribution of the damage thresholds between 0 and a maximum value ε_m, thus, $p(\varepsilon) = \frac{1}{\varepsilon_m}$ and $P(\varepsilon) = \frac{\varepsilon}{\varepsilon_m}$. The stationary solution, the critical load and the corresponding critical strain can be obtained as:

$$\sigma_o = E\varepsilon(1 - \frac{\varepsilon}{\varepsilon_m}), \tag{8.18}$$
$$\sigma_c = E\frac{\varepsilon_m}{4}, \qquad \varepsilon_c = \frac{\varepsilon_m}{2}.$$

Finally, the solution of the integral Eq. (8.8) taking the initial condition also into account can be cast into the implicit form

$$t = -\frac{\beta}{2E} \left\{ \frac{1}{\sqrt{1-\frac{4\sigma_o}{E\varepsilon_m}}} \ln \frac{\frac{\varepsilon}{\varepsilon_m}\left[1+\sqrt{1-\frac{4\sigma_o}{E\varepsilon_m}}\right]+\frac{2\sigma_o}{E\varepsilon_m}}{\frac{\varepsilon}{\varepsilon_m}\left[1-\sqrt{1-\frac{4\sigma_o}{E\varepsilon_m}}\right]+\frac{2\sigma_o}{E\varepsilon_m}} - \ln \frac{E\varepsilon^2 - E\varepsilon_m\varepsilon + \sigma_o\varepsilon_m}{\sigma_o\varepsilon_m} \right\} \tag{8.19}$$

for $\sigma_o < \sigma_c$ (below the *critical point*), and

$$t = \frac{\beta}{E} \left\{ \frac{1}{\sqrt{\frac{4\sigma_o}{E\varepsilon_m}-1}} \left[arctg \frac{2\frac{\varepsilon}{\varepsilon_m}-1}{\sqrt{\frac{4\sigma_o}{E\varepsilon_m}-1}} - arctg \frac{-1}{\sqrt{\frac{4\sigma_o}{E\varepsilon_m}-1}} \right] - \frac{1}{2}\ln \frac{E\varepsilon^2 - E\varepsilon_m\varepsilon + \sigma_o\varepsilon_m}{\sigma_o\varepsilon_m} \right\} \tag{8.20}$$

for $\sigma_o > \sigma_c$ (above the *critical point*). The behavior of those analytical solutions are illustrated in Fig. 8.3 for several different values of σ_o.

The time to failure t_f can be determined by setting $\varepsilon = \varepsilon_m$ in Eq. (8.20), which results in the form

$$t_f \approx \frac{\beta\pi}{2}\sqrt{\frac{\varepsilon_m}{E}}\left(\sigma_o - \sigma_c\right)^{-1/2}, \tag{8.21}$$

in accordance with the above general arguments.

A further important general property of $\varepsilon(t)$ that can be deduced from Eqs. (8.3,8.8) is that at the time to failure t_f the deformation rate $\frac{d\varepsilon}{dt}$ diverges. For disorder distributions $P(\varepsilon)$ defined in a finite interval the exponent is universal

$$\frac{d\varepsilon}{dt} \approx (t_f - t)^{-1/2}. \tag{8.22}$$

In order to obtain information about the gradual breaking of fibers during the creep process, in the experiments the acoustic signal emitted by breaking events in a short time interval is investigated [109, 110]. In our fiber bundle model the number of fibers $N_b(t)$ which have been broken up to time t can be determined as

$$N_b(t) = NP(\varepsilon(t)), \tag{8.23}$$

and hence, its derivative provides the quantity

$$\frac{1}{N}\frac{\partial N_b}{\partial t} = \frac{dP}{d\varepsilon}\frac{d\varepsilon}{dt} = \frac{p(\varepsilon)E\varepsilon}{\beta}\left[\frac{\sigma_o}{E\varepsilon\left[1-P(\varepsilon)\right]} - 1\right], \tag{8.24}$$

which is a measure for the acoustic response. The behavior of Eq. (8.24) for the uniform distribution is illustrated in Fig. 8.4, where it can be observed that the acoustic activity, *i.e.* fiber breaking, practically disappears in the plateau region of $\varepsilon(t)$ (compare to Fig. 8.3), however, it diverges at t_f due to the diverging deformation rate.

Since during a creep test $\varepsilon(t)$ is monitored from which $\frac{d\varepsilon}{dt}$ can be calculated, furthermore, $\frac{\partial N_b}{\partial t}$ is measured by means of acoustic emission techniques, Eq. (8.24) makes possible to determine experimentally the distribution of the failure thresholds $p(\varepsilon)$.

Simulation technique

The analytic results of the previous sections were obtained for infinite bundles. Computer simulations of the creep rupture of finite bundles are needed to justify the validity of analytic predictions for finite systems, and to be able to model the rupture process of

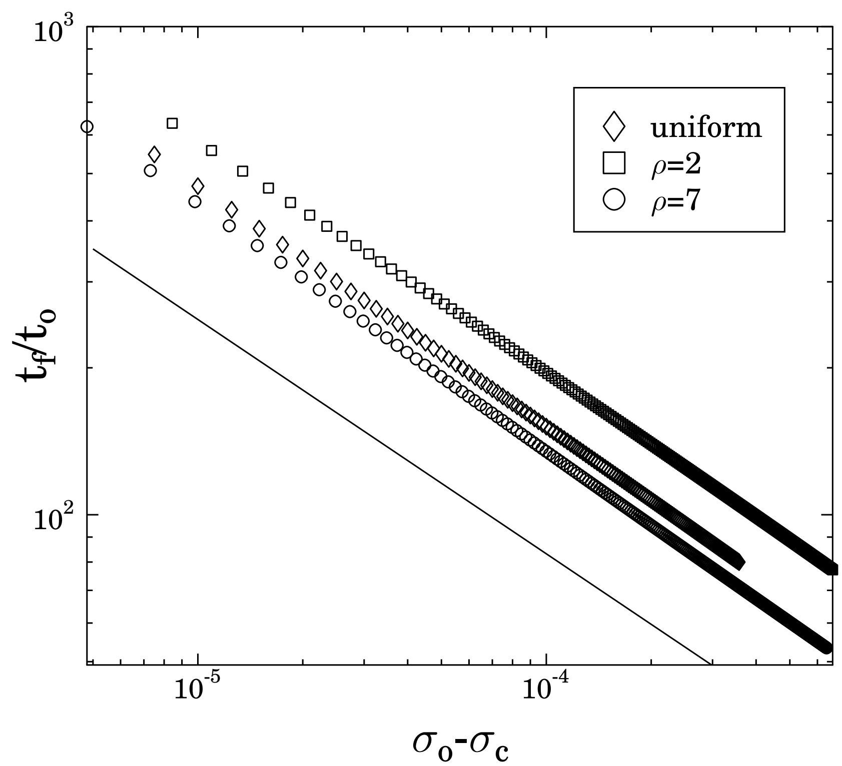

Figure 8.5: The lifetime of a bundle of 10^7 fibers as a function of $\sigma_o - \sigma_c$ above the critical point for three different disorder distributions, *i.e.* uniform and Weibull distributions with $\rho = 2$ and 7 have been considered. The straight line of slope -0.5 is a to guide the eye.

realistic finite systems. In the framework of GLS an efficient simulation technique can be worked out for the failure process. Based on the arguments of the previous subsection, the GLS simulation of the creep process of a bundle of N fibers proceeds as follows:

- random breaking thresholds $\varepsilon_i,\ i = 1, \ldots, N$ are drawn from a probability distribution p, then the thresholds are put into increasing order.
- The time $\Delta t(\varepsilon_i, \varepsilon_{i+1})$ between the breaking of the ith and $i+1$th fibers is calculated according to

$$\Delta t(\varepsilon_i, \varepsilon_{i+1}) = -\frac{\beta}{E}\left[\ln\left(\varepsilon_{i+1} - \frac{\sigma_i}{E}\right) - \ln\left(\varepsilon_i - \frac{\sigma_i}{E}\right)\right]. \tag{8.25}$$

- The time elapsed till the breaking of the ith fiber is obtained as:

$$t(\varepsilon_i) = \sum_{j=0}^{i-1} \Delta t(\varepsilon_i, \varepsilon_{i+1}),$$

from which the deformation as a function of time $\varepsilon(t)$ can be determined by inversion.

To test the validity of the universal power law behavior of t_f as a function of the distance from the critical load given by Eq. (8.17), simulations were performed with various disorder distributions, *i.e.* besides the uniform distribution the Weibull distribution was used. The value of the characteristic strain σ_o^b was set to one, and the shape of the distribution was controlled by varying the value of ρ. The results are presented in Fig. 8.5, where an excellent agreement between the simulations and the analytic results can be observed. Fig. 8.5 supports that the exponent of t_f as a function of $\sigma_o - \sigma_c$ is universal, it does not depend on the specific form of the disorder distribution.

Finite size effect

In the above analytic treatment the size of the system, *i.e.* the number of fibers in the bundle, is infinite. However, it can be expected that the lifetime of a finite bundle has a non-trivial size scaling even in the case of global load sharing.

In order to determine how t_f depends on N, Eq. (8.26) has to be averaged over many realizations of the disorder distribution, which can be performed analytically. The details

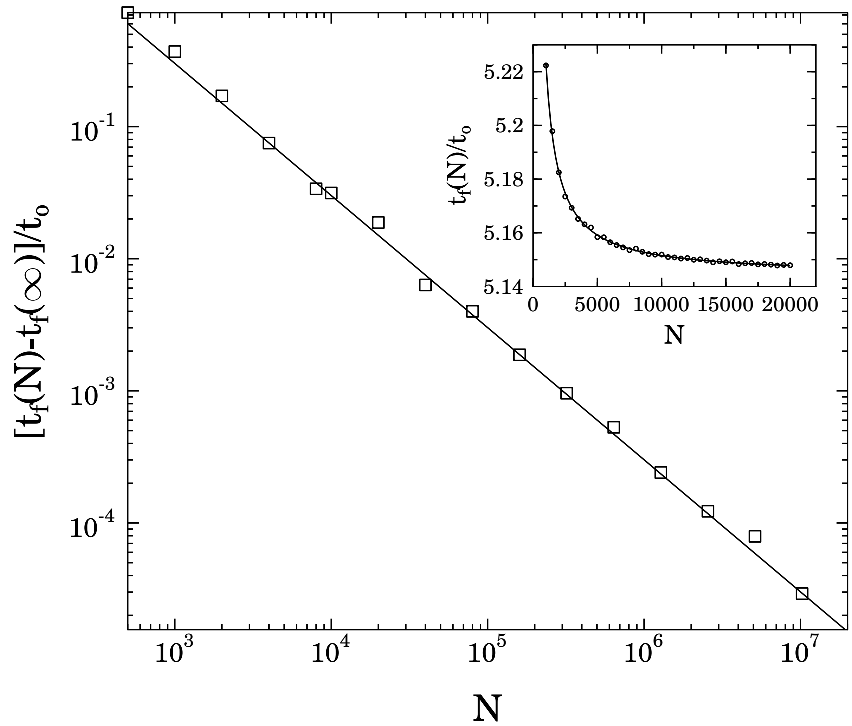

Figure 8.6: The size dependent lifetime of the bundle. The inset shows the lifetime of relatively small systems in a linear plot, while in the main figure the difference of the lifetime of finite bundles and the infinite one obtained from Eq. (8.26) can be seen in a double logarithmic plot. The slope of the fitted straight line is -0.99 ± 0.02.

of the analytic calculations are summarized in the Appendix of this chapter. Finally, the average lifetime $\langle t_f(N) \rangle$ of a bundle of N fibers can be cast into the form

$$\langle t_f(N) \rangle \approx t_f(\infty) + \frac{\beta \sigma_o}{N} \int \frac{E\varepsilon P(\varepsilon)\left[1 - P(\varepsilon)\right]}{\left[\sigma_o - E\varepsilon(1 - P(\varepsilon))\right]^3} d\varepsilon. \qquad (8.26)$$

Eq. (8.26) shows that for finite bundles the average lifetime $\langle t_f(N) \rangle$ converges to the lifetime of the infinite bundle $t_f(\infty)$ as $\sim 1/N$ with increasing number of fibers N. It is interesting to note that in the case of global load sharing the average strength of the bundle σ_c does not have any size dependence.

To study the finite size scaling of the time to failure t_f a uniform distribution was used for the failure thresholds. The value of the external load was fixed above σ_c and the number of fibers N was varied from 5×10^2 to 10^7. Averages were calculated over 10^4 samples for each system size N. The results obtained by simulations are presented in Fig. 8.6, where an excellent agreement of simulations and analytic results can be observed for four orders of magnitude in the system size N.

Statistics of events

As fibers fail one-by-one, furthermore, under GLS conditions, breakings occur in the order of increasing breaking thresholds ε_i and the time $\Delta t(\varepsilon_i, \varepsilon_{i+1})$ elapsed between the breaking of i-th and $i+1$-th fibers can be analytically obtained. The inter-event time Δt is a fluctuating quantity which depends both on the breaking thresholds and the load level. The statistics of inter-event times characterized by the distribution $f(\Delta t)$ provides information on the microscopic dynamics of creep. $f(\Delta t)$ is presented in Fig. 8.7 for a system of $N = 2 \times 10^7$ fibers.

Simulations revealed that $f(\Delta t)$ exhibits a power law of the form

$$f(\Delta t) \sim \Delta t^{-b} \tag{8.27}$$

both below and above the critical point whenever the macroscopic stationary state characterized by the plateau of $\varepsilon(t)$ is attained. However, the value of the exponent b is different on the two sides of the critical point, *i.e.* below σ_c the exponent of the distribution is $b = 1.95 \pm 0.05$ independent of σ_o, while above σ_c we obtained $b = 1.5 \pm 0.05$. Increasing the load above σ_c the stationary state gradually disappears implying that the power law regime of $f(\Delta t)$, which precedes the exponential cut-off, is getting shorter but the exponent remains the same (see Fig. 8.7). It follows for the creeping bundle that: the threshold dynamics of the system is characterized by a separation of time scales of the external driving and the relaxation process leads to the emergence of a macroscopic stationary state accompanied by power law distributed microscopic events.

8.1.2 Local load sharing

Simulation technique

To clarify how the damage process and the behavior of the life time t_f is affected by the range of interaction among fibers, *i.e.* by the range of load sharing we performed calculations with local load sharing. Since this case cannot be treated analytically, we perform numerical simulations in the Kelvin viscoelastic model shown in the figure 8.1.

As in the global load sharing case we suppose a set of N parallel fibers each one having statistically distributed strength taken from a probability distribution function $P(\varepsilon)$ and identified by an integer i, $1 \leq i \leq N$ on a square lattice. After fiber failure the load is redistributed equally among the intact nearest neighbors. As the load is locally distributed the numerical task is more complicated than in the global case since the local stress is different for each fiber.

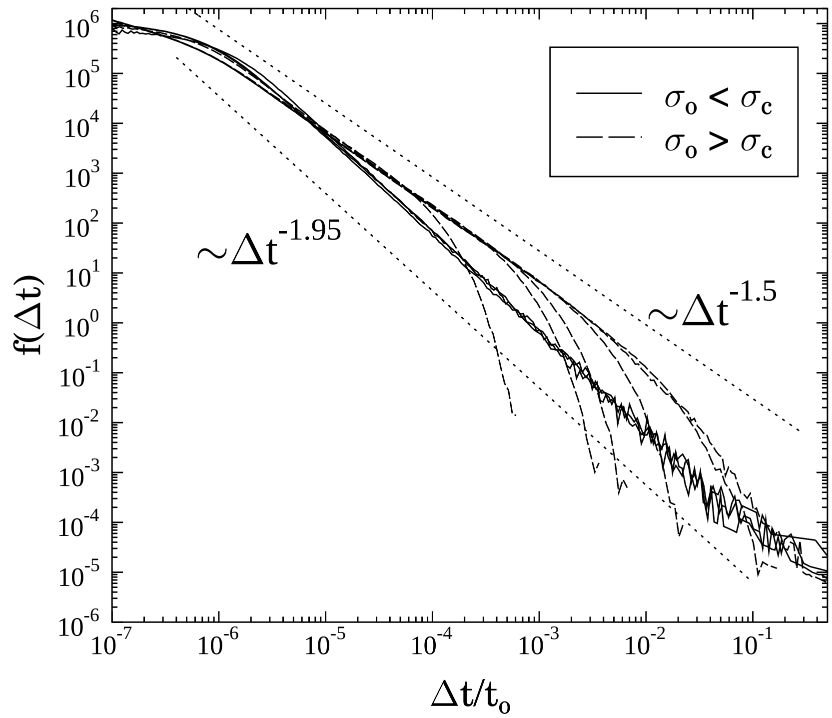

Figure 8.7: The distribution of inter-event times Δt for GLS ($\gamma = 0$). Power law behavior can be observed over up to five orders of magnitude.

Firstly, on all the fibers the same load is imposed. Then the algorithm to simulate the creep process is as follows:

- The equation of motion Eq. 8.1 is integrated with a given time step Δt for each fiber of the system.
- If one of the fiber strain reaches its threshold value it breaks.
- The load carried by the failed fiber is redistributed equally on the intact nearest neighbors, and the load of the broken fiber is set to zero.
- This procedure goes on until the breaking process stops, either when all the fibers are broken ($\sigma_o > \sigma_c$) or when all the remaining intact fibers are strong enough to survive (for $\sigma_o < \sigma_c$).

Since now the strain of the fibers is a local quantity $\varepsilon_i(t)$, the macroscopic strain can only

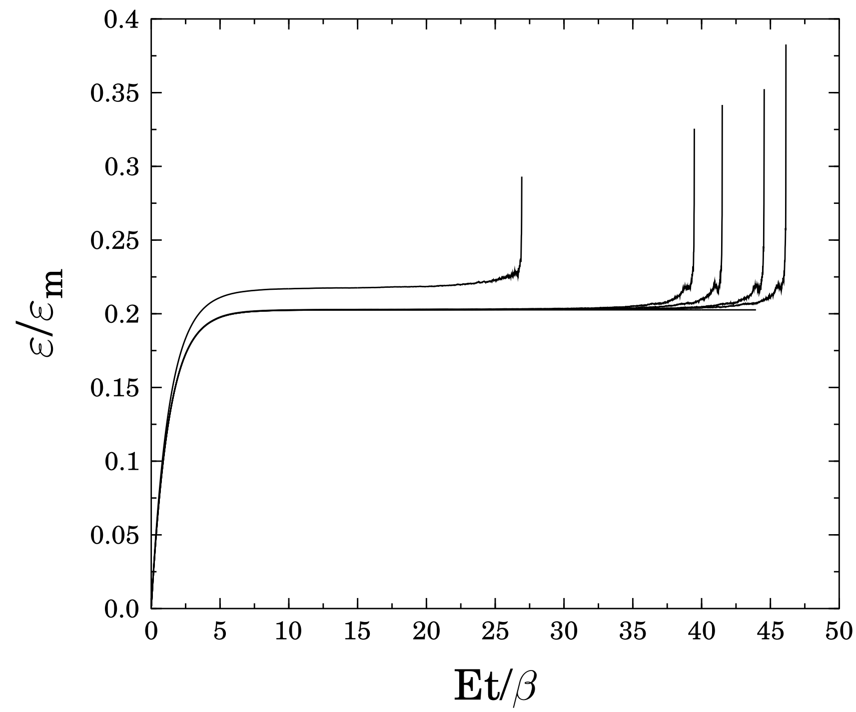

Figure 8.8: The numerical result of $\varepsilon(t)$ for several values of σ_o below and above σ_c in local load sharing approach.

be defined as the mean value $\overline{\varepsilon}(t)$ of $\varepsilon_i(t)$,

$$\overline{\varepsilon}(t) = \frac{\sum \varepsilon_i(t)}{N_{nb}} \tag{8.28}$$

The dependence $\overline{\varepsilon}(t)$ vs time for different values of external stress is presented in Fig. 8.8. As in the global case there is a critical stress value σ_c. In numerical experiments using external stress values lower than σ_c the macroscopic strain $\overline{\varepsilon}(t)$ of the sample evolves to an asymptotic state. And if $\sigma > \sigma_c$ the global failure of the sample occurs in a finite time. As it can be checked in Fig. 8.8 the global failure is more abrupt than in the global case (compare to Fig. 8.3) which is characteristic for brittle materials. The exact value of the critical load σ_c is determined as the static fracture strength of a dry fiber bundle with local load sharing assuming perfectly elastic behavior of fibers.

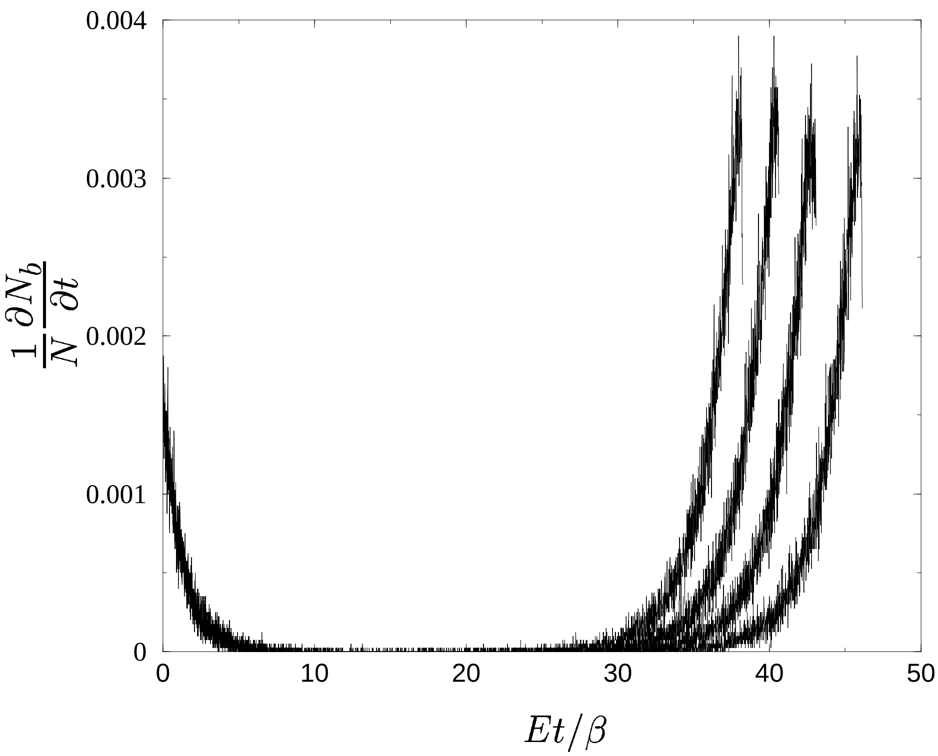

Figure 8.9: The numerically calculated breaking rate for several values of σ_o below and above σ_c, in local load sharing approach

In Fig. 8.1.2 the numerical breaking rate $\frac{1}{N}\frac{\partial N_b}{\partial t}$ is also presented for different external stress values. Again an intensive activity appears at the beginning of the creep process. During the *plateu* period (constant strain ε) almost no activity is detected and finally the catastrophic failure is preceded by increasing failure activity.

Comparing the time to failure results of the local load sharing simulations to the global load sharing ones we observe that above σ_c the failure of the viscoelastic bundle occurs much more abruptly than in the global case. Varying σ as a control parameter the two regimes of the creep rupture process are characterized by an infinite life time below σ_c and by a finite one above the critical point. The nature of the transition between the regimes in the global and local load sharing models can be characterized by studying $1/t_f$ as a function of the control parameter σ_o. In Fig. 8.10 we observe that below the critical point, when no global failure occurs, $1/t_f$ is zero, while above σ_c it takes a finite value for both global and local load sharing. However, the behavior of $1/t_f$ in the vicinity of σ_c is completely different in the two cases, for global load sharing the transition is continuous. Nevertheless, for local load sharing $1/t_f$ has a finite jump, analogously to a second and first order phase transition, respectively.

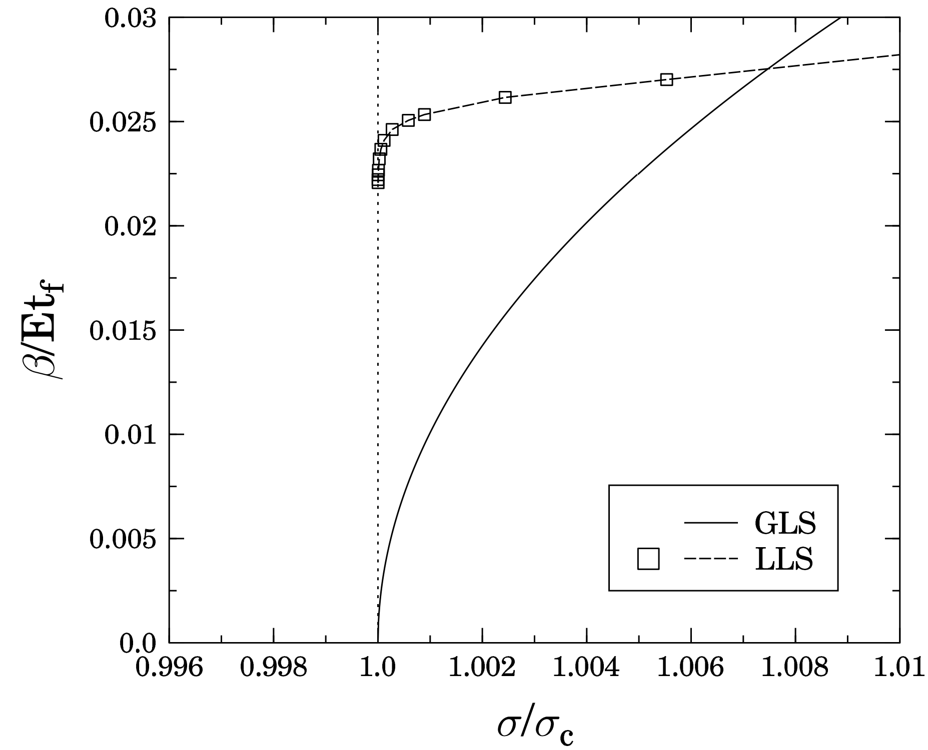

Figure 8.10: Comparison of $1/t_f$ for the LLS and GLS cases as a function of the normalized external load.

8.1.3 Variable range of interaction

To explore the effect of the details of load redistribution on the creep rupture process we studied how the behavior of the system changes in the vicinity of the critical point when the load sharing gets localized. Our fiber bundle model with variable range of interaction, presented in Chapter 6, is able to interpolate between the limiting cases of global and completely local load sharing considered above. Simulations have been performed varying the effective range of interaction of fibers by controlling the exponent γ of the load sharing function (see Chapter 6).

Simulation technique

The system is composed of N parallel fibers identified by an integer i, $1 \leq i \leq N$ on a square lattice, which initially have identical Young-modulus E_f but with random failure thresholds d_i, $i = 1, \ldots, N$. The failure strength d_i of individual fibers is an independent identically distributed random variable with a probability density $p(d)$ and a cumulative

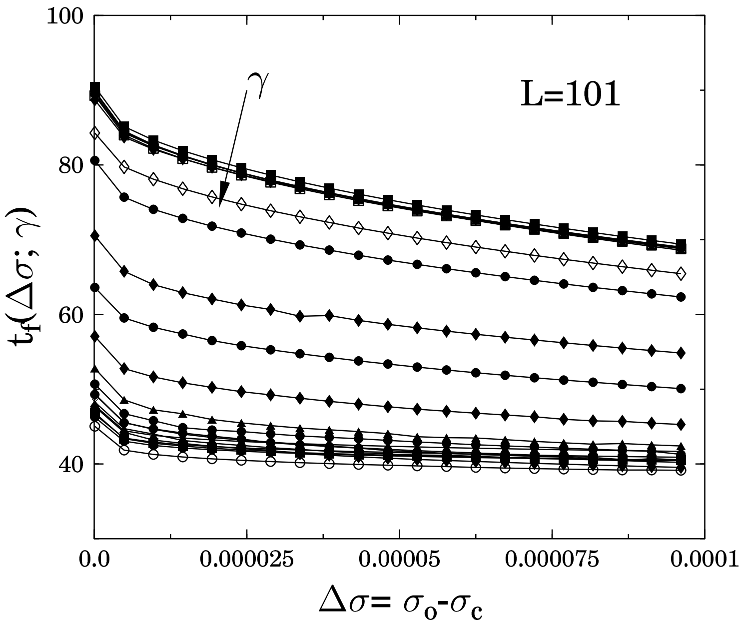

Figure 8.11: The lifetime t_f as a function of $\sigma_o - \sigma_c$ for different values of the exponent γ between 0 and 10.

probability distribution $P(d) = \int_0^d p(x)dx$.

Firstly, on all the fibers the same load is imposed. Then after the ith fiber break, the additional load received by an intact fiber j depends on its distance r_{ij} from fiber i which has just been broken. Hence the load received by a fiber follows the power law form of Eq. (6.2). Then the algorithm to simulate the creep process is as follows: The stress in the surviving element i at time t_{k+1} *i.e.* $\sigma_f^i(t_{k+1})$ is related to the stress at time t_k in the following manner:

$$\sigma_f^i(t_{k+1}) = \sigma_f^i(t_k)(1 - e^{-\frac{E}{\beta}\Delta t_{k+1}}) \tag{8.29}$$

with

$$\Delta t_i = t_{k+1} - t_k. \tag{8.30}$$

Note that t_k denotes the time of the $k-th$ breaking. Using Eq. (8.29), the time elapsed that each element of the system would spend before it breaks under the present local load can be deduced as:

$$\Delta t_i = -\frac{\beta}{E} \ln \left(1 - \frac{\sigma_f^i(t_{k+1})}{\sigma_f^i(t_k)} \right). \tag{8.31}$$

Moreover, when the element i breaks, its stress can be assumed to be equal to its thresholds value d_i, substituting $\sigma_f^i(t_{k+1}) = d_i$ results in:

$$\Delta t_i = -\frac{\beta}{E} \ln\left(1 - \frac{d_i}{\sigma_f^i(t_k)}\right). \tag{8.32}$$

The minimum over the set Δt_i is the time interval between the kth and the $k+1$th breakings

$$\Delta t_{k+1} = \min_{i \in I} \Delta t_i. \tag{8.33}$$

and the time elapsed till the breaking of the $k+1$th fiber is obtained as

$$t_{k+1} = \sum_{j=1}^{k+1} \Delta t_j, \tag{8.34}$$

Time to failure

Fig. 8.11 presents the lifetime t_f of a bundle of fibers arranged on a square lattice of side length $L = 101$ as a function of the distance from the critical point $\Delta\sigma = \sigma_o - \sigma_c$ for several values of the exponent γ. It can be observed that the $t_f(\Delta\sigma;\gamma)$ curves form two groups of different functional form: The upper group is obtained for $0 \leq \gamma \leq 1.95$ when the load sharing is global. In the lower group, obtained for $\gamma > 2.9$ when the load sharing gets localized, $t_f(\Delta\sigma;\gamma)$ rapidly takes a constant value showing an abrupt transition at the critical load σ_c with no scaling, reminiscent of a first order transition. The results imply the existence of two universality classes in creep rupture characterized by a completely global (GLS), or a completely local (LLS) behavior depending on the effective range of interaction γ with a rather sharp transition between them. In order to quantify the behavior of $t_f(\Delta\sigma;\gamma)$ under the variation of γ we calculated the normalized quantity

$$S(\gamma) = \frac{[t_f(\gamma) - t_f(10)]}{[t_f(0) - t_f(10)]}, \tag{8.35}$$

where $t_f(\gamma)$ denotes the value of t_f at the smallest value of $\Delta\sigma$ used to calculate $t_f(\Delta\sigma;\gamma)$ at a given γ. Fig. 8.12 shows that $S(\gamma)$ provides a quantitative description of the creep rupture transition in terms of the effective range of interaction so that $S(\gamma)$ takes value unity for the GLS, and has a value close to zero for the LLS class, respectively. We can also observe in Fig. 8.12 that the transition between the two universality classes gets sharper around $\gamma_c \approx 2$ with increasing system size. Real materials described by a finite value of γ must fall into one of the above universality classes. The existence of only two universality classes implies that the mean field analytical results can be extended beyond $\gamma = 0$, *i.e.*, they apply for a wider interaction range which is relevant for real materials.

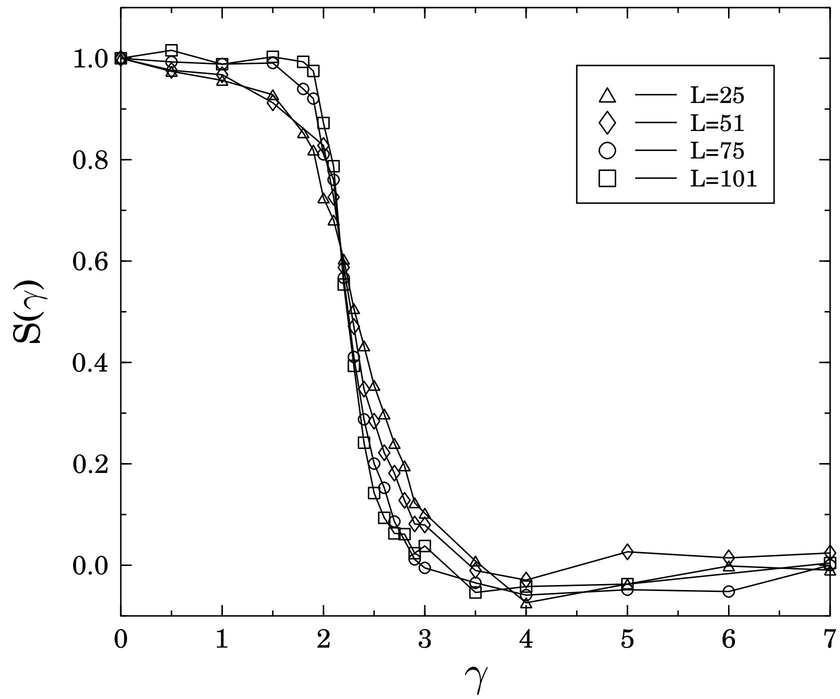

Figure 8.12: $S(\gamma)$ is presented for several system sizes L.

Extensive simulations revealed that whenever a macroscopic stationary state is attained by the system, the distribution of inter-event times follows a power law irrespective of the range of interaction γ. Below the critical point the exponent b of the distribution has a value $b = 1.95 \pm 0.05$ independent of γ, while above the critical point b is different in the two universality classes as illustrated by the Fig. 8.13. In the LLS class the exponent b has practically the same value below and above σ_c.

The breaking process of fibers occurring in a solid under various loading conditions can be monitored by acoustic emission techniques which has also been applied to study creep rupture. The statistics of inter-event times has been studied in various types of materials like wood, plaster, basalt, and fiber glass. It was found experimentally that the distribution of inter-event times always exhibits a power law behavior, however, the values of b were found to depend on the material falling between 1.2 and 1.9 [61, 62, 88] for $\sigma_o > \sigma_c$. Hence, our theoretical findings are in quite reasonable agreement with the available experimental results. Moreover, the different values of b below and above σ_c predicted by our model for long range interactions would correspond to different Omori's exponents for foreshocks and aftershocks in earthquake dynamics, which has also been observed recently [111].

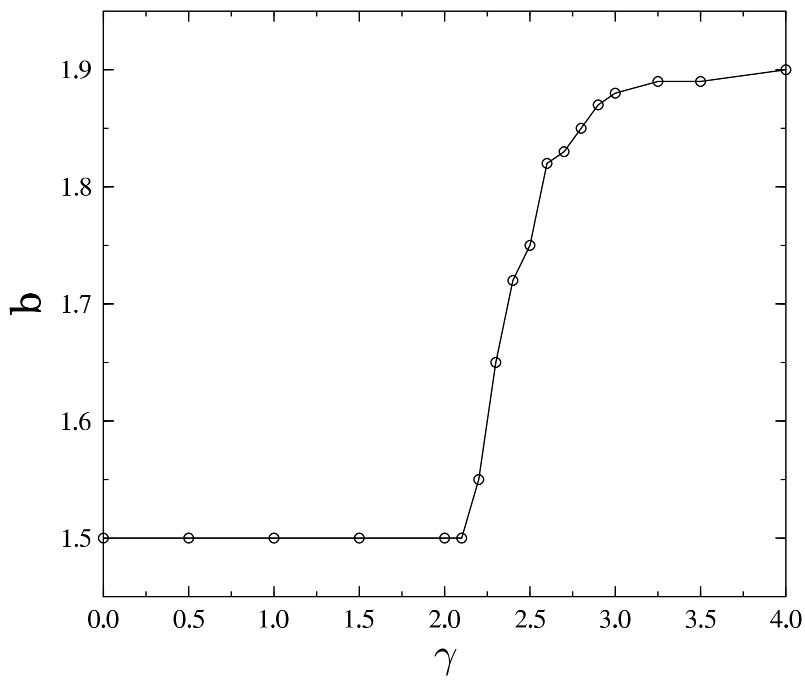

Figure 8.13: The exponent b of the Δt distribution $f(\Delta t)$ as a function of the range of interaction γ for $\sigma_o > \sigma_c$.

8.2 Conclusions

We have studied the creep rupture of bundles of viscoelastic fibers occurring under uniaxial constant tensile loading. A novel fiber bundle model is introduced which combines the viscoelastic constitutive behavior and the strain controlled breaking of fibers. Although study of the model has been presented varying the range of interaction of fibers. Analytical and numerical calculations showed that above a critical external load the deformation of the system monotonically increases in time resulting in global failure at a finite time t_f, while below the critical load the deformation tends to a constant value giving rise to an infinite lifetime. We have identified two universality classes of creep rupture depending on the range of interaction of fibers. The critical behavior of the microfracturing process can be seen as the result of the self-organization of the system into a macroscopic stationary state whose duration depends on the external perturbation (load). In this sense the system is at some point of marginal stability jumping form one metastable state to another with power-law distributed waiting times. This suggests the existence of a critical dynamics underlying the process that seems to indicate self-organized criticality in creep. Our theoretical results provide a consistent explanation of recent experimental findings in the damage process of creep rupture [61, 62, 88, 112].

8.3 Appendix

Here we provide the derivation of the average lifetime for the general case when the lifetime t_f of a bundle with a specific realization of the disorder can be cast in the form

$$t_f = \sum_{i=0}^{N-1} \left[G(\frac{i}{N}, x_{i+1}) - G(\frac{i}{N}, x_i) \right], \tag{8.36}$$

i.e. t_f is a sum of terms which depend on the number of broken fibers i and on a single breaking threshold x_i that can be given as strain or stress. The x_i-s are obtained by choosing N breaking thresholds independently from a cumulative probability distribution $P(x)$ and putting them into increasing order. This treatment includes both models discussed in the present paper. The expectation value of a function $f(x_i)$ can be determined as

$$\langle f(x_i) \rangle = \int \frac{N!}{(i-1)!(N-i)!} P(x)^{i-1} \left[1 - P(x)\right]^{N-i} \times p(x) f(x) dx. \tag{8.37}$$

The probability distribution in Eq. (8.37) that the value of the ith largest breaking threshold falls between x and $x + dx$ has a sharp peak for large N values for each i. The above integration can be carried out by expanding the distribution about its peak. After expanding the result in terms of $1/N$ and neglecting higher order terms we arrive at

$$\langle f(x_i) \rangle = f(\overline{x}_i) + \frac{1}{2N} P(\overline{x}_i)(1 - P(\overline{x}_i)) \times \left[\frac{f''(\overline{x}_i)}{[P'(\overline{x}_i)]^2} - \frac{f'(\overline{x}_i) P''(\overline{x}_i)}{[P'(\overline{x}_i)]^3} \right], \tag{8.38}$$

where $\overline{x}_i$ is defined implicitly by $P(\overline{x}_i) = i/(N+1)$. Applying Eq. (8.38) to Eq. (8.36) the resulting summation can be approximated by integrals replacing i/N by the equivalent $P(\overline{x}_i)(1 + 1/N)$. Neglecting corrections of higher order in $1/N$ after straightforward calculations we arrive at

$$\langle t_f \rangle \approx \int dx \partial_2 G(P(x), x) + \frac{1}{2N} \int dx P(x) \left(1 - P(x)\right) \partial_1^2 \partial_2 G(P(x), x), \tag{8.39}$$

where $\partial_2 G(y, x) \equiv \partial G(y, x)/\partial x$, and $\partial_1^2 \partial_2 G(y, x) \equiv \partial^3 G(y, x)/\partial^2 y \partial x$. Substituting the actual form of $G(y, x)$ for a specific model the complete form of the size scaling of lifetime can be obtained. However, it can be seen in the general expression Eq. (8.39) that the first term provides the lifetime of the infinite bundle and the only size dependence is in the prefactor of the second term. Eq. (8.39) states that if the lifetime can be written in the form of Eq. (8.36) the lifetime of finite bundles converges to that of the infinite one as $1/N$ with increasing number of fibers N.

Chapter 9

Slow relaxation of fiber composites

An important microscopic mechanism which can lead to macroscopic creep is the slow relaxation following fiber failure. In this case, the components of the solid are linearly elastic until they break, however, after breaking they undergo a slow relaxation process, which can be caused, for instance, by the sliding of broken fibers with respect to the matrix material or by the creeping matrix [39]. To take into account this effect, in this chapter we present an approach based on the model introduced in Refs. [82], where the response of a viscoelastic-plastic matrix reinforced with elastic and also viscoelastic fibers have been studied.

9.1 Model

The model consists of N parallel fibers, which break in a stress controlled way, *i.e.* subjecting a bundle to a constant external load fibers break during the time evolution of the system when the local load on them exceeds a stochastically distributed breaking threshold $\sigma_i, i = 1, \ldots, N$. Intact fibers are assumed to be linearly elastic *i.e.* $\sigma = E_\mathrm{f}\varepsilon_\mathrm{f}$ holds until they break, and hence, for the deformation rate applies

$$\dot{\varepsilon}_\mathrm{f} = \frac{\dot{\sigma}}{E_\mathrm{f}}. \tag{9.1}$$

Here ε_f denotes the strain and E_f is the Young modulus of intact fibers, respectively. The main assumption of the model is that when a fiber breaks its load does not drop to zero instantaneously, instead it undergoes a slow relaxation process introducing a time scale into the system. In order to capture this effect, the broken fibers with the surrounding matrix material are modeled by Maxwell elements as illustrated in Fig. 9.1, *i.e.* they are conceived as a serial coupling of a spring and a dashpot which results in a non-linear response

$$\dot{\varepsilon}_{\mathrm{b}} = \frac{\dot{\sigma}_{\mathrm{b}}}{E_{\mathrm{b}}} + \frac{\sigma_{\mathrm{b}}^{\mathrm{m}}}{\beta}, \tag{9.2}$$

where σ_b and ε_{b} denote the time dependent load and deformation of a broken fiber, respectively. The relaxation of the broken fiber is characterized by three parameters E_b, β, and m, where E_b is the effective stiffness of a broken fiber, and the exponent m characterizes the strength of non-linearity of the element. We study the behavior of the system for the region $m \geq 1$.

9.1.1 Global load sharing

Analytical model

Assuming global load sharing for the load redistribution, the constitutive equation describing the macroscopic elastic behavior of the composite reads as

$$\sigma_{\mathrm{o}} = \sigma(t)\left[1 - P(\sigma(t))\right] + \sigma_{\mathrm{b}}(t)P(\sigma(t)). \tag{9.3}$$

Eq. (9.3) takes into account that broken fibers carry also a certain amount of load $\sigma_b(t)$, furthermore, $P(\sigma(t))$ and $1 - P(\sigma(t))$ denote the fraction of broken and intact fibers at time t, respectively. It can be seen from Eq. (9.3) that under a constant external load σ_0, the load of intact fibers σ will also be time dependent due to the slow relaxation of the broken ones.

Due to the boundary condition illustrated in Fig. 9.1, the two time derivatives have to be always equal

$$\dot{\varepsilon}_{\mathrm{f}} = \dot{\varepsilon}_{\mathrm{b}}. \tag{9.4}$$

The differential equation governing the time evolution of the system can be obtained by expressing σ_{b} in terms of σ from Eq. (9.3) and substituting it into Eq. (9.2) and finally into Eq. (9.4)

$$\dot{\sigma}\left\{\frac{1}{E_{\mathrm{f}}} - \frac{1}{E_{\mathrm{b}}}\left[1 - \frac{1}{P(\sigma)} + \frac{p(\sigma)}{P(\sigma)^2}(\sigma - \sigma_{\mathrm{o}})\right]\right\} = \frac{1}{\beta}\left[\frac{\sigma_{\mathrm{o}} - \sigma\left[1 - P(\sigma)\right]}{P(\sigma)}\right]^m. \tag{9.5}$$

In order to determine the initial condition for the integration of Eq. (9.5) the breaking process of fibers has to be analyzed. Subjecting the undamaged specimen to an external

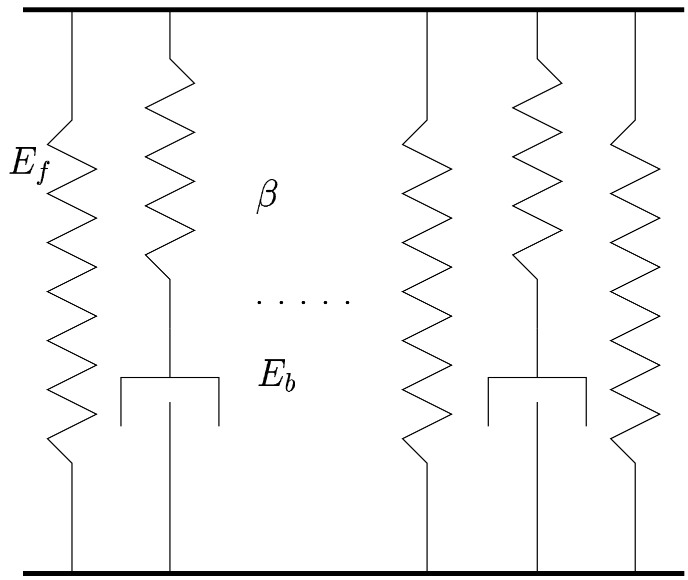

Figure 9.1: The model solid when intact fibers are linearly elastic, and the broken ones with the surrounding matrix are modeled by Maxwell elements.

stress σ_o all the fibers attain this stress value immediately due to the linear elastic response. Hence the time evolution of the system can be obtained by integrating Eq. (9.5) with the initial condition $\sigma(t=0) = \sigma_o$. Since intact fibers are linearly elastic, the deformation-time history $\varepsilon(t)$ of the model can be deduced as $\varepsilon(t) = \frac{\sigma(t)}{E_f}$, which has an initial jump to $\varepsilon_o = \frac{\sigma_o}{E_f}$. It follows that those fibers which have breaking thresholds σ_i smaller than the externally imposed σ_o immediately break. To characterize the macroscopic behavior of the composite the solutions $\sigma(t)$ of Eq. (9.5) have to be analyzed at different values of the external load σ_o. Similarly to the previous creep model (see Chapter 8), two different regimes of $\sigma(t)$ can be distinguished depending on the value of σ_o: if the external load falls below a critical value σ_c a stationary solution σ_s of the governing equation exists which can be obtained by setting $\dot{\sigma} = 0$ in Eq. (9.5)

$$\sigma_o = \sigma_s \left[1 - P(\sigma_s)\right]. \tag{9.6}$$

This means that until Eq. (9.6) can be solved for σ_s the solution $\sigma(t)$ of Eq. (9.5) converges asymptotically to σ_s resulting in an infinite lifetime t_f of the composite. Note that Eq. (9.6) also provides the asymptotic constitutive behavior of the model which can be measured by quasistatic loading. If the external load falls above the critical value the deformation rate $\dot{\varepsilon} = \frac{\dot{\sigma}}{E_f}$ remains always positive resulting in a macroscopic rupture in a finite time t_f. It follows from Eq. (9.6) that the critical load σ_c of creep rupture coincides

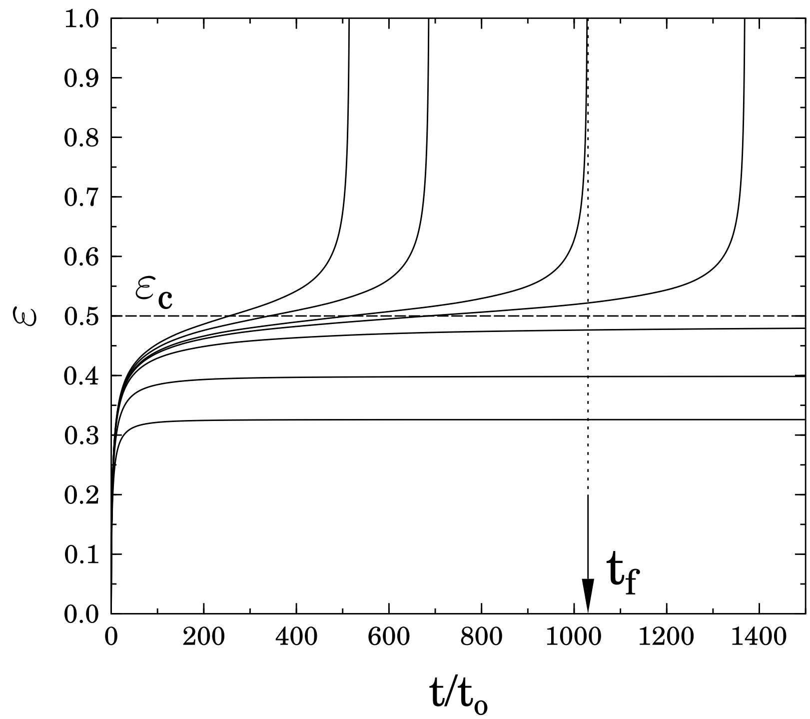

Figure 9.2: Simulation of ε as a function of t for several value of σ_o below and above σ_c. $N = 10^7$ fibers were used.

with the static fracture strength of the composite.

The behavior of the system again shows universal aspects in the vicinity of the critical point. Below the critical point the relaxation of $\sigma(t)$ to the stationary solution σ_s is governed by a differential equation of the form

$$\frac{d\delta}{dt} \sim \delta^m, \tag{9.7}$$

where δ denotes the difference $\delta(t) = \sigma_s - \sigma(t)$. Hence,the characteristic time scale τ of the relaxation process only emerges if $m = 1$, furthermore, in this case also

$$\tau \sim (\sigma_c - \sigma_o)^{-\frac{1}{2}} \tag{9.8}$$

holds when approaching the critical point. However, for $m > 1$ the relaxation process is characterized by

$$\delta(t) = at^{\frac{1}{1-m}}, \tag{9.9}$$

where $a \to 0$ with $\sigma_0 \to \sigma_c$.

Similarly to the previous creep model (see chapter 8), it can also be shown that the lifetime t_f of the bundle has a power law divergence when the external load approaches the critical point from above

$$t_f \sim (\sigma_0 - \sigma_c)^{-(m-\frac{1}{2})}, \quad \text{for} \quad \sigma_o > \sigma_c. \tag{9.10}$$

The exponent is universal in the sense that it is independent on the disorder distribution, however, it depends on the stress exponent m, which characterizes the non-linearity of broken fibers.

Simulation technique

Subjecting a finite bundle of N fibers to an external stress σ_o those fibers whose failure threshold falls below σ_o break immediately. The number N_o of initially breaking fibers can be estimated from the disorder distribution as $N_o \approx NP(\sigma_o)$. In the presence of broken fibers the system slows down and the remaining fibers of the bundle break one-by-one in the increasing order of their breaking thresholds

$$\sigma_{N_o+1} < \sigma_{N_o+2} < \sigma_N. \tag{9.11}$$

In order to construct an efficient simulation technique one has to determine the time elapsed between two consecutive breakings during the creep process.

The macroscopic constitutive equation for a system of N fibers when i fibers have already failed can be written as

$$\sigma_o = \sigma \frac{N-i}{N} + \sigma_b \frac{i}{N}. \tag{9.12}$$

Making use of Eqs. (9.2,9.4), the differential equation describing the time evolution of the load of intact fibers σ can be cast into the form

$$\dot{\sigma} \left[\frac{1}{E_f} - \frac{1}{E_b} \left(1 - \frac{N}{i} \right) \right] = B \left(\frac{N}{i} \right)^m f_i(\sigma)^m, \tag{9.13}$$

where $f_i(x)$ is introduced for brevity as

$$f_i(x) = \sigma_o - \frac{N-i}{N} x \tag{9.14}$$

The time $\Delta t(\sigma_i, \sigma_{i+1})$ elapsed between the breaking of the ith and $i+1$th fiber can be determined by integrating Eq. (9.13) from σ_i to σ_{i+1}, which yields for $m \neq 1$

$$\Delta t(\sigma_i, \sigma_{i+1}) = \frac{K_i}{(m-1)} \left[f_i(\sigma_{i+1})^{1-m} - f_i(\sigma_i)^{1-m} \right], \tag{9.15}$$

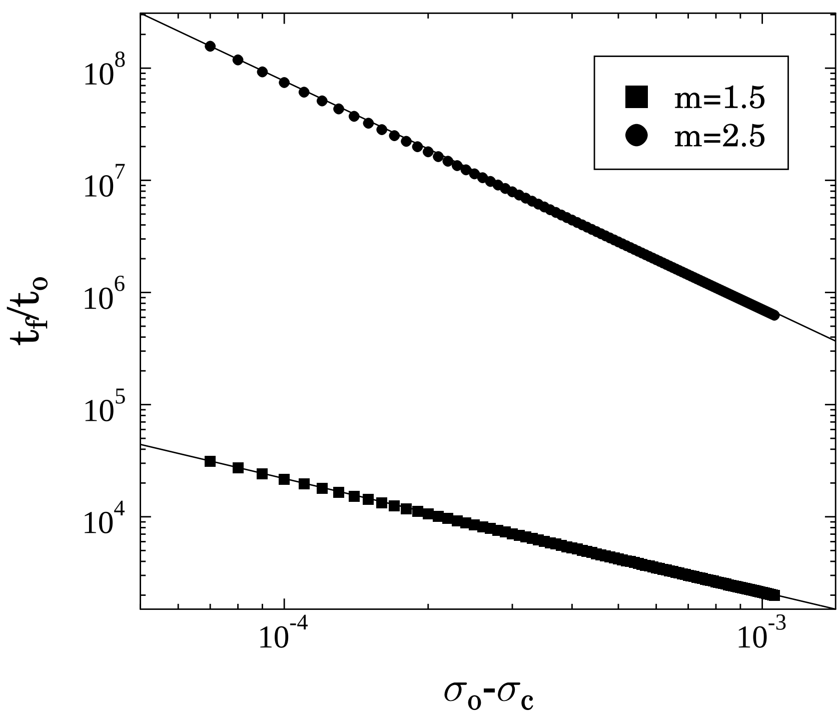

Figure 9.3: Lifetime t_f as a function of the distance from the critical point $\sigma_o - \sigma_c$ for two different values of the parameter m. The number of fibers in the bundle was taken $N = 10^7$.

and the multiplication factor K_i reads as

$$K_i = \frac{N}{N-i}\left(\frac{i}{N}\right)^m \frac{1}{B}\left[\frac{1}{E_f} - \frac{1}{E_b}\left(1 - \frac{N}{i}\right)\right]. \tag{9.16}$$

For $m = 1$ the corresponding equation has the form

$$\Delta t(\sigma_i, \sigma_{i+1}) = K_i \left[\ln f_i(\sigma_{i+1}) - \ln f_i(\sigma_i)\right]. \tag{9.17}$$

Then the simulation proceeds as in the case of viscoelastic bundles but in the above formulas the number of broken fibers i varies as $i = N_o, N_o + 1, \ldots, N - 1$, so the time as function of σ can be obtained as

$$t(\sigma_i) = \sum_{j=N_o+1}^{i} \Delta t(\sigma_j, \sigma_{j+1}) \tag{9.18}$$

from which the deformation as a function of time $\varepsilon_i(t)$ can be determined, since $\sigma = E_f \varepsilon_f$ always holds. The lifetime t_f of the system can be obtained by summing up all the Δt's.

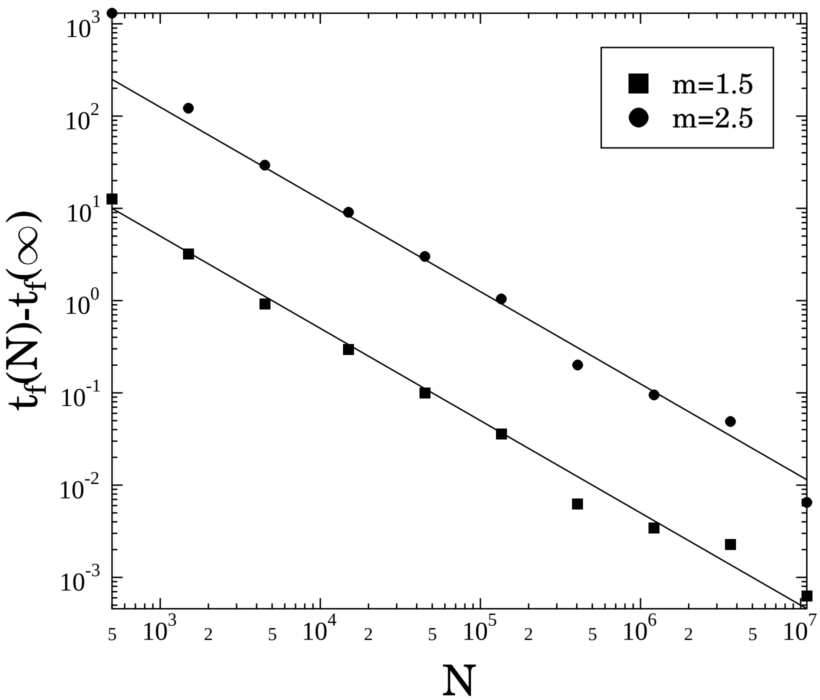

Figure 9.4: Size dependence of the lifetime t_f for two different values of the parameter m.

For the purpose of explicit calculations a uniform distribution was prescribed for the breaking thresholds σ_i between 0 and 1. The deformation as a function of time is plotted in Fig. 9.2 for several different values of the external load below and above the critical load. Similarly to the previous model the two regimes of the creeping system can be clearly distinguished.

To study the behavior of the time to failure as a function of the distance from the critical point, simulations were performed for several different values of the exponent m. In Fig. 9.3 the results are presented for $m = 1.5$ and $m = 2.5$. The slope of the fitted straight lines agrees very well with the analytic predictions of Eq. (9.10).

The size scaling of the time to failure t_f was analyzed by simulating the creep rupture of bundles of size $N = 5 \cdot 10^2 - 10^7$ setting a uniform distribution for the breaking thresholds. We found that $t_f(N)$ converges to the lifetime of the infinite system $t_f(\infty)$ according to the universal law Eq. (8.26) independently on the value of the exponent m. In Fig. 9.4 the best fit was obtained for both curves with slope -1.0 ± 0.05 for both m values.

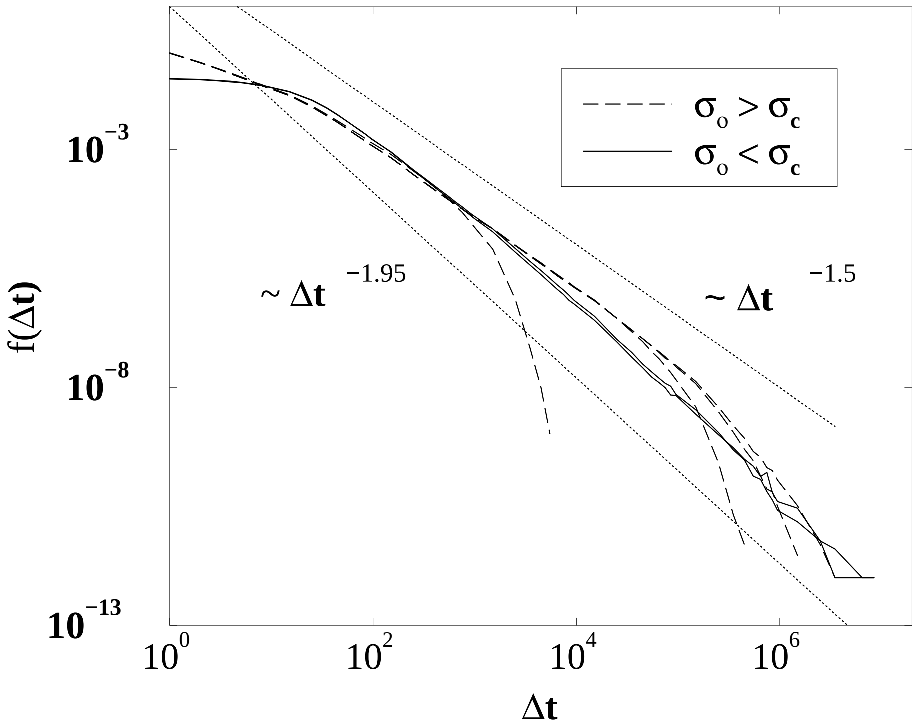

Figure 9.5: The distribution of inter-event times Δt for $\gamma = 0$. Power law behavior can be observed over up to five orders of magnitude.

Statistics of events

The inter-event time Δt is a fluctuating quantity which depends both on the breaking thresholds and the load level. The statistics of inter-event times characterized by the distribution $f(\Delta t)$ provides information on the microscopic dynamics of creep. $f(\Delta t)$ is presented in Fig. 9.5 for a system of $N = 3 \times 10^7$ fibers.

Simulations revealed that $f(\Delta t)$ exhibits a power law of the form

$$f(\Delta t) \sim \Delta t^{-b} \tag{9.19}$$

both below and above the critical point whenever the macroscopic stationary state characterized by the plateau of $\varepsilon(t)$ is attained. However, the value of the exponent b is different on the two sides of the critical point, *i.e.* below σ_c the exponent of the distribution is $b = 1.95 \pm 0.08$ independent of σ_o, while above σ_c we obtained $b = 1.5 \pm 0.07$. Increasing the load above σ_c the stationary state gradually disappears implying that the power law regime of $f(\Delta t)$ preceding the exponential cut-off is getting shorter but the exponent remains the same (see Fig. 9.5). It follows that the slow relaxing bundle also

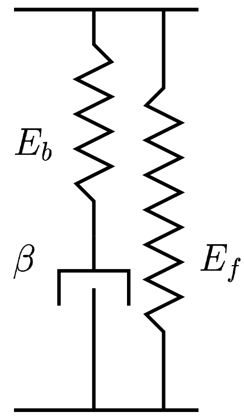

Figure 9.6: Coupling between a pure elastic element and a Maxwell element

self-organizes into a critical state in the same manner than the creeping bundle of fibers previously presented in chapter 8. Note that the exponents keep their universal values.

9.1.2 Variable range of interaction

Relaxation of a single Maxwell element

Firstly, we explore on the relaxation process of a single linear Maxwell element coupled in *parallel* with an elastic surrounding under a fixed external load σ_o. The coupling is shown in Fig. 9.6. There E_f is the stiffness of the elastic element, E_b and β are the characteristic constants of the Maxwell viscoelastic element.

As the two elements are connected in *parallel* the external stress during the process is equal to the sum of the stresses in each element which can be written as

$$\sigma_o = \sigma_b + \sigma_f, \tag{9.20}$$

where σ_b and σ_f are the stresses in the Maxwell element and the elastic element respectively. The constitutive behavior of a linear Maxwell element reads as

$$\frac{\dot{\sigma}_b}{E_b} + \frac{\sigma_b}{\beta} = \dot{\varepsilon}_b. \tag{9.21}$$

Which is a special case of Eq. 9.2 for $m = 1$. On the other hand for the elastic element it looks as

$$\frac{\dot{\sigma}_f}{E_f} = \dot{\varepsilon}_f, \tag{9.22}$$

The boundary condition $\dot{\varepsilon_b} = \dot{\varepsilon_f}$ must always be fulfilled. The solution of the equations 9.21, 9.22 emerges as

$$\sigma_b(t) = \frac{\sigma_o}{2} e^{-\frac{t}{\lambda}}, \tag{9.23}$$

and

$$\sigma_f(t) = \sigma_o - \frac{\sigma_o}{2} e^{-\frac{t}{\lambda}}, \tag{9.24}$$

where λ is a characteristic relaxation time which depends on the parameters of the elements in the following way:

$$\lambda = \frac{E_b \, E_f}{(E_f + E_b)\, \beta}. \tag{9.25}$$

Hence, the stress in the Maxwell element has an exponential relaxation and the elastic element is continuously supporting it. So that, the Maxwell element behaves as a *source* of stress and the elastic element as a sink. In $t = \infty$ the elastic element will carry the whole external stress σ_o.

For a non-linear Maxwell element (Eq. 9.2) the corresponding results read as:

$$\sigma_b(t) = \sigma_o \, \left(1 + \frac{(m-1)\sigma_o^{m-1}}{\lambda} t\right)^{\left(\frac{1}{1-m}\right)}, \tag{9.26}$$

and

$$\sigma_f(t) = \sigma_o - \sigma_o \, \left(1 + \frac{(m-1)\sigma_o^{m-1}}{\lambda} t\right)^{\left(\frac{1}{1-m}\right)}. \tag{9.27}$$

Simulation technique

Based on the previous simple system above we can simulate a fiber bundle model with slowly relaxing fibers in the framework of the local load sharing approach.

The system is composed of N parallel fibers identified by an integer i, $1 \le i \le N$ on a square lattice, which initially have identical Young-modulus E_f but random failure thresholds d_i, $i = 1, \ldots, N$. The failure strength d_i of individual fibers is an independent homogeneously distributed random variable with a probability density $p(d)$ and a cumulative probability distribution $P(d) = \int_0^d p(x)dx$.

After one fiber breaks, the local stress of the broken fiber exponentially decreases with a characteristic time λ. Then, the excess of stress is re-distributed among the intact elements

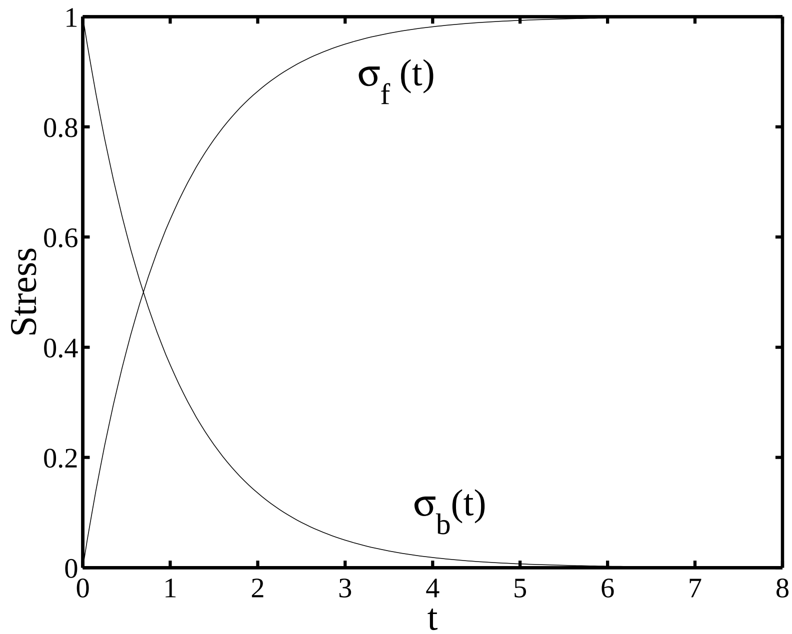

Figure 9.7: Example of the stress sharing between the Maxwell and the elastic element. One can observe that the remaining intact fiber overtake the load of the broken one.

of the system, following a variable range of interaction rule which was already described in chapter 6.

Hence, the stress in the surviving element i at time t_{k+1} *i.e.* $\sigma_f^i(t_{k+1})$ is related to the stress at time t_k in the following manner

$$\sigma_f^i(t_{k+1}) = \sigma_f^i(t_k) + \sum_{j \in I} \frac{\sigma_b^j(t_k) r_{i,j}^{-\gamma}}{Z_j} e^{-\frac{\Delta t_{k+1}}{\lambda}}, \tag{9.28}$$

with $\Delta t_i = t_{k+1} - t_k$ The sum runs over the set I of all broken elements and $r_{i,j}$ is the distance of fiber i to the source point (x_j, y_j) which has at time t_k the stress value $\sigma_b^j(t_k)$ and Z_j is the normalization constant (see chapter 6).

Using Eq. 9.28, the time elapsed for each element of the system before it breaks can be deduced. Moreover, when the element i breaks, its stress can be assumed equal to its threshold value d_i. Solving Eq. 9.28 for the time interval Δt_i and substituting $\sigma_f^i(t_{k+1}) = d_i$ results in

$$\Delta t_i = -\lambda \log \frac{d_i - \sigma_f^i(t_k)}{\sum_{j \in I} \sigma_b^j(t_k) r_{i,j}^{-\gamma} / Z_j}. \tag{9.29}$$

The minimum of the set Δt_i is the interval of time between the kth and the $k+1$th breakings

$$\Delta t_{k+1} = \min_{i \in I} \Delta t_i, \tag{9.30}$$

and the time elapsed till the breaking of the $k+1$th fiber is obtained as

$$t_{k+1} = \sum_{j=1}^{k+1} \Delta t_j. \tag{9.31}$$

Obviously, this algorithm is more simple if global load sharing is assumed, and Eq.(9.29) is given as:

$$\Delta t_i = -\lambda \log \frac{(N\sigma_o - (N - N_o + i))d_i}{T_{i-1}} \tag{9.32}$$

where N_o is the number of broken elements at zero time $(t = 0)$ and

$$T_{i-1} = \sum_{k=0}^{i-1} d_k e^{\frac{t_k}{\lambda}} \tag{9.33}$$

Time to failure

Fig. 9.8 presents the lifetime t_f of a bundle of fibers of linear size $L = 81$ as a function of the distance from the critical point $\Delta\sigma = \sigma_o - \sigma_c$ for several values of the exponent γ. We observe that the $t_f(\Delta\sigma;\gamma)$ curves form two groups of different functional form: The upper group is obtained for $0 \leq \gamma \leq 2$ when the load sharing is global. In the lower group, obtained for $\gamma > 2$ when the load sharing gets localized, $t_f(\Delta\sigma;\gamma)$ rapidly takes a constant value showing an abrupt transition at the critical load σ_c with no scaling, reminiscent of a first order transition. Note that similar results were obtained, for an array of creeping fibers, which were represented by Kelvin's viscoelastic elements and the same load transfer rule was used (see chapter 8).

Following of the presentation of Chapter 8, in order to describe the behavior of $t_f(\Delta\sigma;\gamma)$ under the variation of γ we calculated the normalized quantity $S(\gamma)$ previously define in Eq. 8.35. $S(\gamma)$ is illustrated for different system sizes in Fig. 9.9. As was already explained in Chapter 8 this magnitude provides a quantitative description of the creep rupture transition in terms of the effective range of interaction so that $S(\gamma)$ takes value unity for the GLS, and it has a value close to zero for the LLS class, respectively. We can also observe in Fig. 9.9 that the transition between the two universality classes gets sharper around $\gamma_c \approx 2$ with increasing system size.

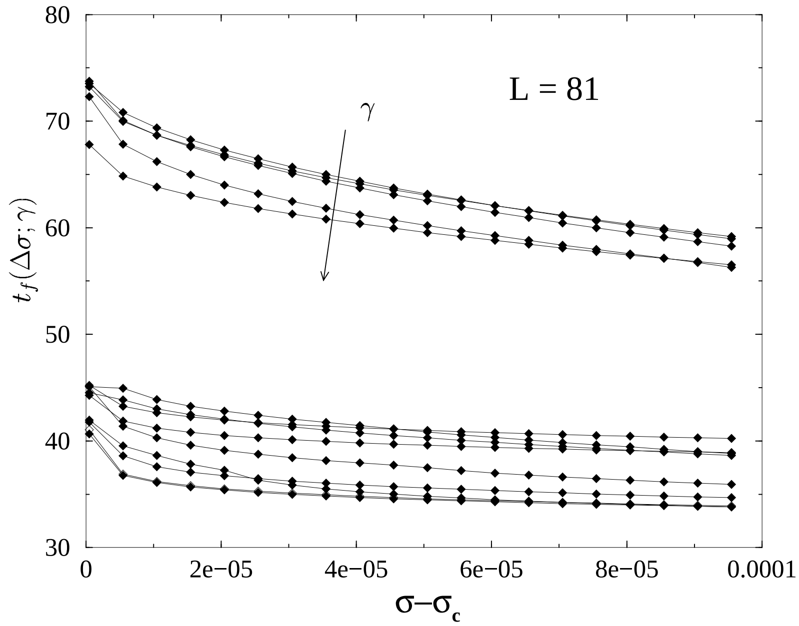

Figure 9.8: The lifetime t_f as a function of $\sigma_o - \sigma_c$ for different values of the exponent γ between 0 and 10. The arrow indicates the direction of increase

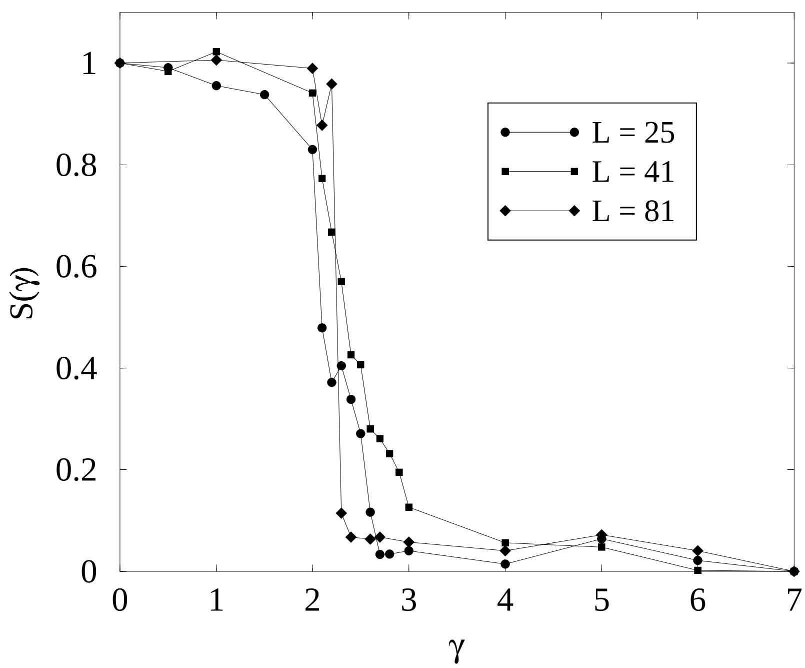

Figure 9.9: $S(\gamma)$ as a function of γ for several system sizes L.

The results confirm the existence of two universality classes in creep rupture of fiber-reinforced composites, which was previously obtained in chapter 8. Those universality classes are characterized by a completely global (GLS), or a completely local (LLS) behavior depending on the effective range of interaction γ with a rather sharp transition between them.

9.2 Conclusions

We have analyzed a model of creeping fibers composites where the time dependence is introduced by the slow relaxation of fibers and their interaction was realistically modeled by the power law transfer function introduced in Chapter 6. Analytical and numerical calculations showed that also during the slow relaxation of broken fibers a transition takes place from a partially failed state of infinite lifetime to a state where global failure occurs at a finite time. Hence, the macroscopic time to failure diverges as power law function, close to the critical stress value σ_c. The critical exponent is independent on the cumulative threshold distribution, but is related with the nature of the relaxation process ($\dot{\varepsilon}$ non-linearity). Similar to the previous chapter, the critical load turned out to be the static fracture strength of the material. The existence of two universality classes in creep rupture of fiber-reinforced composites was confirmed by our results, using a model with variable range of interaction. The model can be relevant to describe metal matrix composites reinforced by brittle fibers where also local load sharing approach is relevant.

Chapter 10

General Conclusions

In this thesis, our goal was to extend the fiber bundle models, used to describe failure of fibers composites, in order to provide a more detailed and realistic description of the failure process of fiber reinforced composites. Severals different damage mechanism relevant for certain classes of materials have been examined. Our analytical and numerical results have been described and some specific new application of those models have been presented.

An extension of the classical fiber bundle model by introducing a continuous damage law, was described in Chapter 4. This model allows for multiple failure of fibers with quenched and annealed disorders. A simple general derivation of the constitutive behavior of the model is provided, which also allows to obtain analytic results for the microscopic damage process. Varying its parameters, the model provides a broad spectrum to describe materials ranging from strain hardening to perfect plasticity, and hence, the model can be relevant to describe the damage process of various types of materials [56, 57, 61–63]. It is a remarkable feature of the model that multiple failure of brittle elements can result in a macroscopically plastic state, which has also been observed experimentally in materials where the damage mechanism is the gradual multiple failure of individual elements. We also focused on the microscopic damage process to understand the emergence of the plastic plateau under strain controlled loading, and the resulted avalanche activity under stress controlled loading of the continuous damage fiber bundle model. Analytic results were obtained to characterize the damage process along the plateau under strain controlled loading, furthermore, for stress controlled experiments a simulation technique was developed and the distribution of avalanches of fiber breakings was explored numerically. Simulations showed that depending on the parameters of the model the distribution of bursts of fiber breakings can be exponential or power law. The results obtained have relevance to understand the acoustic emission measurements performed on various elastoplastic materials [61–63].

In Chapter 5 we have presented an experimental and theoretical study about the evolution of the force chains during the compression of a granular medium. For the theoretical description we applied the concept of fiber bundle models based on the analogy of fibers of composites and the array of force chains in a compacted granular material.

Our model for hardening force networks inverts the mechanism of the continuous damage model for fiber-reinforced composites (Chapter 4). The individual lines of the network are considered as fibers which instead of rupturing under tension do harden under pressure due to contact rearrangements. If the increase of stiffness and the increase in the restructuring threshold stress are equal, the model can be solved analytically. We provide a nonlinear constitutive behavior in good quantitative agreement with the experimental results. Moreover, the stress σ shows a power law divergence when ε approaches the certain critical value ε_c ($\sigma \sim (\varepsilon - \varepsilon_c)^\beta$). The value of the exponent is universal ($\beta = -1$),*i.e.* it does not depend on the form of disorder distribution, while the value of ε_c depends on it. The rearrangement of granular materials results in a spontaneous release of acoustic energy radiating waves similar to those observed in other brittle materials under load. The amplitude distribution of acoustic signals was found experimentally to follow a power law of an exponent $\delta = 1.15 \pm 0.05$ which is in good agreement with the analytic solution of the model $D(s) = s^{-1}$.

In order to model realistic situation, where load sharing in materials fells between the limiting cases of GLS and LLS; we have developed a fracture model of the fiber bundle type where the interaction among fibers is considered to decay as a power law of the distance from an intact element to the rupture point (see Chapter 6). Two very different regimes are found as the exponent of the stress-transfer function varies and a crossover point is identified at $\gamma = \gamma_c$. The strength of the material for $\gamma < \gamma_c$ does not depend on both the system size and γ qualifying for mean-field behavior, whereas for the short range regime, the critical load decreases with the system size as $\sigma_c \sim 1/\ln(N)$. The behavior of the model on both sides of the crossover point was numerically studied by recording the avalanche and the cluster size distributions. The numerical results suggest that the crossover point falls in the vicinity of $\gamma_c = 2.0$.

The size effect of tension strength of softwood loaded parallel to fiber direction has been studied experimentally and theoretically in chapter 7. The macroscopic constitutive behavior of the specimens was rather brittle and the strength values showed a statistical variation which could be well fitted in terms of a Weibull distribution. It was revealed that the average strength is a decreasing function of the cross-sectional specimen size. In order to provide a theoretical interpretation of the experimental results with respect to the size effect and the modeling of the load sharing mechanism, the wood material was modeled as a natural fiber composite with extremely small volume fraction of matrix material. Comparing the strength distribution of single fibers and the macroscopic samples we deduced that the load redistribution among wood fibers is short ranged giving rise to a low precursory activity preceding final failure and small clusters of broken fibers. For a qualitative characterization of the load sharing it has been assumed that the load-transfer function has a power law form and its effective exponent has been estimated.

We studied the creep rupture of fibrous materials in the framework of fiber bundle models taking into account two possible microscopic mechanisms of creep: (i) in the first (Chapter 8) approach the fibers themselves are viscoelastic and they break when their deformation exceeds a stochastically distributed threshold value, (ii) in the second model (Chapter 9) the fibers are linearly elastic until they break, however, after breaking their relaxation is not instantaneous but the creeping matrix introduces an intrinsic time scale for the relaxation. The first model can be relevant for natural fiber composites like wood which are composed of viscoelastic fibers, while the second model can provide an adequate description of metal matrix composites reinforced by brittle fibers. Analytical and numerical calculations showed in both models that increasing the external load on a specimen a transition takes place from a partially failed state with infinite life time to a total failure state with finite life time t_f. We have identified two universality classes of creep rupture depending on the range of interaction of fibers. The critical behavior of the microfracturing process can be seen as the result of the self-organization of the system into a macroscopic stationary state whose duration depends on the external perturbation (load). In this sense the system is at some point of marginal stability jumping form one metastable state to another with power-law distributed waiting times. This suggests the existence of a critical dynamics underlying the process that seems to indicate self-organized criticality in creep.

Outlook

Although fiber bundle models have already been studied in great details, there still exists a lot of new possible applications. Typical laminar composites are made up of different layers of fiber bundles .This follows from the technological specifications which fix the layer composition and the relative orientation between the fibers. The shear-failure in this kind of composites is interesting. The damage evolution and the stress redistribution during this failure process are still not well understood. Many other universal properties could still be obtained. In future, these kind of systems can be better addressed through more complex models developed on the basis of the FBM's.

Currently the evolution of the force chain array inside a compact granular system is not fully understood. Several recent experiments have used different types of materials for the beads and more advanced acoustic emission techniques that include source localization. In this way the evolution of the compact granular media close to the critical volume fraction could now be studied. Moreover, the localization and the description of the local restructuring events could be used to develop a new NDT to study the force distribution inside a compact granular media.

The fracture model with variable range of interaction presented in Chapter 6 can be further improved. For example, the screening influence of the broken fiber clusters could also be taken into account. This may significantly enhance the accuracy of the global strength prediction. Moreover, the possible influence of the disorder on the crossover value γ_c is still an open question. For this reason some analytical arguments are still missing in this respect and a detailed numerical study is needed to clarify this. Such approach may also allow us to develop a more realistic fiber-reinforced composites model in which the stress parallel to the fiber direction could be modeled as a shear-lag interaction. This idea is not completely new, but the efficiency of our algorithm might enable to make calculations with bigger system sizes, an important aspect in this problem.

In Chapter 7 the size dependency of tension strength in soft-wood have been theoretically and experimentally accessed. Further experiments with intermediate size scales are needed to confirm the results in a more quantitative manner. Some aspects of the damage evolution of the wood tension loading parallel to the fiber are not very well described by the FBMs. Nevertheless, our numerical results and existing analytical work by other groups are expected to be the starting point for studying the failure of some real wood structures . This will have significant technological relevance.

Concerning the creep modeling, recent experiments have shown the existence of a critical stress value σ_c in the creep of the soft-wood [112]. These experiments have been performed applying different load values to several sets of wood specimens. The results indicate that with increase of the fixed external load σ_o, a transition takes place from a partially failed state with infinite life time to a total failure state with finite life time t_f. Although our models support that the critical stress value σ_c should be equivalent to the global strength of the sample, in the experiments the critical stress value is found to be around $20\% - 30\%$ lesser than the global strength. Further theoretical studies are needed to clarify this.

I conclude this thesis following one Philosophical Dialectic Principia. It is well understood that the truth is always relative. The absolute truth is just an abstraction which can never be reached. The scientific community will always get a better approximation of the reality. For our children, our theories will only be the first step, that fortunately someone has made before.

Bibliography

[1] Sornette D. Elasticity and failure of a set of elements loaded in parallel. *J. Phys. A*, 22:L243, 1989.

[2] D. Sornette. Failure thresholds in hierarchical and euclidian space by real space renormalization group. *J. Phys. France*, 50:S. 745, 1989.

[3] P.D. Hemmer and A. Hansen. The distribution of simultaneous fiber failures in fiber-bundles. *J. Appl. Mech.*, 59(4):909–914, 1992.

[4] S. R. Pride and R. Toussaint. Thermodynamics of fiber bundles. *Physica A*, 312:159, 2002.

[5] W.A. Curtin. Theory of mechanical properties of ceramic-matrix composties. *J. Am. Ceram. Soc.*, 75(11):2837, 1991.

[6] W.A. Curtin. The tough to brittle transition in brittle matrix composites. *J. Mech. Phys. Solids*, 41(2):217–245, 1993.

[7] S.J. Zhou and W.A. Curtin. Failure of fiber composties: A lattice green function model. *Acta metall. mater.*, 43(8):3093–3104, 1995.

[8] Fredrik Thuvander, E. Kristofer Gamstedt, and Per Ahlgren. Distribution of strain to failure of single wood pulp fibres. *Nordic Pulp and Paper Reseach Journal*, 16(1):46–56, 2001.

[9] H.E. Daniels. The statistical theory of the strength of bundles of threads. *Proc. R. Soc. A*, 183:405–435, 1944.

[10] Coleman B. D. Statistics and time dependence of mechanical breakdown in fibers. *J. Appl. Phys*, 29:968–983, 1958.

[11] Drouillard T.F. and Beall F.C. AE literature-wood. *J. Acoustic Emission*, 9:215–222, 1990.

[12] H. J. Herrmann and S. Roux. *Statistical Models for the Fracture of Disordered Media*. Elsevier Science Publishers B.V., 1990.

[13] B. K. Chakrabarti and L.G. Benguigui. *Statistical Physics of Fracture and Breakdown in Disordered Systems*. Clarendon Press Oxford, 1997.

[14] J. Andersons, R. Joffe, M. Hojo, and S. Ochiai. Glass fibre strength distribution determinated by common experimental methods. *Composites Science and Technology*, 62:131–145, 2002.

[15] J. Andersons, R. Joffe, M. Hojo, and S. Ochiai. Fibre fragment distribution in a single-fibre composite tension test. *Composites: part B*, 32:323–332, 2001.

[16] J. Andersons, U. A. Handge, and I. M. Blumen. Analysis of brittle coating fragmentation under tension for weibull strength distributions. *Eur. Phys. J. B*, 17:261–268, 2000.

[17] S. Zapperi, A. Vespignani, and H.E. Stanley. Plasticity and avalanche hehaviour in microfracturing phenomena. *Nature*, 388:658–600, 1997.

[18] S. L. Phoenix and I. Beyerlein. Statistic strength theory for fibruos composites materials. *Ask Falk*, 2002.

[19] M. Kloster, A. Hansen, and P.C. Hemmer. Burst avalanches in solvable models of fibrous materials. *Phys. Rev. E*, 56(3):2615–2625, 1997.

[20] Alex Hansen and P. C. Hemmer. Burst avalanches in bundles of fibers: Local vs globla load-sharing. *Physics Letters A*, 184:394–396, 1994.

[21] S. D. Zhang and E. J. Ding. Burst-size dsitribution in fiber-bundles with local load shearing. *Physics Letters A*, 193:425–430, 1994.

[22] W. E. Newman and S. L. Phoenix. Time-dependent fiber bundles with local load sharing. *Phys. Rev. E*, 63:021507, 2001.

[23] R.L. Smith. The asymptotic distribution of the strength of a series-parallel system with equal load-shearing. *The Anals of Probability*, 10(1):137–171, 1982.

[24] R. L. Smith and S. L. Phoenix. Asymtotic distributions for the failure on fibrous materials under series-parallel structures and equal load-sharing. *Journal of Applied Mechanics*, 1981.

[25] W.I. Newman, A. M. Gabrielov, T. A. Durand, S. L. Phoenix, and D. Turcode. An exact renormalization model for earthquakes and materials failure. *Physica D*, 77:200–216, 1994.

[26] D.G. Harlow and S.L. Phoenix. The chain-of-bundles probability model for the strength of fibrous materials i: Analysis and conjectures. *J. Composite Materials*, 12:195–214, 1978.

[27] S. Roux. Thermally activated breakdown in the fiber-bundle model. *Phy. Rev. E*, 62(5):6164–6169, 2000.

[28] S. Mahesh, I.J. Beyerlein, and S.L. Phoenix. Size and heterogeneity effects on the srength of fibrous composites. *Physica D*, 133:371–389, 1999.

[29] T. J. Mackin and F. W. Zok. Fiber bundle puschout: A technique for the measurement of interfacial sliding properties. *Journal of the American Ceramic Society*, 75(11):3169–3171, 1992.

[30] I. L. Menezes-Sobrinho, A. T. Bernardes, and J.G. Moreira. Failure regimes in (1+1)d in fribrous meterials. *Phys. Rev.E*, 63:25104(R), 2001.

[31] W. I. Newman, D. L. Turcotte, and A. M. Gabrielov. Log-period behavior of a hierarchical failure model with applications to precursory seismic activation. *Phys. Rev. E.*, 52(5):4827–4834, 1995.

[32] S. Pradhan and B. K. Chakrabarti. Precursors of catastrophe in the bak-tang-wiesenfeld, manna, and random-fiber-bundle models of failure. *Phys. Rev. E.*, 65:016113, 2002.

[33] Dynamic critical behavior S. Pradhan, P. Bhattacharyya, and B. K. Chakrabarti. Dynamic critical behavior of failure and plastic deformation in the random fiber bundle model. *Phys. Rev. E*, 66:016116, 2002.

[34] E. L. Bonnaud and J. M. Neumeister. Inertia damping effects on the damage-dependent burst size distribution of fiber bundles. *Physics Letters A*, 290:261–269, 2001.

[35] F. Kun and H.J. Herrmann. Damage development under gradual loading of composites. *Journal of Material Science*, 35:4685, 2000.

[36] RC Hidalgo, F. Kun, and H. J. Herrmann. Bursts in a fiber bundle model with continuous damage. *Phys. Rev. E*, 64:066122, 2001.

[37] RC Hidalgo, F. Kun, and H. J. Herrmann. Creep rupture of viscoelastic fiber bundles. *Phys. Rev. E*, 64:032502, 2002.

[38] RC Hidalgo, Y. Moreno, F. Kun, and H. J. Herrmann. A fracture model with variable range of interaction. *Phys. Rev. E*, 65:46148, 2002.

[39] F. Kun, RC Hidalgo, H. J. Herrmann, and K. F. Pál. Scaling laws of creep rupture fiber bundles. *Phys. Rev. E*, 67:061802, 2003.

[40] G. Dill-Langer, RC Hidalgo, Y. Moreno, F. Kun, S. Aicher, , and H. J. Herrmann. Size dependence of strength in natural fiber composites. *Physica A*, 325:547, 2003.

[41] O. E. Yewande, Y. Moreno, F. Kun, RC Hidalgo, and H. J. Herrmann. Time evolution of damage under variable ranges of load transfer. *Accepted by Phys. Rev. E*, 2002.

[42] F. Kun, Y. Moreno, RC Hidalgo, and H. J. Herrmann. Universality classes in creep rupture. *cond-mat/0211331 Accepted by Euro. Phys. Lett.*, 2003.

[43] L. Moral, Y.Moreno, J. B. Gomez, and A. F. Pacheco. Exact numerical solution for a time-dependent fiber-bundle model with continuous damage. *Journal of Physics A: Mathematical and General*, 34:9983, 2001.

[44] L. Moral, Y. Moreno, J. B. Gomez, and A. F. Pacheco. Time dependence of breakdown in a global fiber-bundle model with continuous damage. *Phys. Rev. E*, 63:066106, 2001.

[45] Y. Moreno, J. B. Gómez, and A. F. Pacheco. Fracture and second-order phase transitions. *Phys. Rev. Lett.*, 85(14):2865–2868, 2000.

[46] Y.Moreno, J. B. Gómez, and A. F. Pacheco. Phase transitions in load transfer models of fracture. *Physica A*, 296:9, 2001.

[47] Y.Moreno, J. B. Gómez, and A. F. Pacheco. Self-organized criticality in a fiber-bundle type model. *Physica A*, 274:400, 1999.

[48] M. Vazquez-Prada, J. B. Gómez, Y. Moreno, and A. F. Pacheco. Time to failure of hierarchical load-transfer models of fracture. *Phys. Rev. E*, 60:2581, 1999.

[49] J. B. Gómez, M. Vazquez-Prada, Y. Moreno, and A. F. Pacheco. Bounds for the time to failure of hierarchical systems of fracture. *Phys. Rev. E*, 58:R1287, 1999.

[50] J. B. Gómez, Y. Moreno, and A. F. Pacheco. Probabilistic approach to time-dependent load-transfer models of fracture. *Phys. Rev. E*, 58:1528, 1998.

[51] N. Weigel, B. Kroeplin, and D. Dinkler. Micromechanical modeling of damage and failure mechanisms in c/c-sic. *Computational Materials Science*, 16:120–132, 1999.

[52] N. Weigel, B. Kroeplin, and D. Dinkler. Micromechanically-based continuum damage mechanics material law for fiber-reinforced ceramics. *Proceedings of ECCM'99*, pages 461–481, 1999.

[53] M. Ibnabdeljalil and W.A. Curtin. Strength and reliability of fiber-reinforced composites: Localized load-shearing and associated sice effects. *Int. J. Solids Structures*, 34(21):2649–2668, 1997.

[54] W.A. Curtin. Dimensionality and size effects on the strength of fiber-reinforced compoistes. *Composites Science and Technology*, 60:543–551, 2000.

[55] Z.Xia, W.A.Curtin, and T.Okabe. Green's function vs.shear-lag models of damage and failure in fiber composites. *Composites Science and Technology*, 62:1279–1288, 2002.

[56] A. E. Naaman and H.W. Reinhardt. *High Performance Fiber Reinforced Cement Composites*. E&FN Spon London, 1995.

[57] A.G. Evans and F.W. Zok. Review. the physics and mechanics of fibre-reinforced brittle matrix composites. *J. of Materials Science*, 29(15):3857–3896, 1994.

[58] F. Kun, S. Zapperi, and H.J. Herrmann. Damage in fiber bundle models. *The European Physical Journal B*, 17:269–279, 2000.

[59] W. A. Curtin. Size scaling of strength in heterogeneous meterials. *Phys. Rev Lett.*, 80:1445, 1998.

[60] S. Zapperi, P. Ray, H. E. Stanley, and A. Vespignani. Avalanches in breakdown and fracture processes. *Phys. Rev.E*, 59:5049, 1999.

[61] A. Guarino, R. Scorretti, and S. Ciliberto. Material failure time and the fiber bundle model with thermal noise. e-print cond-mat/9908329.

[62] C. Maes, A. Van Moffaert, H. Frederix, and H. Strauven. Criticality in creep experiments on cellular glass. *Phys. Rev. B*, 57:4987–4990, 1998.

[63] A. Petri, G. Paparo, A. Vespignani, A. Alippi, and M. Costantini. Experimental evidence for critical dynamics in microfracturing processes. *Phys. Rev. Lett.*, 73:3423, 1994.

[64] Cox H. L. The elasticity and strength of paper and other fibrous materials. *Brit. J. Appl. Phys.*, 3:72, 1952.

[65] Hedgepeth J. M. Stress concentrations in filamentary structures. *NASA TN D-882*, 1961.

[66] Hedgepeth JM and Van Dyke P. Local stress concentrations in imperfect filamentry composites materials. *J. Comp. Mater.*, 1:294–309, 1967.

[67] John A. Nairn. On the use of shear-lag methods for analysis of the stress transfer in unidirectional composites. *Mechanics of Materials*, 26:63–80, 1997.

[68] Beyerlein I. J. and Landis C.M. Shear model for failure simuation of unidirectional fiber composites including matrix stiffness. *Mech. Mater.*, 31:331–350, 1999.

[69] Landis C. M., McGlockton M. A., and McMeeking R. M. An improved shear lag model for broken fiber in composites materials. *Journal of COMPOSITES MATERIALS*, 33(7):667–680, 1999.

[70] C.M. Landis, I.J. Beyerlein, and R.M. McMeeking. Micromechanical simulation of the failure of fiber reinforced composites. *Journal of the Mechanics of Physics of Solids*, 48:621–648, 2000.

[71] Z.Xia, T.Okabe, and W.A.Curtin. Shear-lag vs finite element models for stress transfer in fiber-reinforced composites. *Composites Science and Technology*, 62:1141–1149, 2002.

[72] T.Okabe, N.Takeda, Y.Kamoshida, M.Shimizu, and W.A.Curtin. A 3d shear-lag model considering micro-damage and statistical strength prediction of unidirectional fiber-reinforced composites. *Composites Science and Technology*, 61:1773 –1787, 2001.

[73] T. L. Laufenberg, L. C.Palka, and J. Dobbin McNatt. Creep and creep-rupture behaviour of wood-based structural panels. preprint, 1999.

[74] S. V. RAngaraj and L.V. Smith. The nonlinearly viscoelastic response of a wood-thermoplastic composites. *Mechanics of the Time-Dependent Materials*, 3:125–139, 1999.

[75] L. Perez, Valerie Pittet, and Parviz Navi. Fiber behaviour under tensile force, experimentation and modelling. In *Wood and Wood Fiber Composites*, pages 125–139, 1995.

[76] C. Le Govic. Sensitivity of creep to different constant enviroments. In *preprint*, 1995.

[77] S. P. Zwerschke, A. Wanner, and E Arzt. Evolution of fiber fragmentation in a short-fiber-reinforced metal-matrix model composite during tensile creep deformation- an acoustic emission study. *METALLURGICAL AND MATERIALS TRANSACTIONS A*, 33A:1549, May 2002.

[78] Otani H, Phoenix L, and Petina P. Matrix effects on the lifetime statistics for carbon fiber-epoxy microcomposites in creep rupture. *J. Mater. Sci.*, 26:1955–1970, 1991.

[79] M.L. Gambone A. H. Rosenberger. Creep of sic/ti-100 composites in a vacuum enviroment. *Acta mater.*, 47(6):1723–1734, 1999.

[80] L. Phoenix and L.J. Tierney. A statistic model for the life dependent failure of unidirectional composites materials under local elastic load-sharing among fibers. *Engng Fracture Mech.*, 18:193–215, 1983.

[81] M. Ibnabdeljalil and L. Phoenix. Creep rupture of brittle matrix composites reinforced wit time dependent fibers: Scaling and monte carlo simulations. *J. Mech. Phys Solids*, 43(6):897–931, 1995.

[82] Z. Z. Du and R. M. McMeekingb. Creep models for metal matrix composites with long brittle fibers. *Journal of the Mechanics and Physics of Solids Volume 43, Issue 5 , May 1995 , Pages 727-740*, 43(5):701–726, 1995.

[83] McLean M. Directionally solidified materials for high temperature service. In *The Metal Society Lodon*, pages 207–230, 1983.

[84] M. McLean. Creep deformation of metal matrix composites. *Comp. Sci. and Technol.*, 23:37–52, 1985.

[85] Daniel Bonn, Hamid Kellay, Michal Prochnow, Karim Ben-Djemiaa, and Jacques Meunier. Delayed fracture of an inhomogeneous soft solid. *Science*, 280:265, 1998.

[86] A. Guarino, S. Ciliberto, and A. Garcimartin. Failure time and microcrack nucleation. *Euro. Phys. Lett.*, 47:456, 1999.

[87] L. Pauchard and H. Meunier. Instantaneous and time-lag breaking of a two-dimensional solid rod under a bending stress. *Phys. Rev. Lett.*, 70:3565, 1993.

[88] A. Guarino, R. Scorretti, S. Ciliberto, and A. Garcimartin. The critical exponents of fracture precursors. e-print cond-mat/9906146.

[89] C. Liu, S.R. Nagel, D.A. Schecter, S.N. Coppersmith, S. Majumdar, O. Narayan, and J.P. Witten. Force fluctuations in bead packs. *Science*, 269:513, 1995.

[90] H. J. Herrmann, RC Hidalgo, and F. Kun. Restructuring of force networks. *Eur. Phys. J. E*, 9:261, 2002.

[91] RC Hidalgo, C. Groe, F. Kun, H. W. Reinhardt, and H. J. Herrmann. Evolutions of percolating force chains in compressed granular media. *Phys. Rev. Letts*, 89:205501, 2002.

[92] C. Groe, RC Hidalgo, F. Kun, H.W. Reinhardt, and H. Herrmann. Acoustic emission analysis as a tool in percolation theory of compressed granular systems. *NDT&E*, 7, 2002.

[93] T. Travers, D. Bideau, A. Gervois, J.-P. Troadec, and J.-C. Messager. Uniaxial compression effects on 2d mixtures of ‘hard’ and ‘soft’ cylinders. *J. Phys. A*, 19:L1033–L1038, 1986.

[94] B. Miller, C. O’Hern, and R. P. Behringer. Stress fluctuations for continously sheared granular materials. *Phys. Rev. Lett.*, 77:3110–3113, 1996.

[95] S. Roux, D. Stauffer, and H. J. Herrmann. Simulation of disordered systems of cylinders. I. Geometrical behavior. *J. Physique*, 48:341–345, 1987.

[96] D. Stauffer, H. J. Herrmann, and S. Roux. Simulation of disordered systems of cylinders. II. Mechanical behavior. *J. Physique*, 48:347–351, 1987.

[97] M. D. Rintoul and S. Torquato. Metastability and crystallization in hard-sphere systems. *Phys. Rev. Lett.*, 77(20):4198–4201, 1996.

[98] H.A. Makse, D.L. Johnson, and L.M. Schwartz. Packing of compressible granular materials. *Phys. Rev Lett.*, 84:4160, 2000.

[99] C. Grosse, H.-W. Reinhardt, and T. Dahm. Localization and classification of fracture types in concrete with quantitative acoustic emission measurement techniques. *NDT&E Intern.*, 30(4):223–230, 1997.

[100] C. Grosse, B. Weiler, and H.-W. Reinhardt. Relative moment tensor inversion applied to concrete fracture tests. *J. of Acoustic Emission*, 14(3-4):S64–S87, 1997.

[101] C. Grosse, M. Motz, H.-W. Reinhardt, and B. Kroeplin. Signal conditioning in acoustic emission analysis using wavelets. *NDT.net*, 7(9), 2002.

[102] C. Grosse, H.-W. Reinhardt, and F. Finck. Signal-based acoustic emission techniques in civil engineering. *J. of Mat. In Civ. Eng.*, 2003.

[103] D. G. Harlow. The pure flaw model for chopped fibre composites. *Proc. R. Soc. London A*, 397:211–232, 1985.

[104] B. Kahng, G. G. Bartrouni, S. Redner, L. de Arcangelis, and H. J. Herrmann. Electrical electrical breakdown in a fuse network with random, continuously distributed breaking strengths. *Phys. Rev. B*, 37:7625, 1988.

[105] J. D. Barrett. Effect of size on tension perpendicular to grain strength of douglas fiber. *Wood Fiber*, 6(2):126, 1974.

[106] J. D. Barrett and A. R. Fewell. Size factors for the bending and tension strength of structural timber. In *Proc. CIB-W18A Meeting*, pages paper 23–10–3, 1990.

[107] S. Aicher, G. Dill-Langer, and W. Kloeck. Evaluation of different size effect models for tension perpendicular to grain strength of glulam. In *Proc. CIB-W18A Meeting*, pages paper 35–6–1, 2002.

[108] F Kollmann. *Technologie des Holzes und der Holzwerkstoffe*. Springer, 1982.

[109] G. Dill-Langer, T. Rigger, l. Hoefflin, and S. Aicher. Localization of acoustic emission sources in timber loaded parallel to grain. *Proceedings 13th International Symp. on NDT of Wood*, Berkely 2002.

[110] G. Dill-Langer and S. Aicher. Monitoring of microfracture by microscopy and acoustic emission. In *Wood and Wood Fiber Composites*, page 93, 2002.

[111] J. V. Andersen, D. Sornette, and K.-T. Leung. Tricritical behavior in rupture induced by disorder. *Phys. Rev. Lett.*, 78:2140, 1997.

[112] G. Dill-Langer, RC Hidalgo, F Kun, S. Aicher, and H. J. Herrmann. Creep rupture of natural fiber composites. *in preparation*, 2003.

Acknowledgments

I wish to express my sincere gratitude to Prof. Dr. Hans J. Herrmann and Dr. Ferenc Kun for their invaluable support and orientation. They guided and helped me whenever I was in need, without them this work would have been impossible.

I am also in debt with many people due to their important apport in my professional develoment R. Mulet, M. Rigol Pérez, E. Altshuler, A. Batista-Leyva, L. Pérez, L. Roca, J.C. Cordero, J.M. de la Peña, E. Fernandez and many others.

I am also very grateful to Y. Moreno, F. Wittel, C. Große, G. Dill-Langer and S. Aicher for the wonderful collaboration we done together along these years.

I would also like to thank my wife Carmen Aimara, my parents Raúl and Bertha and my friends A. Martinez and L. Madrazo who always were with me, giving their support and love.

Moreover, I thank all the friends that made from my stay in Germany a beautiful part of my life, specially L. López, A. Ehl, S. Moran, J. Garibay, M. Massoni, J.D. Muñoz, V. Arrieta, O.L. Castro, F. Alonso-Marroquín, M. Rigol Madrazo, J. Jovel, V. Schwemmle, M. Hasse, L. Aguilera, B. and V. Bibhu, M. Sidra, A. Mora, F. Fonseca, S. McNamara, M. Wackenhut, R. Mahmoodi,M. Maddadi, R. Garcia, M. Lätzel, R. Mück, S. Luding, the OLA and the ICA1.

Finally, I wish to thank the project SBF381 C7 of the German Research Foundation (Deutsche Forschungsgemeinschaft) and the NATO grant PST.CLG.977311. for the financial support.

Raúl Cruz Hidalgo
Stuttgart August 18, 2003